Evaluation of the Attachment and Viability of Cultured Cells under Addition of Antitumor Reagents Using Quartz Crystal Microbalance and Microscopy

DOCTORAL THESIS

By

ALSALEEM ABDULLAH HUSSAIN A

（アルサリーム　アブドッラ　ホセイン　エー）

School of Bioscience and Biotechnology

Tokyo University of Technology

Tokyo, Japan

March 2022

Contents

Abstract

With scientific advances in biological research, cultured cells are being used as simulations of living organisms with the goal of building synthetic biosystems for research in the fields of bioengineering and medical applications. One of the most important of these uses is studying the adhesion and separation of cultured cells on surfaces. In addition, studying their life and death is important as a result of exposure to stimuli and chemical pressures. The study of cell morphology is important in these studies, as it shows changes in the shapes of cells as a result of the influence of stimuli or inhibitors on them. Moreover, cultured cells differ in their shapes depending on the type of surface and type of extracellular matrix (ECM).

In order to observe cell morphology and the effects of ECM in response to an antitumor reagent for cultured cells and monitor the attachment process, I have developed a quartz crystal microbalance (QCM) system with a micro-CMOS camera and a Peltier device. The system enables microphotograph imaging and temperature controlling simultaneously with QCM measurement, where I have improved imaging and measurement performance to get more repeatable data. The lighting unit and electronic focus control of the lens have been added, and linked to the thermoregulatory unit for precise control and rapid temperature change. This system was used in a CO_2 incubator. The electrodes of QCM were made after optimizing and tuning their working conditions from transparent indium tin oxide (ITO) electrodes with a thin thickness and high transmittance, which enable to obtain a transparent mode microphotograph.

I have studied different types of ECM that will contribute to cell attachment on ITO electrical surfaces to monitor and analyze changes in cells. After forming poly-L-lysine (PLL), collagen, and thermoresponsive polymer poly(N-isopropylacrylamide) (PNIPAM) layers on QCM surfaces, human hepatoma cell line (HepG2) cells were cultured at 37 ˚C. The attachment process of cells cultured on poly-L-lysine (PLL), collagen, and thermo-responsive polymeric polymer (N-isopropylacrylamide) (PNIPAM) were studied. At the same time, micro photographs of the cells were recorded to observe the morphological changes.

During cell attachment process, resonance frequency decreased and resonance resistance increased, which meant that cells attached on the quartz crystal surface. In case of PLL and collagen the resonance frequency and resonance resistance showed the attachment finished within 24 h. This corresponded to the cell image observed with the micro-CMOS camera. To determine the relationship between change of resonant frequency and cell number on a QCM, a cell-cell interaction model has been proposed using the binomial equation in the model mass effect. In the proposed equation, the variable mass ratio (variable mass: m_v / steady

mass: m_s) was 1.75, and the close contact probability of cells was 1/2400, which was determined to correct the resonance frequency modeling curves of the experimental results. Analysis of the fitting curves showed that the curves fitted to the first order lag response and the time constants of the first order lag response were 11 h for PLL, 16 h for collagen and 38 h for PNIPAM films. These findings were supported by photographic images showing wider spread cells on PLL and collagen than PNIPAM. The response of cells on PNIPAM was measured during a thermal cycle from 37 to 20 °C and then from 20 °C to 37 °C.

For the cell response process after injection of the antitumor cisplatin, two response steps were observed in both QCM data and microscopic images, where the cells loosened in the first step and shrank in the second step. Log-normal distributions were applied to match both steps by the resonant frequency responses of both processes. The measured curves and the modeling curves are in good agreement with QCM data. By fitting results, I obtained survival rates of 0.1 and 0.2 when the cisplatin concentrations were 83.3 and 16.7 μmol/L, respectively.

In this thesis, I have developed a measurement system that allows monitoring of cells in a CO_2 incubator. Using this system, I observed how the cell interacts with ECM and attaches to surfaces, as well as the structural changes associated with these interactions. In addition to monitoring the effects of chemical and stress stimuli, and analyzing the physical properties of cells, transition of the state of cytoskeleton and antitumor drag activity was measured. Moreover, fitting curves of the model equations were investigated by matching them with the experimental curves of the resonant frequency change. The resonance frequency analysis could provide analysis of mass, viscosity, life and death of cells that are difficult to obtain through microscopic measurements alone.

When using traditional measurement methods for determine cell death, only the state of an elapsed time is measured since the measurement is performed after a certain period of time has passed. Similarly, these methods cannot show the progress or status when more time has passed. On the other hand, the method of this study is possible to measure how the morphology is continuously changing. In addition, the method in this study is also possible to analyze the mechanism of cell change. Through this system, it can be used to analyze the cell adhesion process of various ECMs. Also, it can be used to analyze changes in cell responses over time and evaluate the rate of cell death that were not able to do before.

Chapter 1: General introduction

1.1 Motivation of the study

In vitro cultured cells are widely used for research in biological instrumentation and biological analyses as simulations of organisms. One of the most important uses in these research works is the test of adhesion and detachment of cultured cells on surfaces by chemical stimuli. In addition, monitoring their life and death due to exposure to some chemical stresses is an important application. The study of cell morphology is of great importance in the fields of biological research, as the morphology changes as a result of effect by stimuli or inhibitors to the cultured cells. Moreover, cultured cells differ in their shapes when spread on surfaces by means of adjuvants (ECM: extracellular matrix) [1,2,3], depending on the type of ECM [4]. Where adheres to surfaces over time based on its interaction with the ECM through four stages: The first stage is spherical with no legs (filiform). The second stage is spherical with one or two filamentous legs. The third stage is spherical with more than two legs. The fourth stage extends on the surface [5].

To understand the effect chemical stimuli and stresses, on cell shape physical properties of cells are analyzed on their cytoskeletal state and activity. One of the common uses for analyzing the physical properties of cells is the use of quartz crystal microbalance (QCM) sensor with transparent electrodes (indium tin oxide: ITO), which enables the monitoring of subtle changes in mass and viscosity in real time and capturing images through it due to its high transparency. On the other hand, the quartz crystal microbalance can evaluate cells without any damage. While the elasticity of cells and the changes in them can be measured directly, and this cannot be done through ordinary microscopes.

Current techniques for cytoskeletal analysis include microscopic observation, dead cell measurement (Lactate dehydrogenase : LDH, LDH Assay), live cell measurement, staining of live and dead cells separately, quartz crystal microbalance, and others. In this chapter, I will show these technology. Also, the aim and contents of this thesis will be described.

1.2 Cell evaluation methods

1.2.1 Dead cell measurement method (LDH assay)

The LDH assay is a method for examining enzyme activity caused by dead cells. LDH is an enzyme present in the cytoplasm that normally does not permeate the cell membrane, but in dead cells, LDH in the cytoplasm leaks out due to damage to the cell membrane. As shown in Figure 2-1, LDH catalyzes the dehydrogenation of lactate to produce pyruvate and NADH.

NAD (nicotinamide adenine dinucleotide) is used as a coenzyme to catalyze the dehydrogenation of lactic acid to produce pyruvic acid and NADH. The resulting NADH reduces WST (water soluble tetrazolium salt) (colorless) to WST formazan (orange) with an absorption of 490 nm via an electron mediator. The amount of formazan produced is proportional to the released LDH activity and is an indicator of the number of injured cells. The characteristics of this measurement method are said to be reliability, speed, and simple evaluation [6].

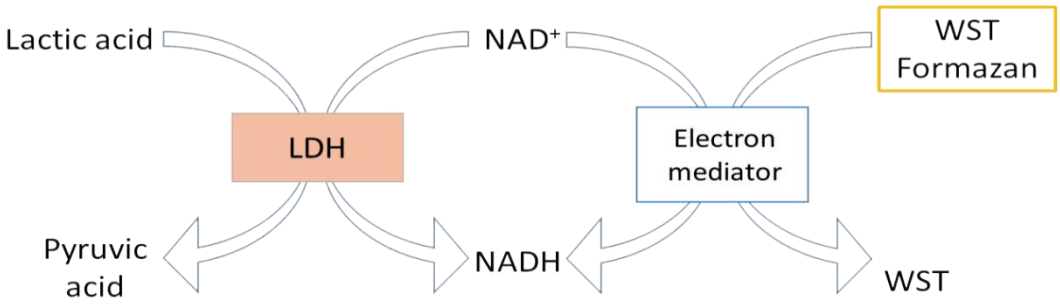

Figure 2-1. LDH assay principle.

1.2.2 Live cell measurement method

1.2.2.1 MTT assay

The MTT (3-(4,5-Dimethylthiazol-2-yl)-2,5-Diphenyltetrazolium Bromide) assay is a common measurement method for assessing the activity of antitumor compounds. The activity of mitochondrial dehydrogenase (particularly succinate dehydrogenase) causes the reduction of the MTT tetrazolium salt to formazan in the mitochondria of living cells. Since the amount of formazan produced correlates with the number of living cells, it is used as a method for measuring the number of living cells [7].

1.2.2.2 Cell Counting Kit-8 (CCK-8)

CCK-8 is a viable cell number measurement kit using a water-soluble tetrazolium salt (WST-8) as a coloring reagent. As shown in Figure 3-1, NADH produced by intracellular dehydrogenase reduces WST-8 to orange water-soluble formazan via 1-Methoxy PMS. When reduced, this reduced water-soluble formazan produces a maximum absorption wavelength near 460 nm. Such live cell measurement methods are mainly used for drug sensitivity evaluation [8,9].

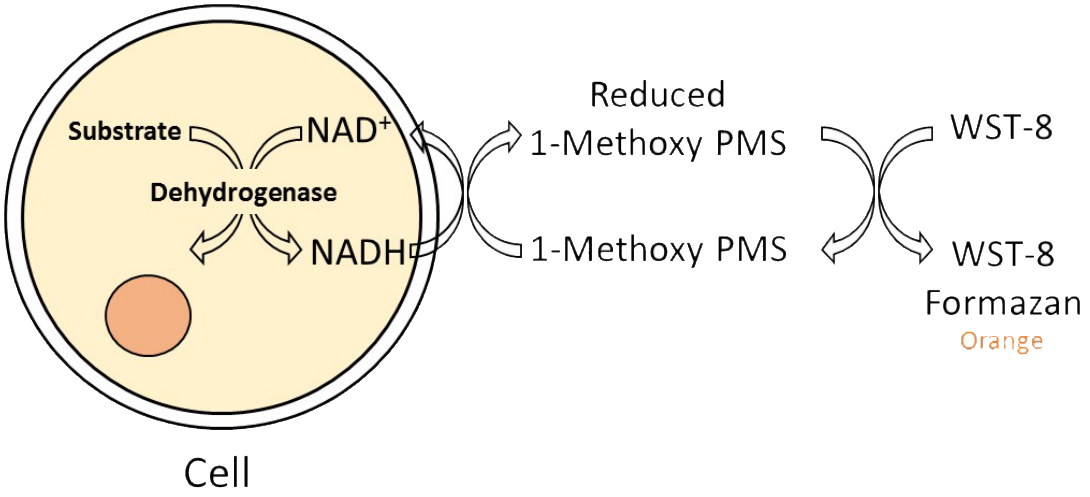

Figure 3-1. Principle of viable cell number measurement method.

1.2.3 Dyeing live cells and dead cells separately (fluorescence staining)

Cellstain ® **Double Staining Kit** [Cellstain Cell Double Staining Kit] is composed of Calcein-AM, this method is used to staining both live and dead cells. It contains a fluorescent dye to stain dead cells. Calcein-AM has the property of permeating the cell membrane to enhance the conversion of the four carboxyl groups of the fluorescent dye Calcein into acetoxymethyl (AM). When it penetrates the membrane of a living cell and enters the cell, it is hydrolyzed by intracellular esterase and releases strong yellow-greenish fluorescence. While PI enters dead cells and stains their DNA by intercalating the double helix structure of intracellular DNA, emitting a uniquely strong red fluorescence.

By applying this method, living cells can be stained yellow-greenish and dead cells can be stained red. This method enables observation of cells under a fluorescence microscope, in addition to flow cytometry [10, 11, 12].

1.2.4 Quartz crystal microbalance

(QCM) used as a sensor for various purposes (Figure 5-1). The frequency resonates changes by mass loading onto the surface of electrodes at nanogram level [13]. It has been used to evaluate physical properties of cells [14, 15, 16, 17, 18, 19, 20], as it can monitor mass change in real time and even quantitatively. This is an important advantage of QCM because the mass sensitivity enables it to be used as an accurate sensor. It has been used to evaluate changes in cultured cells in several previous studies, and it is classified as one of the accurate methods of evaluating cells. For this, QCM is used for monitoring the cells in this study.

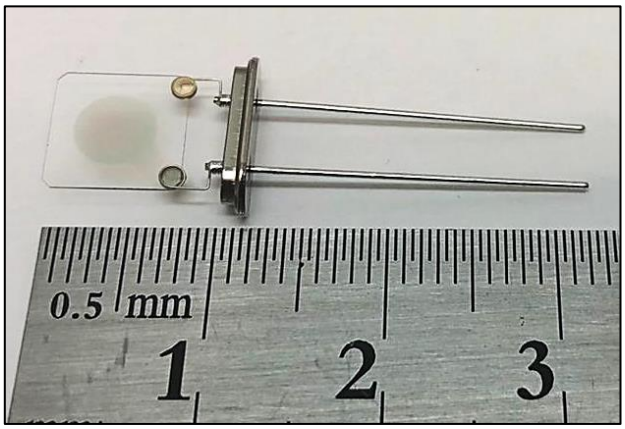

Figure 5-1. Quartz crystal microbalance.

When applying the other current techniques for cells analysis and monitor, the change state in cells is measured only after a period of time, and these techniques cannot show progress or status as more time has passed. Therefore, I made a system consisting of a quartz crystal microbalance and a micro CMOS camera simultaneously. It can be used to analyze the cell adhesion process with various ECMs. In addition, it can be used to study the effect of antitumor on cells that was not able to do before.

1.3 The aim of this thesis

A lot of research works used multiple methods to monitor cells, and some of them used quartz crystal microbalance in cellular measurements. Through this study, I studied the initial stage of the cellular attachment process using a quartz crystals microbalance. I also studied the resonance frequency change to determine its correlation with cell number. The cellular changes with the response curve of attachment process of were studied by mathematical modeling. The response of a cell attachment process in the presence antitumor reagents were also studied by calculating fitting curves of the model equations onto the experimental curves of the resonant frequency change. In addition, not only the measurement with quartz crystal microbalance, but also a microscopic observation was provided that was useful for simultaneously monitoring the change in cell morphology. The aim of this study is to revel the cell attachment process and response process of cell death by antitumor reagent.

In this thesis, a new quartz crystal microbalance system has been developed which is considered the first method in the world. This system supports the previous methods, but uses QCM measurement technology and a micro-CMOS camera simultaneously with a model for analysis. In addition, it works with easy and low cost applications and gives quick results without exposure to experiments on humans or animals. This system can help in studying and evaluating some drugs or toxins on cultured cells and conducting preliminary tests on them in simple and quick ways, and knowing their effectiveness before applying them directly to humans or animals. This system is mainly composed of quartz crystal microbalance and a micro CMOS camera. The system includes a Peltier device for precise and rapid temperature controlled, and can work inside a CO_2 incubator. With this system, extracellular matrixes can be investigated their effect on the attachment of cells cultured to quartz crystal microbalance surfaces with precise temperature control. Extracellular matrices (PLL, Collagen, PNIPAM) were used as structural support for cells to adhere and bind on quartz crystal microbalance surfaces. I monitored the changes in the cytoskeleton using quartz crystal microbalance and then analyzed them by the response curve of the attachment process by mathematical equations. In addition to the morphological monitoring accompanying these changes at real time, it is possible to assess the morphology and physical properties that reflect and to describe the state of the cell, such as the change in the cytoskeleton, the characteristics of the attachment of cells cultured to the surface of the quartz crystal microbalance, and the cell activity. In addition, the measurement system was applied on studying with antitumor drug to the effect of on cells. Also, I compared them with the mathematical curve of response to attachment process.

According to reflections of the state of cytoskeleton and activity as a result of exposure to such antitumor on the surfaces of the quartz crystal microbalance.

In order to describe these contents, the thesis is composed as follows. In Chapter 1, a motivation of the study, cell evaluation methods, and the aim of this thesis are described. In Chapter 2, the principle of the quartz crystal microbalance and its utility in measurements, biological assessments, and pharmacological responses are explained. In addition to explaining the curves of the model equations applied to experimental curves of the resonance frequency change, as well as the improvement and preparation of the quartz crystal microbalance for ITO electrodes and its use in extracellular matrixes (ECM) and drug toxicity evaluations. In Chapter 3, the development of the measuring device is explained. In Chapter 4, the cell matrix (ECM), the types that were used, and methods for assessing cell adhesion are described in relation to their use with cultured HepG2 cells. Finally, in Chapter 5, the results of monitoring HepG2 cells under the application of chemical stress factors are presented and their effect on cell activity is discussed via the curves of the mathematical equations applied and according to the changes in the cytoskeleton of the cultured cells, and the conclusions are stated.

Chapter 2: Quartz crystal microbalance

2.1 Background and Purpose of this section

Bioanalytical methods are used in several fields, one of the most important of these methods is measurement using QCM, which can be used in biofilm analysis and cultured cells analysis because of its ability to monitor mass and viscosity changes in real time. Since the fifties of the last century, Sauerbery revealed that quartz crystal microbalance has the ability to detect changes in mass through changes in resonance frequency [13], as it has the ability to detect very small changes in mass of about 1 nanogram due to its high sensitivity. Since his discovery, QCM has been used in the field of analytical chemistry, but its use was limited at that time, as it was believed that QCM could not oscillate in the liquid phase. In the 1980s, Nomura and Minemura were able to use it in the liquid phase [21,22]. The effect of the liquid viscosity on the QCM resonance frequency was also studied, in addition to clarifying the relationship of QCM resonance resistance to the liquid viscosity and density [23, 24]. The resonance resistance has also been used as a method to show the energy dissipation on QCM, in addition to its use in analyzing thin films viscosity [25, 26]. The plotting method of comparing resonance frequency versus the resonant resistance was considered a valuable method in analyzing the changes in QCM [27]. The damping factor was also used as a similar index of resonance resistance [28].

With the beginning of the 1990s, QCM began to be used in studies of cultured cells [29, 30]. The resonant frequency and resonance resistance of QCM has been used in many studies on cultured cells, through these studies the characteristics of QCM with cells have been studied to understand the initial attachment of cells [31-35]. Also studied the effects of cellular attachment in the ECM, such as effects of hydrophilicity and hydrophobicity [36-41]. Furthermore, QCM has been used to study the effects of applying chemical stressors and stimuli on cells [42-52], and cell cycle monitoring has also been reported [53,54].

The change in the resonance frequency was also studied to clarify its association with the number of cells, and the cellular correlation with the mathematical structure curve was also studied. Several studies have shown that frequency change did not show a linear relationship with cells number [29,31,34,43,55], while the logarithmic plots of the resonance frequency change and the resonant resistance showed a linear relationship with the number of cells [48]. As reported by Redepenning et al., the first-order attachment process curve of cells is fit to the initial frequency change [29], and Wuzhou et al, also stated that the response curves for cell

attachment process can be fit to the exponential curves [56].

To study the response of a cell cultured with QCM , it is important to understand its characteristics. When the surface of the QCM contacts with liquid or viscous materials, the horizontal surface vibrations of the QCM propagate to the materials that have contacted its surface, but the amplitude of the vibration decreases with increasing distance. The depth limit of propagation of vibrations is the depth of penetration, as the penetration depth limits the effect of mass on the QCM, it also limits the resonant frequency change. This effect has been reported in the previous reports to study cells cultured with QCM [35,51]. Therefore, it is necessary when analyzing the resonance frequency, considering the depth of penetration.

Several important studies of the responses of cells cultured without QCM have been performed. Ozawa et al. studied the simulation of cell death using a chemical kinetics model [57]. Also Montalenti et al. studied cells kinetics with cisplatin considering cell cycle delay [58]. A real-time electrical impedance detection method was used on cultured cells to monitor the cells' response to cisplatin, and the response curves for cisplatin injection were monitored for 40 h [59].

Through the use of QCM, I monitored the effect of ECM on the adhesion of cultured cells on the surface of a quartz crystal microbalance is monitored, in addition to monitoring cell morphology and its changes in a CO_2 incubator using a device that integrates a quartz crystal microbalance and a small microscope. One of the purposes of this thesis is to analyze cell adhesion response based on measurement data using quartz crystal microbalance, as well as the use of microscopy in real-time of measurement to obtain images of changes, and to comprehensively understand the response mechanism.

Also, the effect of antitumor drug on cultured cells is continuously monitored at the same time as cell shape observation in a CO_2 incubator using a device that integrates a quartz crystal microbalance and a small microscope. Among the purposes of this thesis are the analysis of cell response to drug and the occurrence of apoptosis based on measurement data using quartz crystal microbalance, as well as the use microscopy in real-time of measurement to obtain images of changes, and to comprehensively understand the response mechanism as well. The resonant frequency response is clarified by building response model equations and determining the parameters of the equations (Table 1, Table 3) which have been mentioned in this thesis.

In this chapter, I introduce overall quartz crystal microbalance, including a theory of a quartz crystal microbalance, the principle of quartz crystal microbalance, the equivalent circuit, the ITO electrodes, and the usefulness of quartz crystal microbalance used for the ECM and drug toxicity. In addition, I explain fitting curves of model equations to the experimental curves

of the resonant frequency change.

2.2 Principle of the quartz crystal microbalance

2.2.1 The basic of quartz crystal microbalance resonator

A QCM consists of a piece of crystal that has been cut with an AT type, and has metal electrodes on both sides. Since the quartz crystal contains 32 groups that are symmetrical across a trigonal system, It is cut according to the different angles into different pieces of quartz plates, as there are several types of quartz plates such as AT-, BT-, CT-, DT-, NT- and GT. These different types are referred to as the Euler group angles. These possess different properties of elastic, piezoelectric, and dielectric characteristics, which are the basic qualities of QCM. In this thesis, an AT-cut quartz crystal was used [60,61].

A quartz crystal microbalance is made by sputtering metal thin films on both sides of a quartz plate obtained by cutting a quartz crystal at an AT-cut (parallel to the X axis and at an angle of 35 degrees 15 minutes from the Z axis) to form electrodes on both sides. By applying a voltage to the electrodes, horizontal shear vibration called thickness slip vibration occurs. The image of the thickness slip vibration is shown in Figure 2-1.

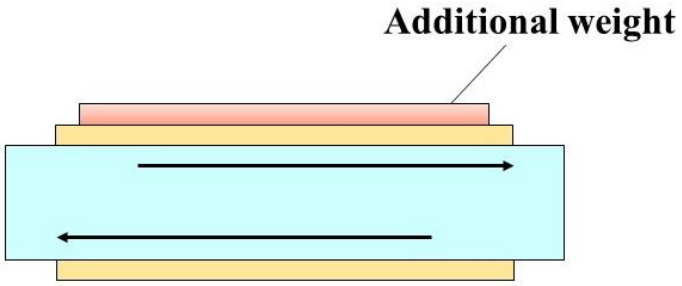

Figure 2-1. Image of thickness slip vibration.

2.2.2 The equivalent circuit of the QCR for physical sensing

In the case of the AT-cut QCR, the vertical electric field generates the shear strain. Therefore, the electrical resonance and the mechanical resonance of the shear oscillation of the QCR are coupled with each other. An AT-cut QCR is regarded to be electrically the same as the equivalent circuit depicted in Figure 2-2. Quantitatively, the left arm of the equivalent circuit represents the parasitic capacitance of the QCR, while the right arm represents the mechanical

oscillation of the QCR. Based on electromechanical analogy, L_1, C_1, and R_1 correspond to energy storage into kinetic energy (i.e., mass), energy storage into elastic energy (i.e., compliance), and energy dissipation (i.e., coefficient of viscous friction), respectively. When certain material, such as a film and/or viscous liquid, contacts with the QCR surface, the L_1, C_1, and R_1 change due to acoustic loading. For this reason, a QCR can be used as a chemical sensor for surface reaction.

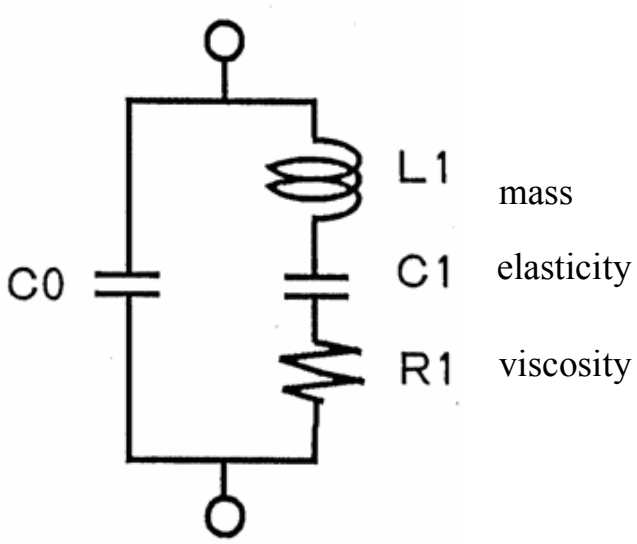

Figure 2-2. A schematic illustration of an AT-cut QCR. In this illustration, a standing wave of the fundamental mode is formed. The left arm of the equivalent circuit represents the parasitic capacitance of the QCR. The right arm represents the mechanical oscillation of the QCR.

When a substance adheres to the electrode portion, the resonance frequency changes (decreases) due to an increase in mass corresponding to the mass of the substance, so that it is used as a microbalance. The quartz crystal microbalance has become a tool for real-time measurements in terms of robustness, low cost, and ease of use [62]. It is also used for various purposes such as measurement of trace amounts of sublimated substances and measurement as an odor sensor.

The relationship between the amount of change in frequency and the mass of adherent substances is expressed by Sauerbrey's equation (1) below [13,63]. When the amount of adherent substances increases, the frequency decreases, and when the amount of adherent

substances decreases, the frequency decreases and then increases. In the crystal unit with a fundamental frequency of 9 MHz used in this thesis, a change of 1 Hz corresponds to a mass change of about 1 ng.

$$\Delta f = \frac{2f_0^2}{\sqrt{\mu_q \rho_q}} \frac{\Delta M}{A} \quad \cdots (1)$$

Δf is the frequency change amount, f_0 is the fundamental frequency, ΔM is the mass change amount, A is the electrode area, μ_q is the crystal shear elasticity, and ρ_q is the crystal density.

In the case of measuring physical properties and reactions, a liquid may be brought into contact with the crystal unit. At that time, the frequency is affected by changes in the viscosity η and density ρ of the liquid in contact with the crystal unit [23,24], This relationship is shown in equation (2).

$$\Delta f = -{f_0}^{3/2} \sqrt{\frac{\rho_l \eta_l}{\pi \mu_q \rho_q}} \quad \cdots (2)$$

Further, the resistance component (resonance resistance) in the electrically equivalent circuit of the crystal microbalance increases reflecting the loss of vibration energy on the surface of the crystal microbalance. Therefore, when the crystal unit is in contact with a viscous fluid or a viscoelastic body, the resonance resistance increases [25,26].

Figure 2-4 summarizes the above contents. Figure 2-4 schematically shows the changes in the resonance frequency and the resonance resistance with respect to the elapsed time. When either the mass or the viscosity decreases, the resonance frequency increases, and when either the mass or the viscosity increases, the resonance frequency decreases. Further, when the viscosity increases, the resonance resistance increases, and when the viscosity decreases, the resonance resistance decreases.

The plot of the resonance frequency and the resonance impedance is called the FR plot. Figure 2-5 shows the FR plot of resonance frequency and the resonance resistance with respect to the elapsed time. In the FR plot, the arrow on the top indicates an increase in viscosity because it changes both the resonance frequency and the resonance impedance, and the arrow on the bottom indicates an increase in mass because it only changes the resonant frequency. Therefore, the mass and viscosity changes can be evaluated by the resonance frequency and the value of the resonance resistance.

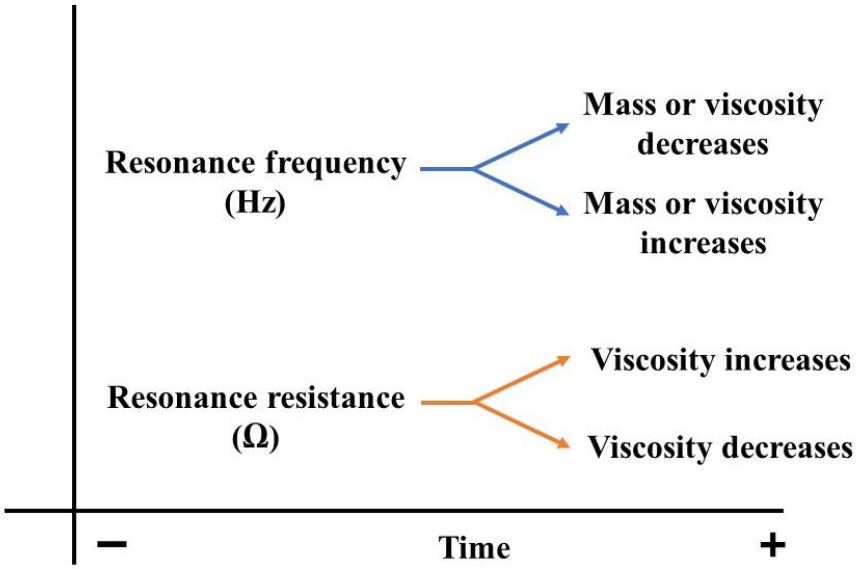

Figure 2-4. Changes in resonance frequency and resonance resistance with respect to elapsed time.

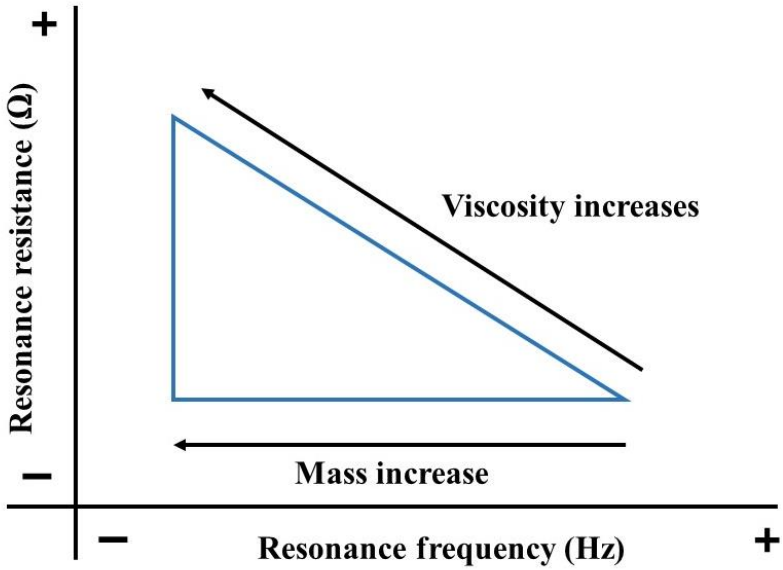

Figure 2-5. FR plot of resonance frequency and the resonance resistance with respect to the elapsed time.

2.2.3 Advanced QCM with ITO electrodes

The film-forming method used in this thesis is RF sputtering, in which an inert gas (mainly Ar) is introduced into a vacuum and a high-frequency voltage is applied between the target and the sample to ionize the inert gas atom. High speed causes gas ions to collide with the surface of the target. This is a technology that violently ejects particles (atoms/molecules) of the film-forming material that make up the target and vigorously adheres to and deposits them on the surface of the base material/substrate to form a thin film. The sputtering method is described in Appendix 1.

In the film formation of the quartz crystal microbalance, ITO (indium tin oxide) was used as the electrode. ITO electrodes have a thin thickness and high transmittance that allow clear images of cell morphological changes to be taken in real time for measurement. Also, it can monitor these changes by measuring changes in the resonance frequency and the resistance frequency of the electrodes as a result of the overall load on them. The transmittance of ITO electrodes is optimized to obtain high-resolution micrographs of morphological changes in real time for measurement. Table 1 summarizes the film-forming conditions performed this time, and Figure 2-6 shows the quartz crystal microbalance produced (in Appendix 2, there is a table showing the ITO electrode film formation, optimization, and setting conditions).

Table 1. ITO electrode film forming conditions.

Output	Ar flow rate	O_2 flow rate	ITO film formation time	Baking temperature
400 W	21.0	0.2	23 min	120°C

Figure 2-6. Quartz crystal microbalance manufactured.

2.3 Principle for cell evaluation

2.3.1 Principle of quartz crystal microbalance used for the ECM and cell adhesion evaluation

The cell adhesion response model in this thesis can be considered as shown in Figure 2-7. Consider the cell as a model of a spring and a dashpot, and consider that the force acts on the cell to adhere to the surface of the quartz crystal microbalance electrode. On the other hand, the quartz crystal microbalance measures the mass by vibrating together with the vicinity of the interface. Therefore, it is considered that the mass detected by the quartz crystal microbalance also increases because the volume near the interface increases due to cell adhesion.

In the model of Figure 2-7, when the force $\gamma\ (t)$ is a step function, the transfer function of cell deformation becomes the first-order delayed transfer function, and cell adhesion is represented by the first-order delayed response model equation (3). In such a first-order lag response, it is important to obtain the time constant because the shape of the response curve changes depending on the time constant.

$$y\ (t)=y_0\left(1-e^{-\frac{t}{T_1}}\right) \quad \ldots \quad (3)$$

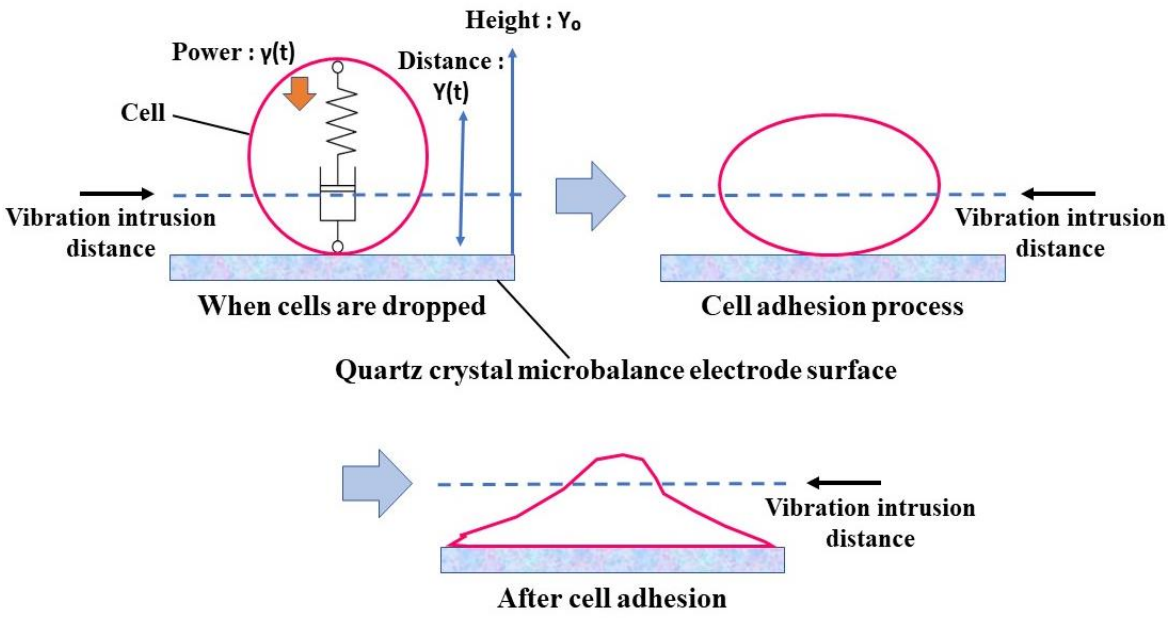

Figure 2-7. Schematic diagram of cell adhesion response model.

Moreover, I have proposed the process of cell−cell interaction with the cell mass model as shown in Figure 2-3, it expresses the cell-cell increase the height of cells that effects to mass increase is not linear to the cell numbers. For example, by the model in the case of three cells, there are three states of "three separate", "one separate and one pair", and "triple one". Using this simple model, the mass index of the three cells (M_3) can be written using the basic probability of cell−cell interaction p as

$$M_3=(3(1-2p)^2+2\cdot 2p(1-2p)+(2p)^2)m_v + 3m_s \qquad (4)$$

where $\alpha(=m_v/m_s)$ is the mass ratio of the variable mass and the steady mass for a cell.

The index of the mass is the sum of the steady mass m_s and the variable mass m_v. The equation of the mass index can be extended to cell number n using the binomial coefficient and rewritten as

$$\begin{aligned} M_n &= \sum_{k=0}^{n-1}\{(n-k)_{n-1}C_k(1-(n-1)p)^{n-k-1}((n-1)p)^k\}m_v + n\cdot m_s \\ &= (n-p\cdot(n-1)^2)m_v + n\cdot m_s \\ &= m_s\cdot((n-p\cdot(n-1)^2)\alpha + n) \end{aligned} \qquad (5)$$

where M_n is the mass index, n is the number of cells, p is the probability of cell proximity, and α is the addition ratio of m_v/m_s.

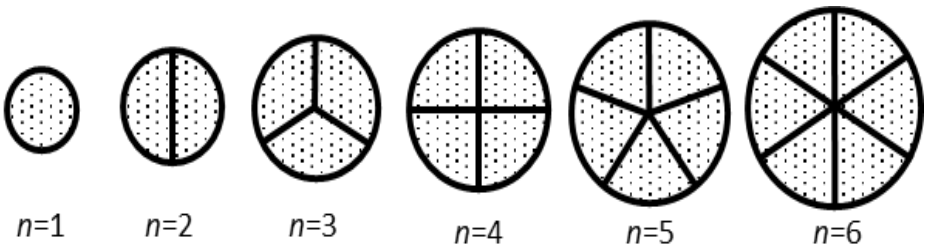

Figure 2-3. A schematic illustration of the proposed model of cell−cell interaction with the cell mass model.

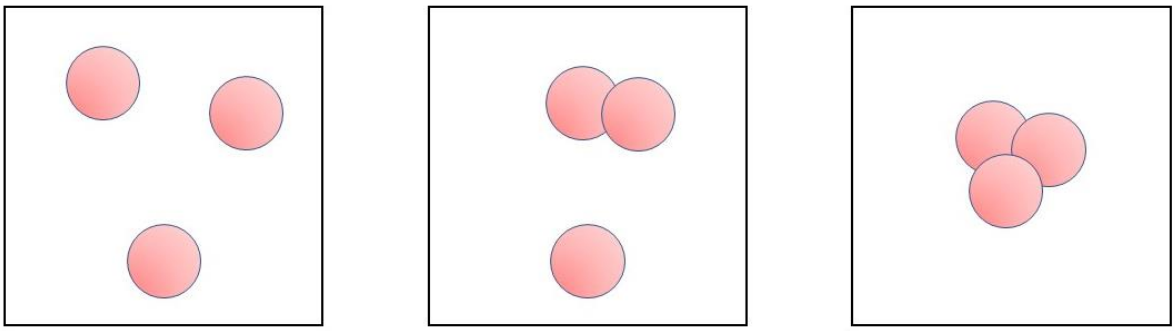

Figure 2-9. Cell-cell interaction model for the cells.

The cell adhesion response analysis formula, which is a model formula for the resonance frequency response, is constructed with cell-cell interaction effect (formula (5)), the formula for the mass factor (formula (6)), and the formula for the change in the number of cells due to cell growth (formula (7)). Then, the equation of the resonance frequency change (Equation (8)) can be obtained. Furthermore, considering that there is a constant mass effect (m0) at the moment when the cell settles on the surface of the crystal unit, the formula of the mass factor is rewritten as formula (9). In addition, when cells settle, they do not reach the surface of the crystal microbalance at exactly the same time. Therefore, if this distribution is considered as a lognormal distribution, equation (8) can include by equation (10), and the frequency change can be expressed by equation (11). The mass factor equation shows a first-order lag response. In the cell number formula, T_2 hours represents the time when the cell number doubles. Finally, the resonance frequency change is obtained by multiplying the mass factor by the number of cells.

Mass factor formula:

$$m_c(t) = m_c \cdot y(t) = m_c \cdot y(\infty)\left(1 - e^{-\frac{k}{D}t}\right) = m_c \cdot y(\infty)\left(1 - e^{-\frac{t}{T_2}}\right) \quad \ldots \ (6)$$

Here, m_c is the basic mass factor (equivalent to one cell), $y\ (t)$ is the unit distance of cell deformation (y (0) = 1).

Cell number formula: $n(t) = n_0 2^{\frac{t}{T_2}}$ ... (7)

Here, $n\ (t)$ is the number of cells, n_0 is the number of initial cells, and T_2 is the cell doubling time.

Resonance frequency change equation:

$$\Delta F = -K_{\mathrm{m}} M_n = -K_{\mathrm{m}} m_{\mathrm{c}} \cdot ((n - p \cdot (n-1)^2)\alpha + n)$$
$$= -K \cdot ((n - p \cdot (n-1)^2)\alpha + n) \quad (8)$$

Here, ΔF is the resonance frequency change, K_m is the mass frequency change coefficient, m_{c} is the mass factor of a cell, and K ($=K_{\mathrm{m}} m_{\mathrm{c}}$) is the basic frequency change factor for a single cell. Using equation 8, the resonant frequency change can be calculated from the cell density by applying the probability p, mass ratio α and cell number in a unit area n.

Formula of initial adhesion mass factor:

$$m_c(t) = m_c \frac{m_0 + K_y \cdot y(t)}{m_0 + K_y \cdot y(\infty)} = m_c \frac{m_0 + K_y \cdot y(t)(1 - e^{-\frac{t}{T_2}})}{m_0 + K_y \cdot y(\infty)} = m_c \frac{\beta + (1 - e^{-\frac{t}{T_2}})}{\beta + 1} \quad (t \geq 0) \quad \ldots \quad (9)$$

Here, m_c is the basic mass coefficient, m_0 is the initial attached mass, K_y is the mass conversion factor from the displacement, and $\beta = \frac{m_c(0)}{m_c(\infty)}$ is the initial attached mass ratio.

Formula of initial adhesion mass factor:

$$m_c(t) = m_c \frac{\beta + (1 - e^{-\frac{t}{T_2}})}{\beta + 1} \cdot \mathrm{CDF.LN}(t. t_m. t_s) \quad \ldots \quad (10)$$

Resonance frequency change equation:

$$\Delta F(t) = -K_{\mathrm{m}} \left\{ (n(t) - p \cdot (n(t) - 1)^2)\alpha + n(t) \right\} \cdot \frac{\beta + \left(1 - e^{-\frac{t}{T_2}}\right)}{\beta + 1} \cdot \mathrm{CDF.LN}(t. t_m. t_s) \quad \ldots \quad (11)$$

Here, the cumulative lognormal distribution function is CDF.LN (t is the elapsed time after cell addition, t_m is the initial adhesion mean time, and t_s is the standard deviation).

2.3.2 Principle of quartz crystal microbalance used for drug toxicity evaluation

Optical methods such as microscopic observation, MTT colorimetry, and flow cytometry (FCM) are generally used for drug toxicity evaluation performed in vitro. However, they are not usable to simultaneous, multi-step operation and real-time and continuous monitoring. Several methods are used to optically assess drug toxicity. In recent years, magnetic elasticity sensors, electrochemical impedance spectroscopy, and quartz crystal microbalance techniques have been used [64]. Quartz crystal microbalance was used to monitor cell dynamics, through it, the adhesion of cultured cells was monitored as mentioned in section (1-2) [65,66]. In addition to monitoring the process of apoptosis caused by drug toxicity [67,68]. Previous studies have shown that the use of the QCM method is useful in the process of observing the surface attachment and morphological changes, whether normal or cancerous cells.

As a drug response model in this thesis, it is considered that the drug response is performed by the process shown in Figure 2-10. The shape of the cells after seeding the cells adheres like an amoeba, but the adhesive area gradually decreases due to the antitumor drug, and the shape of the cells also becomes round. In addition, the cells gradually contract as the process progresses.

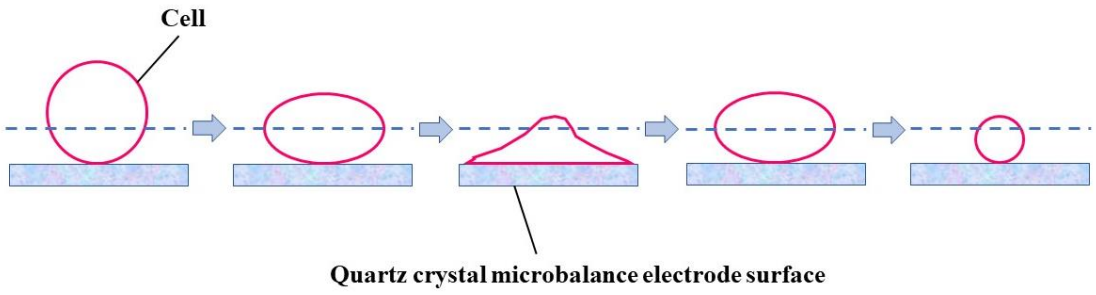

Figure 2-10. Schematic diagram of changes in cell shape due to drug response.

In the process of cell shape change by antitumor drug, cells change after a certain period of time, but it is considered that the change time varies. Therefore, I considered a model that disperses according to a lognormal distribution centered on the mean response time, integrates

this lognormal distribution, and considers two cumulative lognormal distribution functions to act on the drug response. One is the process in which the adhesive area is reduced by the antitumor drug and the cells are rounded, and the other is the process in which the cells are contracted by the antitumor drug. For the process of cell contraction, the reverse cumulative lognormal distribution was considered as a response model. Graphs of the lognormal distribution density function and the cumulative lognormal distribution function are shown in Figures 2-11 and 2-12.

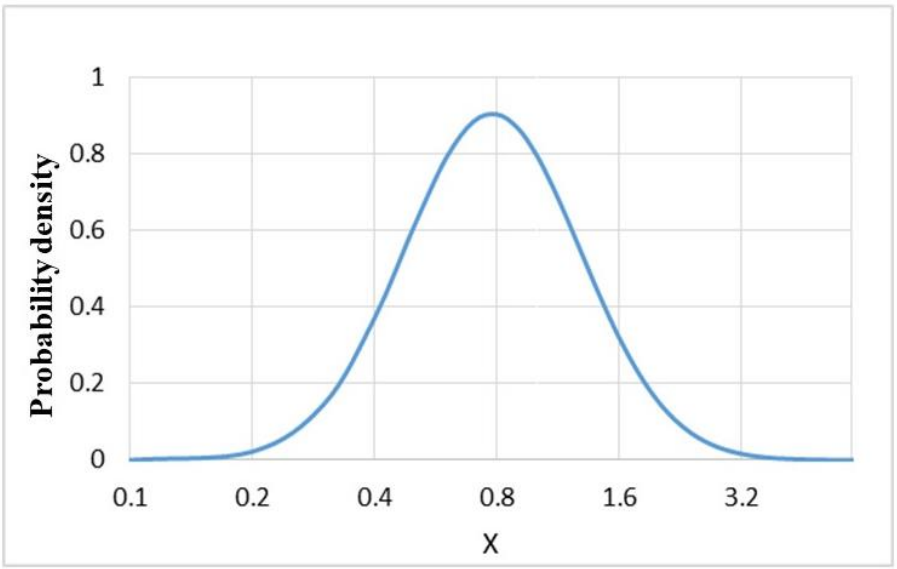

Figure 2-11. Lognormal distribution density function ($\mu = ln(\bar{x}) = 0, \sigma_{ln(\bar{x})} = 0.5$)

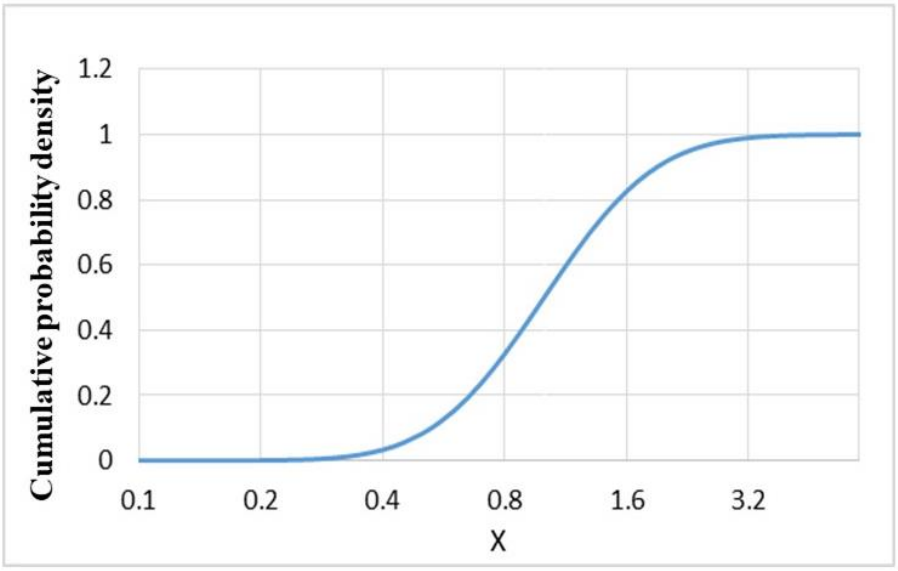

Figure 2-12. Cumulative lognormal distribution function ($\boldsymbol{\mu = ln(\bar{x}) = 0, \sigma_{ln(\bar{x})} = 0.5}$)

The drug response analysis formula is shown in Equation (12). When the cell viability 1-γ after dropping the antitumor drug is low, the amount of change is large, and when the cell viability is high, the amount of change is small. By drug response analysis, it is possible to determine the time during which cells are rounded by an antitumor drug, the time during which cells are involved in contraction, and the survival rate. This makes it possible to compare parameters according to the type and concentration of antitumor drug. Using the typical values of parameters, I simulated the response curves for several survival rates in Figure 2-13.

$$\Delta F(t) = -K_{\mathrm{m}}\{(n(t) - p \cdot (n(t) - 1)^2)\alpha + n(t))\} \cdot \frac{\beta + \left(1 - e^{-\frac{t}{T_2}}\right)}{\beta + 1} \cdot \mathrm{CDF.LN}(t.t_m.t_s)$$
$$\cdot \left(1 - \gamma\left(k_1 \mathrm{CDF.LN}(t - t_{inj}.m_1.s_1) - k_2 \mathrm{CDF.LN}\left(t - t_{inj}.m_2.s_2\right)\right)\right) \quad \ldots \quad (12)$$

Here, γ is the dead cell rate, t is the elapsed time from cell addition, t_{inj} is the antitumor drug addition time, m is the mean response time, s is the standard deviation, k_1 is the mass coefficient of the first response, and k_2 is the mass coefficient of the second response.

Figure 2-13(a) shows typical resonant frequency responses when the target seeded cell density is 320, 630 and 1300 cells/mm^2. The amount of change in the resonant frequency increases with increasing cell density. The important point here is that the shapes of the response curves differ slightly according to different cell densities. While Figure 2-13(b) shows the change in resonance frequency versus density of seeded cells based on the results obtained from Figure 2-13(a). Here the results indicate that the resonance frequency changes 6, 12, 18, 24 h after seeding cells. The relationship between the amount of change in resonance frequency and the amount of seeded cells density is not linear, the relationship is affected by the incubation time, and this reason is likely related to the progression of the interaction between cells. As already shown, the cell-cell interaction makes the resonance frequency change smaller. Using the equation 11, Figure 2-13(c) shows the curve fitting results for the plot of resonance frequency change versus cell density when the time has passed 6, 12, 18 and 24 h from seeding the cell. And figure 2-13(d) shows the estimated modeling curves for figure 2-13 (a).

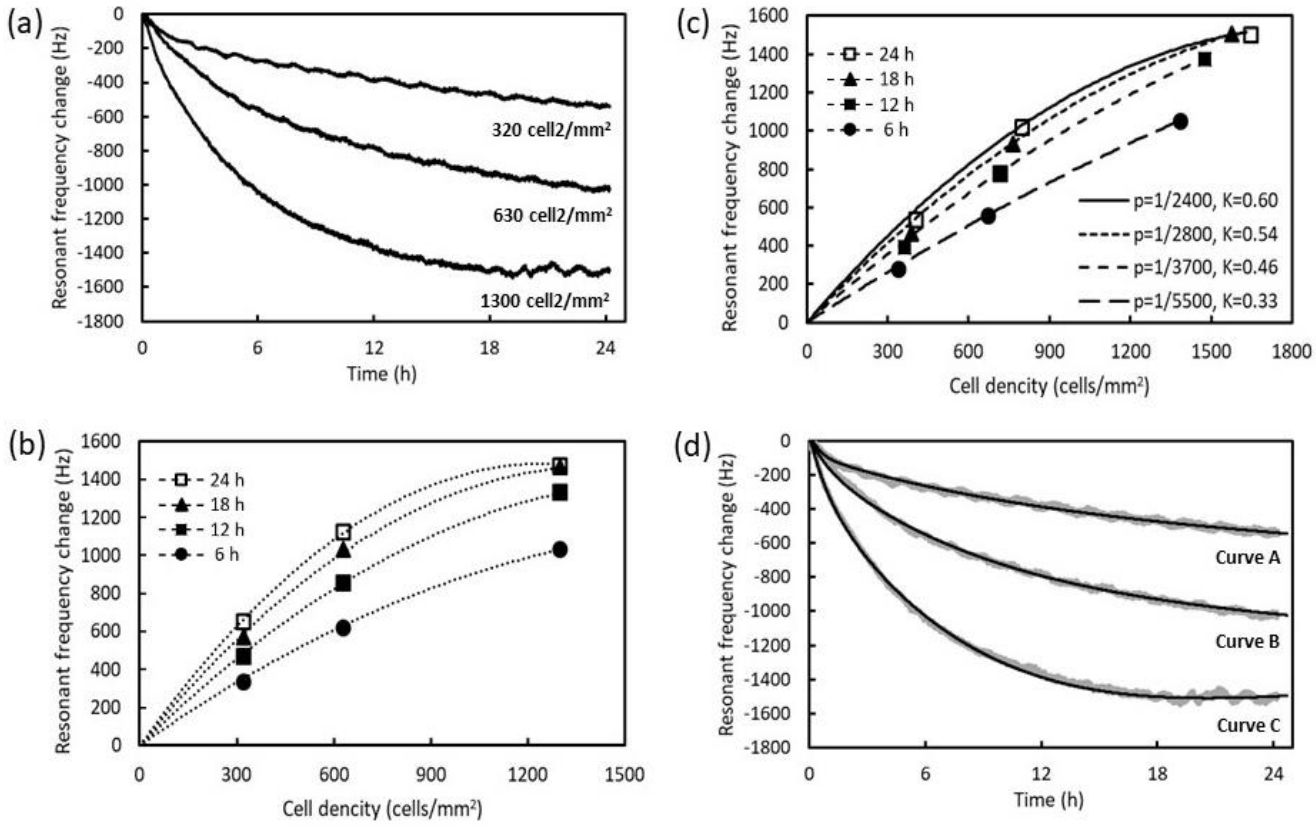

Figure 2-13. The figures indicate the resonant frequency response as a result of cell seeding. (a) The result of typical resonant frequency responses is shown when cells were seeded at three densities of 320, 630 and 1300 cells/mm2. (b) Shown the plot obtained depending on the change of resonance frequency as a result of changing the density of seeded cells which was obtained from Figure 2(a). (C) Shown the curve fitting results for the plot of resonance frequency change versus cell density when the time has passed 6, 12, 18 and 24 h from seeding the cell. (d) Shown the estimated modeling curves for part (a).

Chapter 3: Development and improvement of the experimental devices

3.1 Introduction

In this thesis, a new crystal microbalance system has been developed to monitor the activity of cultured cells, and to observe the attachment of cells to quartz crystal surfaces by ECM, as well as its response to chemical stimulation. The system mainly consists of a quartz crystal microbalance and a CMOS camera that has been linked to a Peltier device for precise control and for rapid temperature change (Figure 3-1), where the system can work inside a CO_2 incubator.

With the system, cell matrix is investigated on the effect of cell attachment quartz crystal microbalance surfaces with precise temperature control. PLL, Collagen, and PNIPAM cell matrices were used as structural support for cells to adhered and bind to quartz crystal microbalance surfaces. I monitored the changes in the cytoskeleton by means of the quartz crystal microbalance, as it will come in Section 4, and then analyzed them by the response curve of the attachment process by mathematical equation. In addition to the morphological monitoring accompanying these changes at real time, it is possible to assess the morphology and physical properties that reflect and describe the state of the cell, such as the change in the cytoskeleton, the characteristics of the attachment of cells cultured to the surface of the quartz crystal microbalance, and the cell activity.

In addition, I cultured cells in the presence of antitumor drug to investigate their effect on cells, especially programmed cell death, and to compare them with the mathematical curve of the response to the attachment process through the plasters on the surfaces of the quartz crystal microbalance as it will come in Chapter 4.

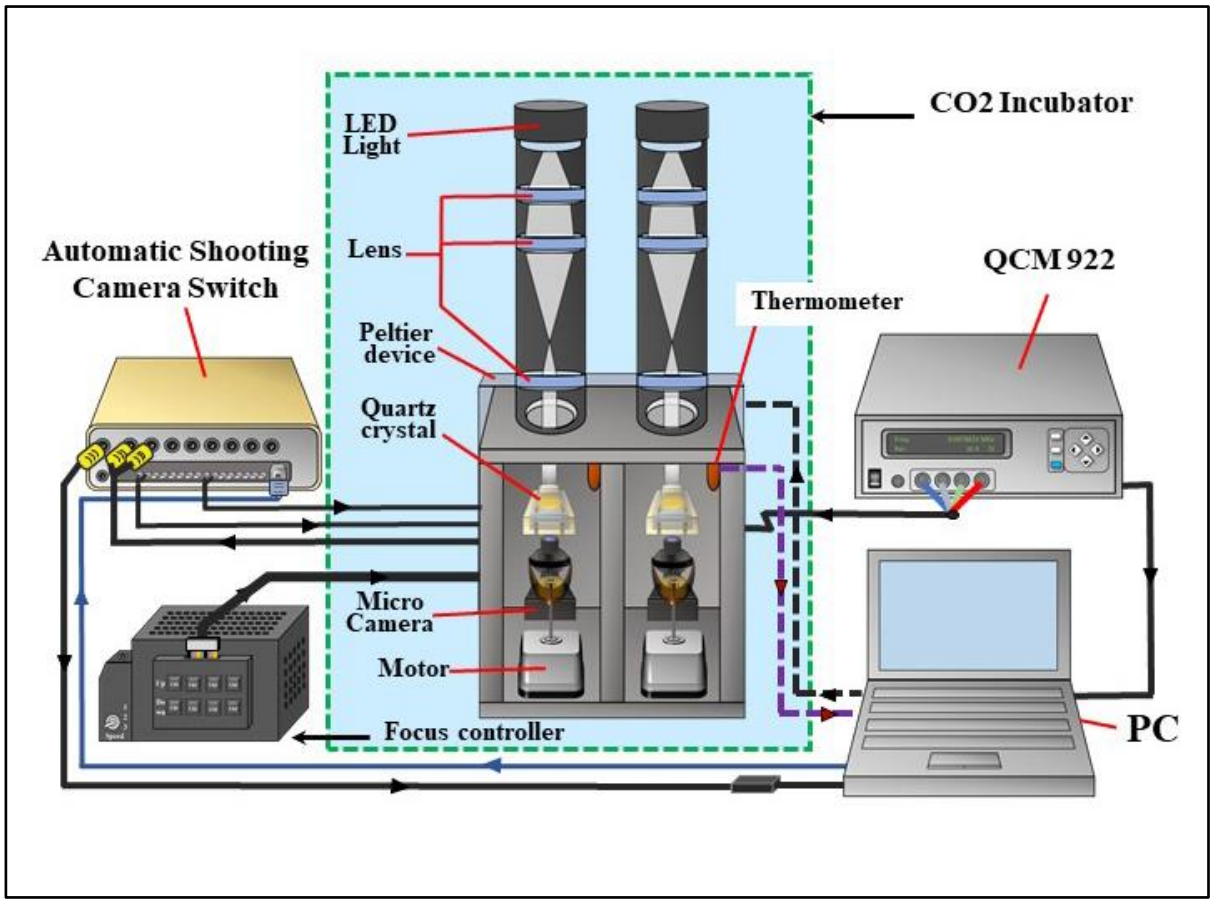

Figure 3-1. Schematic diagram of device configuration shows the aluminum block is divided into two compartments for two measuring units. Each measuring unit comprises a quartz crystal chamber, a small microscope with a CMOS camera at the lower side, and a focus-controlling motor that has been linked to a Peltier device.

3.2 Purpose

The device has been rebuilt for the purpose of obtaining more repeatable data by building an improved measurement system. In particular, to improve imaging and measurement performance, the system was modified by adding a lighting unit, an imaging unit, electronic focus control of the lens and a unit specialized in thermoregulation. Figure 3-2 refers to the Peltier device, while Figure 3-3 shows the equipment after improvement of experimental device.

Figure 3-2. Peltier device.

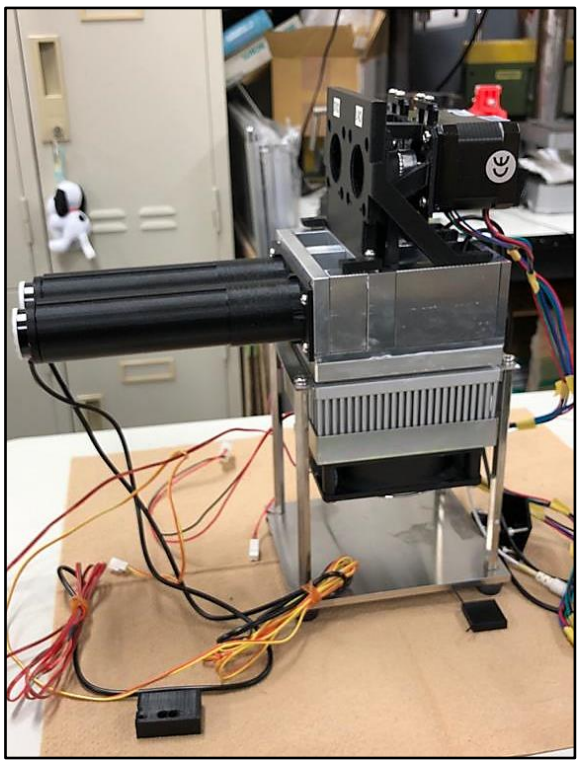

Figure 3-3. Experimental device after improvement.

3.3 Composition of the experiment device

Figure 3-1 shows the schematic illustration of the experimental device. The experimental device consists of aluminum walls, they are divided into two rooms so that each a measurement unit is inserted into each room. In addition, some rules and fasteners made by 3D printer have been used to help connect the components of the device (Figure 3-4). Each room features a small CMOS-camera (LOSKA IP68, Japan) from the lower side and a camera-focus control motor, as well as white LED light from the top. The CMOS-camera size was 168 x 89 x 46 mm. The white LED light was 24 mm diameter, connected with tube was diameter of 24 mm x 130 mm height, Inside the tube there are 3 lenses to collect and highlight the chamber of agriculture, it was obtain from a handy microscope (TV-120M, Kenko, Japan). All rooms are connected to the Peltier-stimulating device (Ampere UTC-1000A, Japan) size was100 mm x 100 mm to rapid control temperature change during measurement (Figure 3-7). A thermal sensor was also connected to one of the rooms to regulate the temperature of the Peltier-stimulating device. The measurement units consist of the QCM inserted between the agriculture chamber and the sensor holder, and a pair of O rings has been placed to prevent the infiltration of the culture medium and cells. The dimensions of the agriculture chamber and sensor holder were width 30 mm × depth 20 mm × height 16 mm. The base resonance frequency of the quartz crystal was 9.2 MHz (AT cut, 7.9 mm × 7.9 mm). ITO was sputtered onto both surfaces of the quartz crystal as electrodes, the diameter and thickness of the electrodes were 5 mm and 250 nm, respectively. Which enable to observe the cells on the electrode surface in transmission mode with the micro-CMOS camera. Thermostat was connected to each room to monitor room temperature during measurement. To switch camera power and light power, the camera/light switching unit is built on the Arduino Nano board with a CD4051 to switch the camera signal via 8-channel mono analog multiplexer for CMOS. In addition, another CD4051 chip and TLP597A photodetector to switch camera power and LED lighting power. To control focus, the focus controller unit is built on the Arduino Mega 2540 board and Ramps 1.4 board, the stepper motors are controlled by tact switches. The change in resonance frequency and resonance resistance was measured by QCA922 (Seiko EG&G, Japan). The experimental device was autoclaved and put into the incubator (32 ◦C, 5% CO_2, humid). The measuring units were inserted inside each room after autoclaved and the white LED light was turned on the agriculture chamber during observation with a micro-CMOS camera. The QCA922, Peltier-stimulating, micro-CMOS, and the white LED were remote-controlled with a PC. All QCM measurements were performed at 37 °C, except for thermal sweep experiments.

3.4 Development and improvement of the measuring devices

3.4.1 Development of thermoregulation portion measurement and operation check

For developing the thermoregulation unit, I constructed a representative model from a group of pieces made by the 3D printer as in Figure 3-4 and simulated it on the ground as in Figure 3-5. After that, the block of the Peltier device was replaced with aluminum parts as shown in Figures 3-6, 3-7, and 3-8. Then all the components were joined together to form an experiment device and the observation unit was encapsulated by polystyrene boards to maintain the temperature (Figures 3-9 and 3-10).

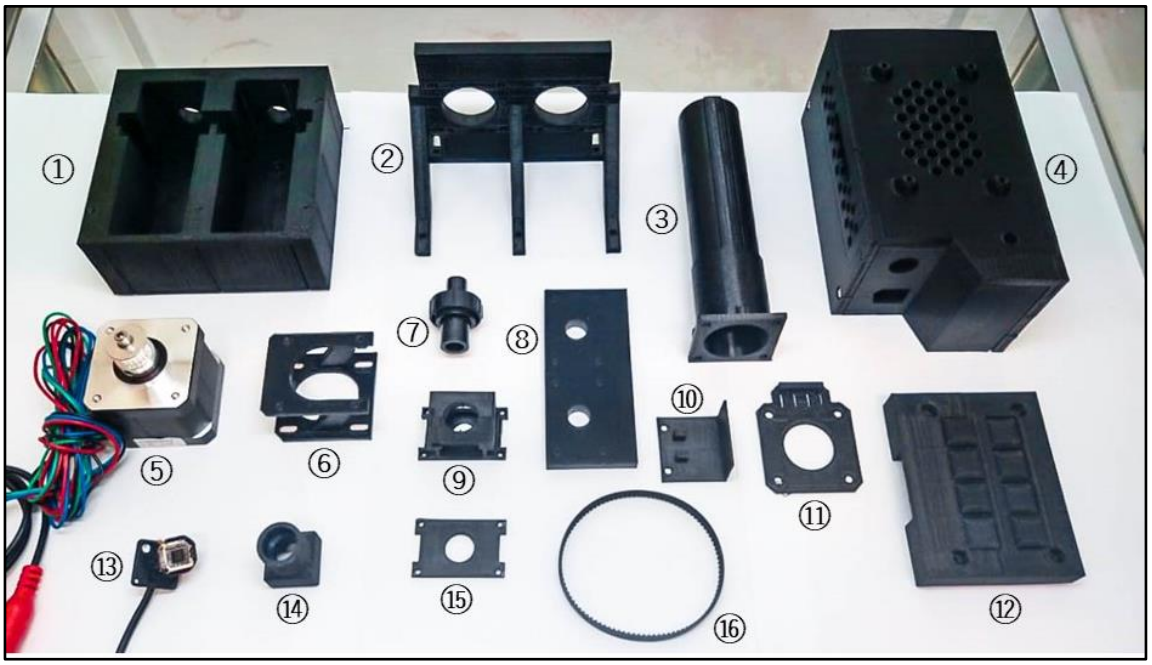

Figure 3-4. Improved parts of experimental equipment

The parts: ① Camera block 1pc, ② Camera stand 1pc, ③ Light tube 2pcs, ④ System box 1pc, ⑤ Motor 2pcs, ⑥ Motor seat 2pcs, ⑦ Lens of camera 2pcs, ⑧ Camera sheet 1pc, ⑨ Camera lens seat 2pcs, ⑩ Measurement cell sheet 2pcs, ⑪ Camera sheet space 2pcs, ⑫ Button system 1pc, ⑬ CMOS camera 2pcs, ⑭ Camera body 2pcs, ⑮ Camera lens sheet space 2pcs, ⑯ Motor belt 2pcs.

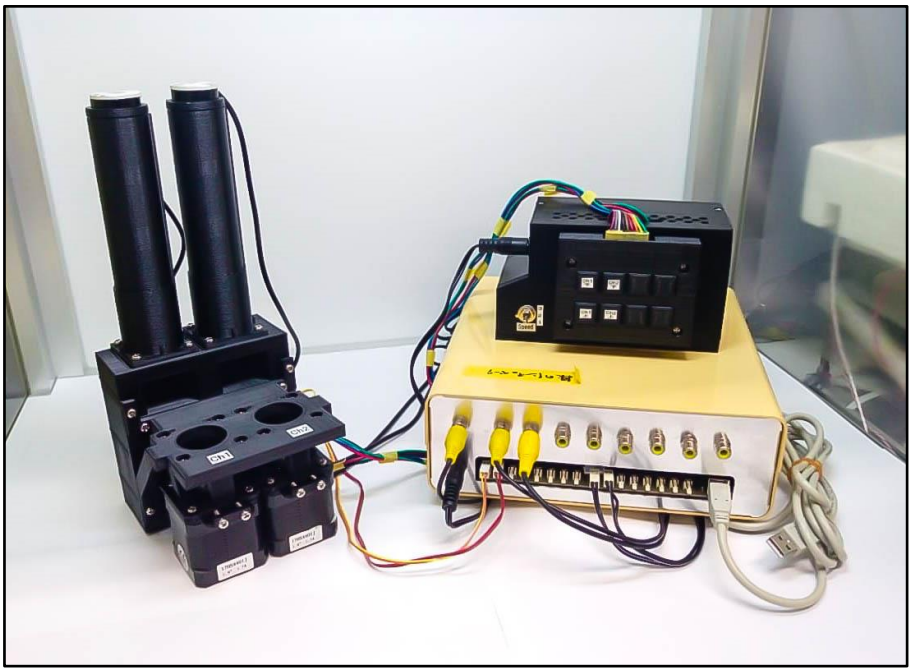

Figure 3-5. Simulation model.

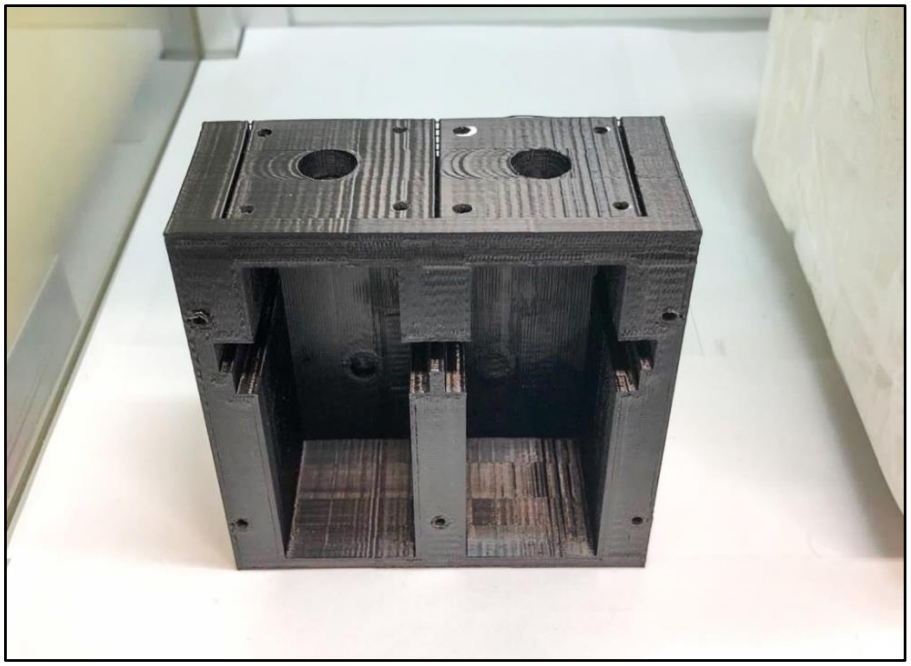

Figure 3-6. 3D printer block.

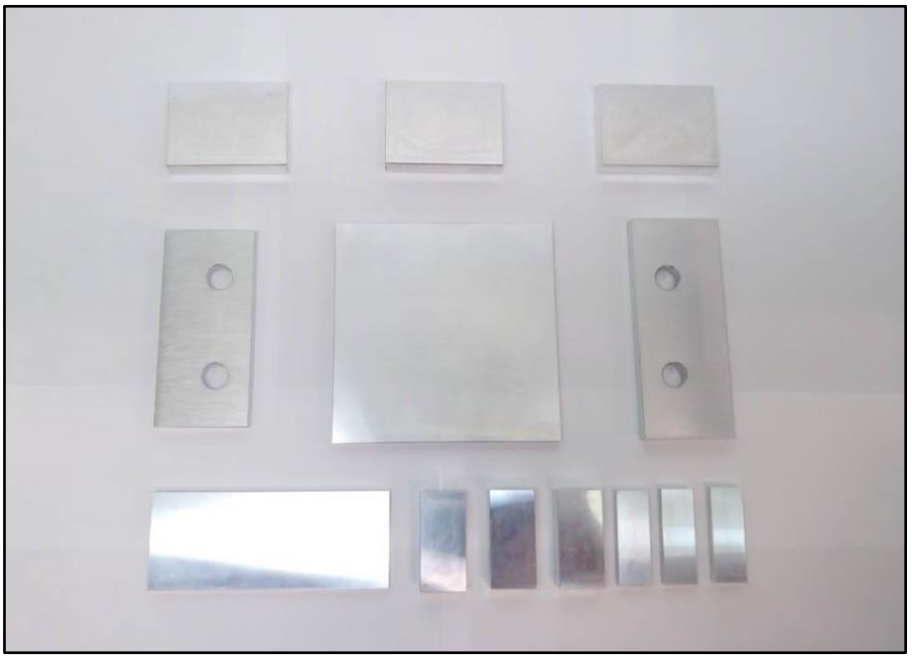

Figure 3-7. Aluminum block parts.

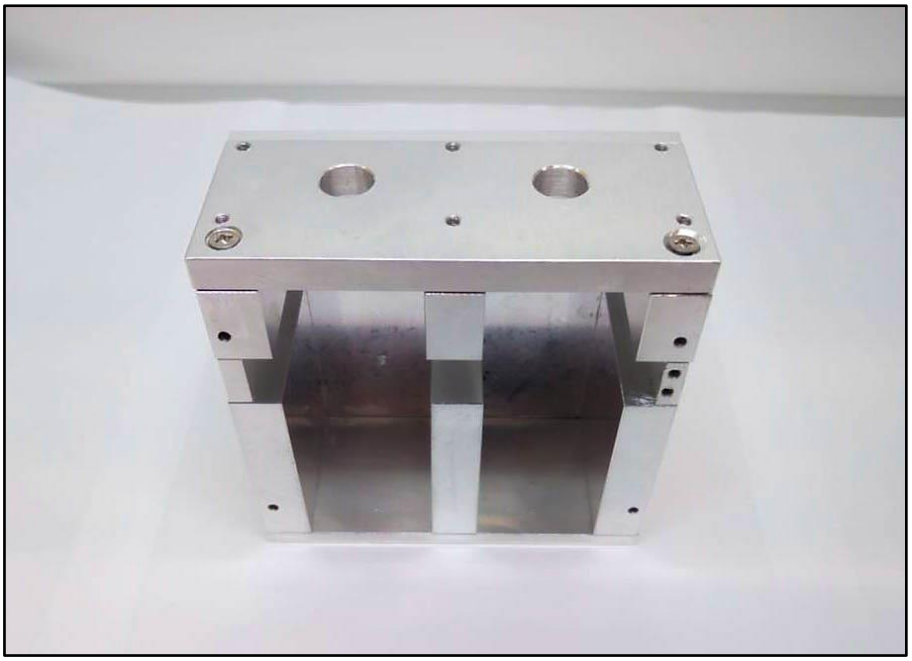

Figure 3-8. Aluminum block.

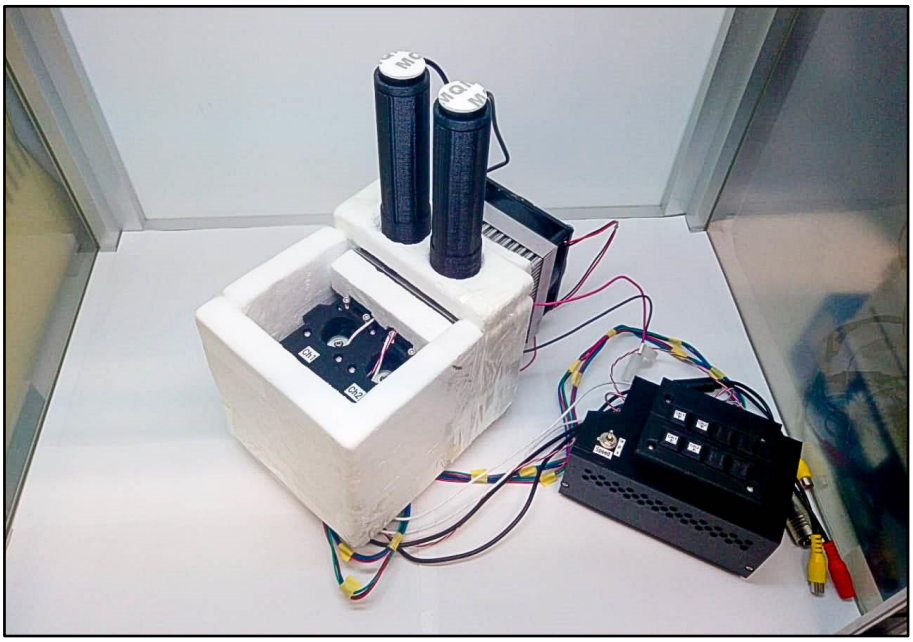

Figure 3-9. Experiment device after encapsulated by styrene boards when the cover is opened.

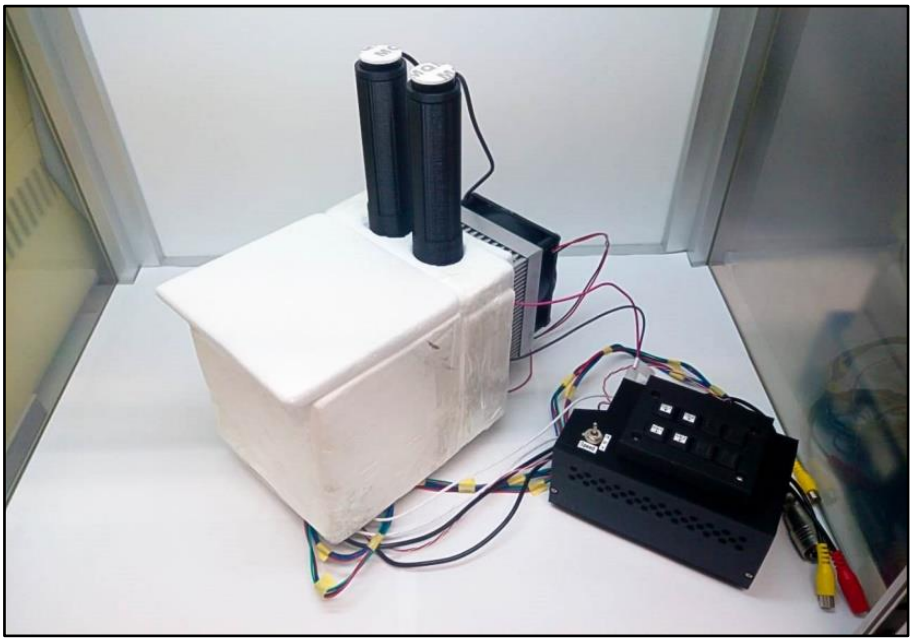

Figure 3-10. Experiment device after encapsulated by styrene boards when the cover is closed.

3.4.1.1 Experimental instruments/reagents

The experimental equipment and reagents used in this experiment are shown below:

- Heat-melting 3D printer
- Camera block 1pc
- CMOS camera 2pcs
- Camera stand 1pc
- Camera sheet space 2pcs
- Camera body 2pcs
- Camera sheet 1pc
- White LED light 2pcs
- Light tube 2pcs
- Lens of light tube 6pcs
- Motor 2pcs
- Motor seat 2pcs
- Motor belt 2pcs
- Lens of camera 2x
- Camera lens seat 2pcs
- Camera lens sheet space 2pcs
- Measurement cell sheet 2pcs
- System box 1pc
- Button system 1pc
- Camera focus adjuster – Arduino Mega 2540 board
- Automatic shooting camera switching machine

- Driver
- Silicon rubber sheet (thickness 0.5 mm)
- CO_2 incubator (temperature 34 ºC)
- Crystal oscillator chemical measurement system QCA922
- Computer
- Measurement software

(WinQCM (Seiko EG & G), USB Video Selector & Capture (laboratory original))

- Sterilized water
- ABS resin

3.4.1.2 Experiments

After all components were joined together to form an experimental device and the observation unit was encapsulated by polystyrene boards, the experiment device after being sterilized was placed in the CO_2 incubator at a temperature of 34 °C, in order to be able to electronically control the temperature of the experiment device through the computer. I set the device to a temperature of 37 °C, while automatically lowering temperature to 17 °C after a specified period of time. Several experimental measurements were performed to ensure the precise thermal unit control of both channels.

3.4.2 Development and optimization of device camera and LED light parts and operation check

For the development and optimization of device camera and LED light parts, I added a CMOS camera with dimensions: 25 x 23 x 23 mm. This camera is equipped with a high-quality sensor with a resolution of 720 x 480 pixels, and it has super powerful night vision which enables us to obtain more accurate and clear images while observing the morphological changes occurring in the cells. It was connected to a focus controller and a focus-controlling motor was installed. In addition, the lighting module was attached to the top of the camera, made of high brightness white LED light and equipped with three lenses at different focus concentrations, to be able to accurately highlight towards the measurement sample parallel to

the CMOS camera. In the measuring device, a correction for the normal optical path was performed with the aim of increasing the contrast in the invisible cellular components of the captured samples. Although it is not structured to have a special phase difference, the phase difference is naturally applied due to the deviation of the optical system. Incident and scattered light in different paths is restricted and converted into straight and regular light by making holes in the inner tubes that carrying the lenses. The light passing through those holes is collected by the collecting lenses until the light reaches the measuring cell in a straight line with increasing contrast in the samples captured during imaging. This unit was connected to the experiment device and then connected to the computer by camera/light switch unit (Figure 3-1).

3.4.2.1 Experimental instruments/reagents

The experimental equipment and reagents used in this experiment are shown below:

Experimental instruments

- Developed experiment device (Figure 3-1)
- CO_2 incubator (temperature 34 ºC)
- Crystal oscillator chemical measurement system QCA922
- Peltier device controller
- Camera/light switch
- Focus controller
- Computer
- Measurement software

(WinQCM (Seiko EG & G), USB Video Selector & Capture (laboratory original)) and thermal control and adjustment program using Visual Basic

- Centrifuge
- Gas burner
- Hemocytometer (counting chamber)
- Culture petri dish (100 mm/Collagen-Coated Dish)

- 15 mL tube centrifuge tube
- Electric pipettor
- Pipette (2 mL, 5 mL)
- Micropipette (20 μL, 200 μL, 1000 μL)
- Chip (20 μL, 200 μL, 1000 μL)
- Driver
- Quartz crystal microbalance
- Measurement cell (attached: O-ring, screw)

Reagents

- DMEM medium (with FBS, Antibiotic-Antimycotic, Amphotericin B solution)
- Trypsin
- PBS
- HepG2 cells
- Polylysine
- Ethanol 76.9–81.4%
- Sterilized water

3.4.2.2 Checking the device

After the quartz crystal microbalance was collected in the measurement cell with a pair of O rings (Figures 3-11 and 3-12), the cells were seeded into the measurement cell on the QCM and deposited inside the experiment device. Several experiments were performed on samples of cultured cells in a CO_2 incubator by the device developed (Figure 3-13), and many high-resolution images of the changes occurring in cells over time were obtained.

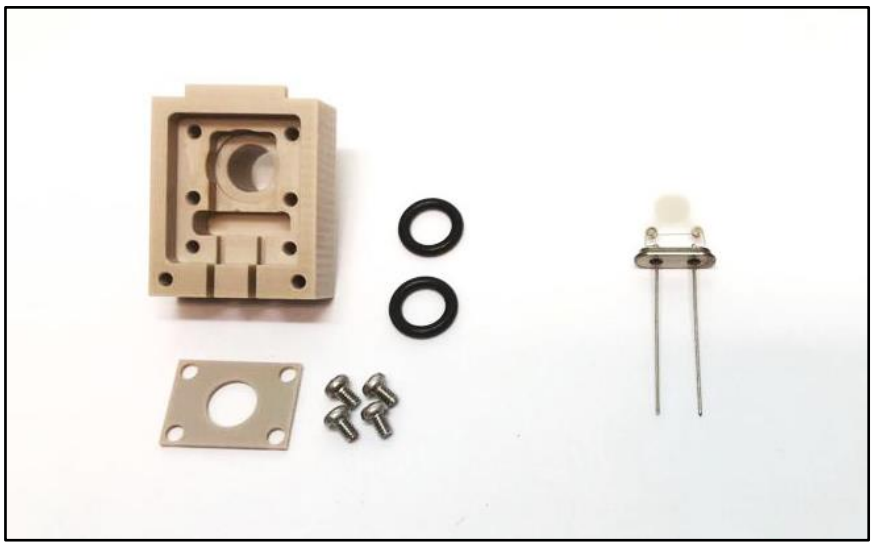

Figure 3-11. The components of the measurement cell, a quartz crystal microbalance, a pair of O-rings, and four screws.

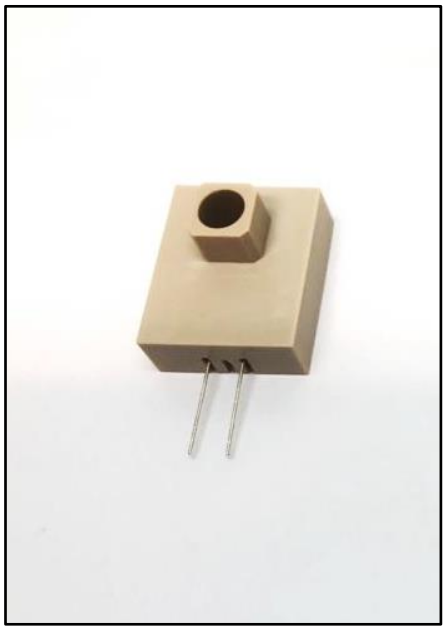

Figure 3-12. The quartz crystal microbalance after setting in the measurement cell.

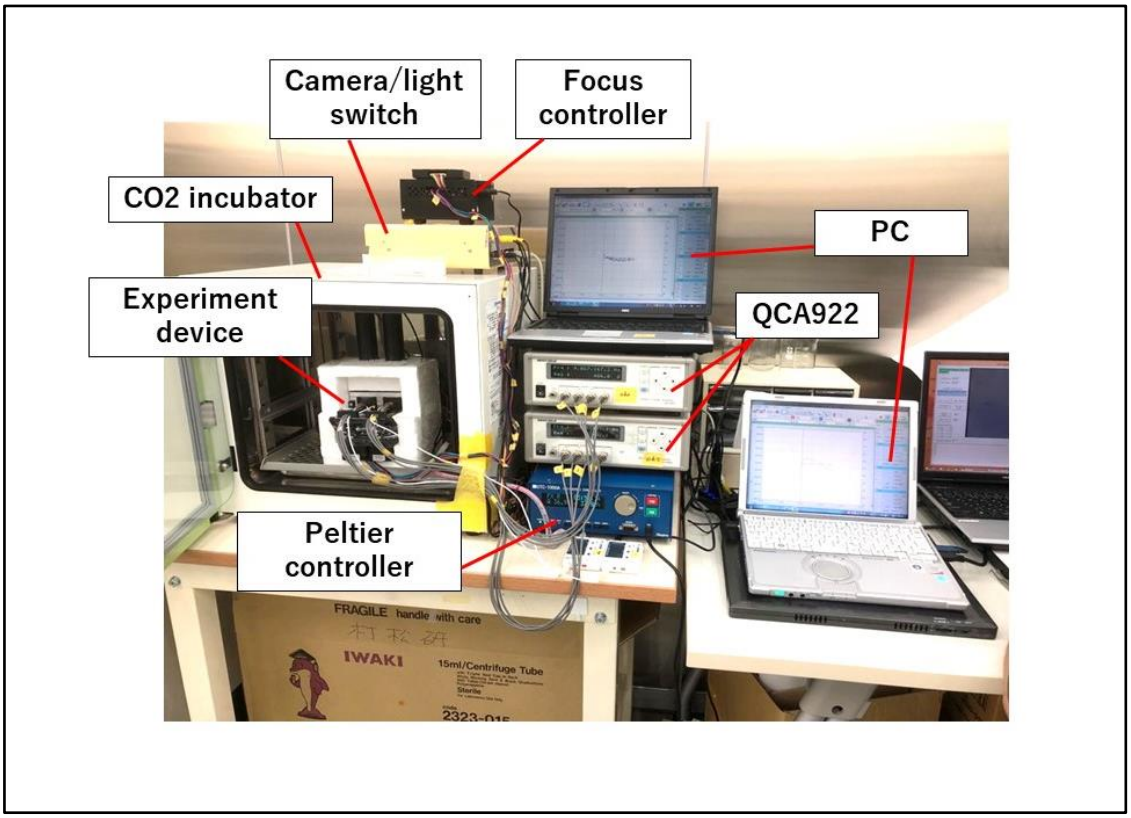

Figure 3-13. The measuring device inside the CO_2 incubator.

3.5 Results and discussion

3.5.1 Thermoregulatoin portion measurement operation check

Several experimental measurements were made to ensure the precise control of the thermal unit of the experiment device. For example, as in Figure 3-14, I set the device to 37 °C for 14 h, with the temperature automatically lowered in 30 min to 17 °C. The results of the measurements showed the success of the experiment device in the ability to control its temperature accurately. The measurement started at 37 °C and continued to be stable for 14 h, after which it began to lower the temperature within 30 minutes to reach a stable temperature of 17 °C within 24 h of the measurement. The results of these experiments constitute the possibility of using the measuring device in conjunction with the real measurements of this thesis with precise temperature control required.

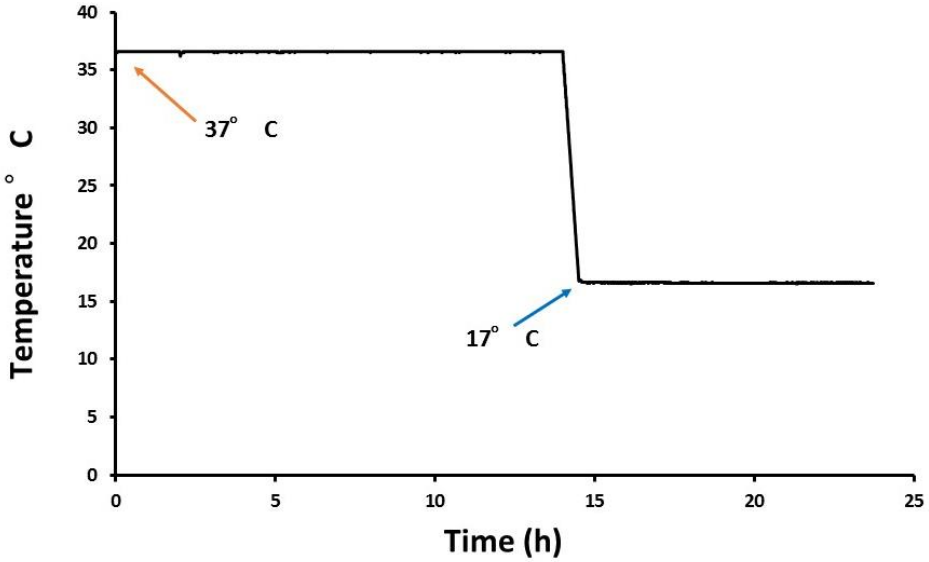

Figure 3-14. The measurement result of channels started at 37 °C and continued to stabilize for 14 h, after which it started automatically lowering the temperature within 30 min to reach a constant temperature of 17 °C within 24 h of the measurement.

3.5.2 Device camera and LED light parts operation check

In Figure 3-15 (a, b), the results of these experiments constitute the possibility of using the experiment device after developing the monitoring and lighting units in conjunction with the thermal control unit in the real measurements of this thesis and thus obtaining the best results as a result of the development of this device.

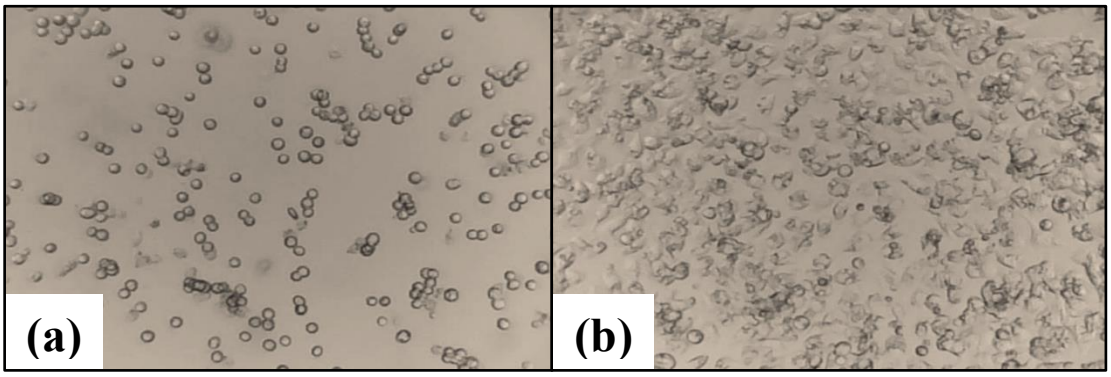

Figure 3-15. (a,b) The results of culturing cells on the glass surface with collagen coating and ITO electrodes: (a) status of cells 10 min after seeding, (b) status of cells after 24 h from seeding the cells.

Chapter 4: Assessment of cell adhesion using cultured cells and ECM

4.1 Introduction

Cell adhesion is essential in connection and regulation between cell tissues. Cell adhesive molecules (integrins) allow cells to connection with each other and with structures in the ECM. Mechanical interactions between cell and ECM can influence cell behavior, function, and control. They are important in developing methods for measuring and studying cell adhesion properties.

The ECM is considered as a smart compound, due to its varied nature and composition. It can help control many cell functions and deliver therapies. In addition, it regulates the dynamic behavior of the cell, thus helping to understand its complex dynamic movements through its diffusion in space by attaching it to the matrix surface by integrins present in the cell surface.

When culturing HepG2 cells on a quartz crystal microbalance, the crystal surface must be treated with the cell adhesion factor. However, if the cell adhesion factor is too thick, it will buffer the sliding vibration of the crystal unit, which may affect accurate measurement. Therefore, the binding properties of cells cultured on the surfaces are studying using ECM.

Collagen and Poly-L-lysine (PLL) have been used in many researches as an ECM [33, 19, 47, 69, 70, 71]. In addition, the Poly(N-isopropylacrylamide) (PNIPAM) film has been used in cell sheet technology research as an ECM as well [72, 73].

Collagen exerts a biological effect on cultured cells as an ECM. It affects cell growth, differentiation, and proliferation, as it has the ability to form a basement membrane. When cells are cultured in a Petri dish on collagen, the cells are considered prevented from increasing in size due to flattening and stretching, and the cells are allowed to maintain their original shape and size. Thus the traditional collagen coating method may inhibit QCM vibration due to the thickness of the cell adhesion layer, so the surface should be coated with a thinner layer of collagen.

When the glass is coated with PLL, the adhesion is improved by changing the charges on the surface. Furthermore, when a PLL layer is coated on the glass surface, the glass surface is positively charged, and cells or tissues containing a negative charge are interconnected by electrostatic bonding. PLL is a kind of basic amino acid, which is a polymer of lysine that has an amino group (positive charge) in the side chain, and the amino group of PLL is electrostatically linked to an OH group on the surface of the glass. Adhesion between cells or tissues and the PLL is electrically coupled by the negative charge on the cell surface and the

positive charge on the PLL. That is, the glass and cells are attached adhesively via PLL. Since the negative charge on the cell surface is used as an adhesion base, it is believed that adhesion of PLL is primarily carried out using adhesion molecules on the microvilli, without integrin-based adhesion.

Cell sheet technology is useful for transplanting cultured cells into a patient's damaged tissue, they help recover tissue functions. To be able to obtain cell sheets, some conditions are required while using thermoresponsive polymer PNIPAM. Whereas, PNIPAM is hydrophobic at temperatures above the lower critical solution temperature (32 °C) and hydrophilic at temperatures below those; therefore, the affinity of PNIPAM to cells increases at temperatures above 32 °C and decreases when it decreases. Thus the sheet of cells can be removed without disrupting the shape of the sheet.

Therefore, studying the interactions of cells with the ECM and the structural changes accompanying those interactions and their attaches to surfaces, it is important in order to understand cell morphology.

4.2 Purpose

To understand cell morphology is important to know how the cell interacts with the ECM and attaches to surfaces. For this reason, I have studied different types of ECM that will contribute to cell attachment on ITO surfaces. The aim in this section is study these different types of ECM and analyzing the interaction between the cultured cells and the surface previously the experiment with QCM to check ECM preparation and cell response. For this, I monitor the potential for the cell binding and analyze the binding process for PLL, collagen, and PNIPAM on a quartz crystal microbalance as well as the cell alteration in PNIPAM films under a controlled temperature.

4.3 Development of the ECM

4.3.1 Experimental instruments/reagents

The experimental equipment and reagents used in this experiment are shown below:

Experimental instruments

・ CO_2 incubator (temperature 37 ℃, CO_2 concentration 5%) "When placed the developed experiment device inside the CO_2 incubator, the temperature is lowered to 34 ℃; In order to control the temperature of the experiment device at the desired

temperature by the computer"

・Microscope

・ Camera

・ Computer

・ Camera software (DigiCamControl)

・ Developed experiment device (Figure 3-1)

・ Crystal oscillator chemical measurement system QCA922

・ Peltier device controller

・ Camera/light switch

・ Focus controller

・ Computer

・ Measurement software

(WinQCM (Seiko EG & G), USB Video Selector & Capture (laboratory original)) and thermal control & adjustment program using Visual Basic

・ Centrifuge

・ Gas burner

・ Hemocytometer (counting chamber)

・ Culture petri dish (100 mm/Collagen-Coated Dish)

・ Tissue culture test plate 12 wells

・ Round slide glass (22 mm/with ITO electrodes & without)

・ 15 mL tube centrifuge tube

・ Electric pipettor

・ Pipette (2 mL, 5 mL)

・ Micropipette (20 μL, 200 μL, 1000 μL)

- Chip (20 μL, 200 μL, 1000 μL)
- Quartz crystal microbalance (ITO electrodes)
- Measurement cell (attached: O-ring, screw)

Reagents

- DMEM medium (with FBS, Antibiotic-Antimycotic, Amphotericin B solution)
- Trypsin
- PBS
- HepG2 cells
- Poly-L-lysine (PLL)
- Collagen
- Poly(N-isopropylacrylamide) (PNIPAM)
- Ethanol 76.9–81.4%
- Acetone 99.8%
- Sterilized water

4.3.2 Experiments

4.3.2.1 Experiments on the slides glass

After rinsing the round glass slides with sterile water and acetone, 5 glass slides were deposited in the wells of a tissue culture test plate (3 slides with ITO electrodes, 2 slides without). In the first time, 1 of the slices with ITO electrode was coated with PLL. In addition to using the 2 slides without ITO electrodes, 1 slice was also coated with PLL and the other was not coated. After that, the culture medium had 1 mL/well added, and the wells were placed in a CO_2 incubator for one hour. After a full hour, the cells were seeded at 3 x 10^3 cells/well and waited for 10 minutes for the cells to settle on the surface, after which the images were taken through the microscope by camera. After a full day, all samples were confirmed, and the images were taken again and results were drawn. After confirming the cells adhesion to the

ITO surfaces coated with PLL, the same method was applied to the remaining slides with ITO electrodes, so that 1 slice was coated with collagen and the other slice coated with PNIPAM. Then the results were compared, to confirm the effectiveness of using these types of ECM to adhesion cultured cells on ITO surfaces.

4.3.2.1.1 Surface modification of the slides glass

4.3.2.1.1.1 Poly-L-lysine coating

PLL is a polypeptide of lysin –[NH–CH($C_4H_8NH_2$)-CO]n– that is widely used as an ECM. The PLL (0.01%, Sigma-Aldrich, USA) was used as an ECM to contribute to the adhesion of cells to the ITO. After 2h measurement by an empty chamber, 60µl of the PLL solution that was diluted 10 times with the filtered sterilization water was dropped onto the electrode surface. The PLL film was deposited in 1h at 37 ◦C. After careful rinsing with PBS, 200µl of the culture medium was filled the measurement chamber.

4.3.2.1.1.2 Collagen coating

Collagen is a triple helix peptide consisting of glycine, proline, 4-hydroxyproline alanine, lysine, and 5-hydroxylysine residues. Lysine residues and 5-hydroxylysine residue –[NH–CH(CH_2–CH_2–CH(OH)–CH_2–NH_2)-CO]– possess amino groups. The Collagen - A 2 mg mL^{-1} Atelocollagen solution - (DME-02, KOKEN, Japan) was used as an another ECM to contribute to the adhesion of cells to the ITO. After 2h measurement by an empty chamber, 60µl of the Collagen solution that was diluted 5 times with 1 mmol L^{-1} hydrochloric acid solution was also dropped onto the electrode surface. The Collagen film was deposited in 30 min at 37 °C. After careful rinsing with PBS, 200µl of the culture medium was filled the measurement chamber.

4.3.2.1.1.3 Preparation of temperature-responsive polymer

The Triethoxysilane-terminated PNIPAM (Mn: 5000; Sigma-Aldrich, USA) was used as an another ECM also to contribute to the adhesion of cells to the ITO. To prepare the PNIPAM films, the ITO surface was thoroughly washed with methanol for 10 min, then heated at 150 °C for 30 min. The surface was then further treated with a solution of 5% triethoxysilane terminated with PNIPAM in methanol for 10 min and treated at 150 °C for 60 min. After which it was rinsed with distilled water and deposited again at 150 °C for 30 min.

4.3.2.1.1.4 Cell culture

With regard to observing the change in the shape and physical properties of cells, the human hepatoma cell line HepG2 was used in the experiments. I used DMEM (Sigma, USA) as culture media additionally supplemented with 1% (v/v) antibiotic–antimycotic (Gibco, Germany) and 10% (v/v) fetal bovine serum (Gibco, USA). The cells were cultured into a 10 cm diameter petri dish in a humidified 5% CO_2 air atmosphere at 37 °C inside a CO_2 incubator. In order to obtain and seed the cells for the culturing chamber, the cells were detached from a Petri dish by rinsing three times with phosphate-buffered saline (PBS without divalent cations) and treated with trypsin/EDTA for 6 min at 37 °C in the CO_2 incubator, then culture medium was added and the cell solution was centrifuged for 4 min with 1500rpm. The pellets were then resuspended in culture medium, then the cell suspension of 0.63 x 10^{-3} [cell/ml] was transferred to the culture chamber.

4.3.2.2 Experiments on the quartz crystal microbalance

Before the measurement, the measurement cell for the crystal unit was assembled. Figure 3-12 shows a photograph of the measurement cell parts and quartz crystal microbalance, and Figure 3-13 shows the procedure after they are collected in the measurement cell. An experiment to measure the effect of cell concentration was done [74]. The target cell concentration in this experiment was 0.63 × 10^3 cells/chamber. Experiments to measure and evaluate the adhesion of cells grown on a quartz crystal microbalance surface with ECM were performed by the following procedures, and then the results of HepG2 cell response were described.

The quartz crystal microbalance was integrated into the measuring cell and washed with sterile water. The measuring cell was connected to the experiment device by QCA multiplier in the incubator, the measuring program “WinQCM” was started, and the measuring cell was allowed to stand about 1 to 2 h until the resonant frequency and resonant resistance became stable. After resonant frequency and resonant resistance became stabled, when measured with ECM, the ECM coated on QCM surface according to the measurement objective. When measured with collagen film, 100 μL of collagen solution was added and when measured with PLL film, 60 μL of PLL (100 μL/mL) was added dropwise to the measurement cell for surface treatment on the crystal unit substrate. When measurement with PNIPAM film, the measurement was paused and the quartz crystal was removed from the measurement cell, after which the quartz crystal was washed with methanol for 10 minutes and heated at 150 °C for 30

min, after which its surface was treated with PNIPAM – triethoxysilane 5% – in methanol for 10 min. After heating the crystal at 150 °C for 60 min, its surface was rinsed with distilled water. The crystal was then heated again at 150 °C for 30 min. After the PNIPAM film was formed, the quartz crystal was returned to the measuring cell. After 1 hour of adding ECM, the ECM was removed with 100 μL of added PBS and gently removed to wash the surface of the quartz crystal microbalance, and then 200 μL of medium was added dropwise, and the mixture was allowed to stand for 2 h. After culturing the HepG2 cells, the cells were seeded into the measurement cell at the target concentration. In a cell reduction monitoring experiment, the temperature was lowered from 37 °C to 20 °C for half an hour, after which the temperature was raised to 37 °C. After 10 minutes of seeding the cells into the measuring cell, the "USB Video Selector & Capture" turned on, and then CMOS camera focus was set, after which cells were imaged at 30 min intervals. The measurement was completed approximately 72 h after seeding the cell. For details of measurement procedures, please refer to Appendix 3.

4.3.3 Response analysis setting items

Table 1 shows the setting items for cell adhesion response analysis. In the cell adhesion response analysis, Excel VBA is used based on the measurement data to obtain the values of these items so that the coefficient of determination of the measurement curve and the model curve is maximized by fitting curves of model equations to the experimental curves of the resonant frequency change as mentioned in Section 2.3.

Table 1. Setting items for cell adhesion response analysis.

Setting items	Details
Time constant 1 T_1 (h)	Time to reach 63% of cell adhesion process
Doubling time 2 T_2 (h)	Time for cells to double
Number of cells n_0	Number of dropped cells
Basic mass coefficient K (Hz/cell)	Basic mass per cell
Initial adhesion mass coefficient β	Cell mass sensed by the crystal oscillator sensor in the early stages of cell adhesion
Initial adhesion average time t_m (h)	Average cell sedimentation time in the early stages of cell adhesion
Initial adhesion standard deviation t_s (h)	Degree of variation in average data of cell sedimentation time in the initial stage of cell adhesion

4.3.4 Results

4.3.4.1 ECM on the slides glass

Figures 4-1 and 4-2 show the results of cell adhesion testing using PLL, Collagen, and PNIPAM on ITO electrodes.

Figure 4-1 (a1,2) shows the results of culturing cells directly on the glass surface without coating and without ITO electrodes; (a1) shows the status of cells 10 min after seeding, while (a2) shows the status of cells after 24 hours from seeding the cells. In this case, I find cells clustering in mini groups and not spreading over the surface. Figure 4-1 (b1,2) shows the results of culturing cells on the glass surface with PLL coating and without ITO electrodes; (b1) shows the status of cells 10 minutes after seeding, while (b2) shows the status of cells after 24 h from seeding the cells. In this case, we find that cells multiply and spread on the surface which means an effective adhesion to the surface. Figure 4-1 (c1,2) shows the results of culturing cells on the glass surface with PLL coating and ITO electrodes; (c1) shows the status of cells 10 minutes after seeding, while (c2) shows the status of cells after 24 h from seeding the cells. In this case, I find that cells also multiply and spread on the surface which means an effective adhesion to the surface.

In Figure 4-2, the experiment was performed directly on the glass surface with ITO electrodes for both collagen and PNIPAM coating. Figure 4-2 (d1,2) shows the results of culturing cells on the glass surface with collagen coating and ITO electrodes; (d1) shows the status of cells 10 min after seeding, while (d2) shows the status of cells after 24 h from seeding the cells. In this case, I find that cells multiply and spread on the surface which means an effective adhesion to the surface. Figure 4-2 (e1,2) shows the results of culturing cells on the glass surface with PNIPAM coating and ITO electrodes; (e1) shows the status of cells 10 min after seeding, while (e2) shows the status of cells after 24 h from seeding the cells. In this case, I find that cells also multiply and spread on the surface which means an effective adhesion to the surface. By comparing these results, the efficacy of using these types of ECM in adhesion of cultured cells to ITO surfaces is evident.

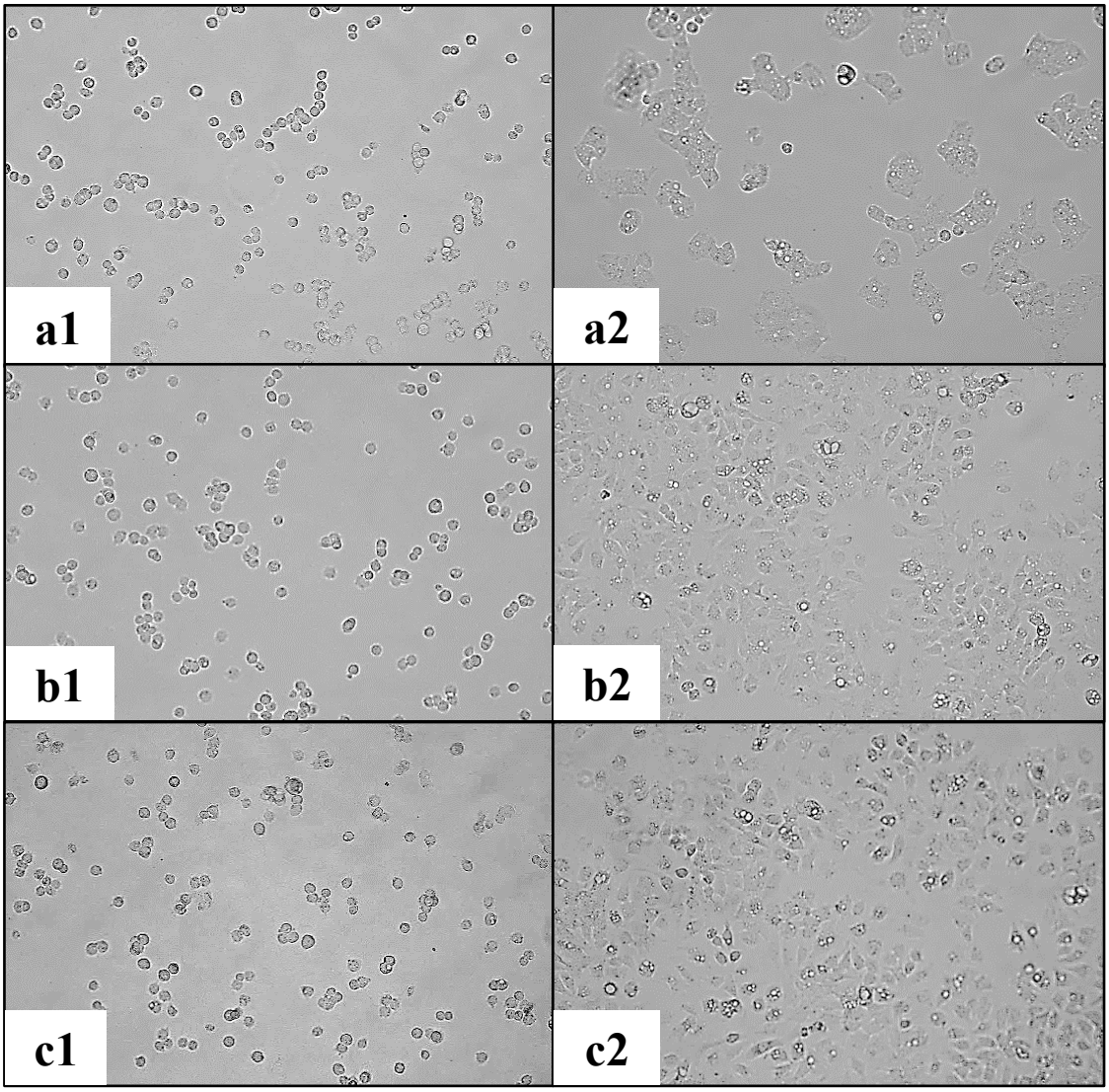

Figure 4-1. (a1,2) The results of culturing cells directly on the glass surface without coating and without ITO electrodes: (a1) status of cells 10 min after seeding, (a2) status of cells after 24 h from seeding the cells. (b1,2) The results of culturing cells on the glass surface with PLL coating and without ITO electrodes: (b1) status of cells 10 min after seeding, (b2) status of cells after 24 h from seeding the cells. (c1,2) The results of culturing cells on the glass surface with PLL coating and ITO electrodes: (c1) status of cells 10 min after seeding, (c2) status of cells after 24 h from seeding the cells.

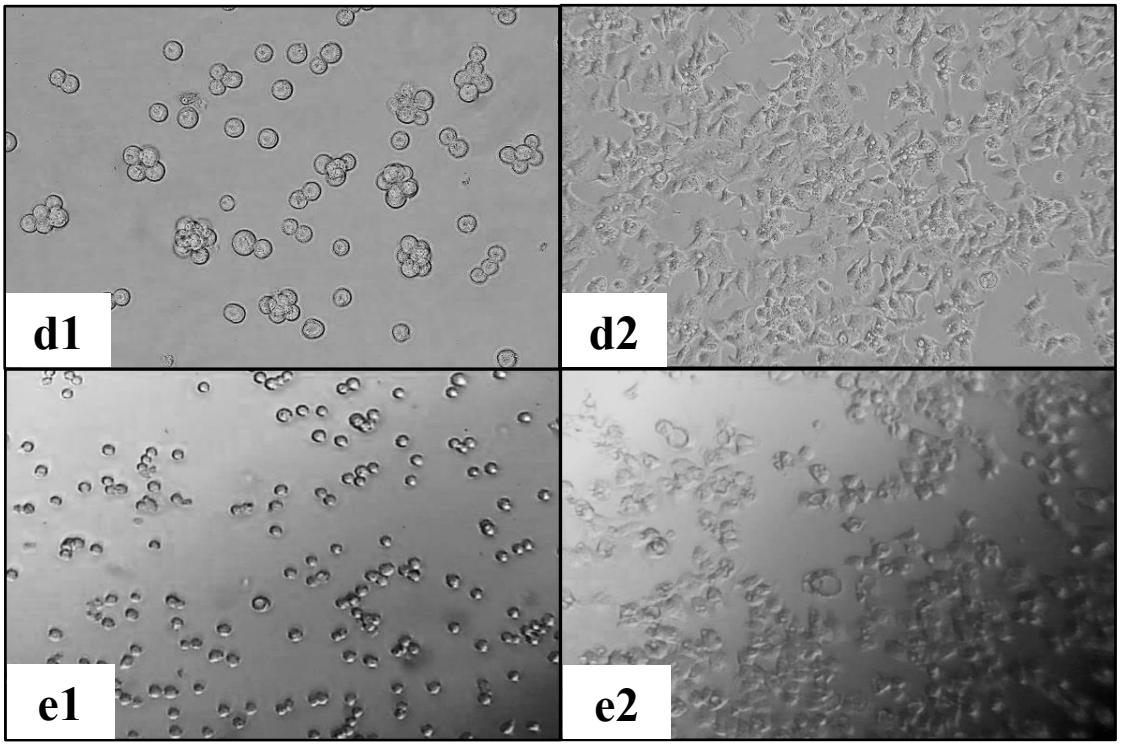

Figure 4-2. (d1,2) The results of culturing cells on the glass surface with collagen coating and ITO electrodes: (d1) status of cells 10 min after seeding, (d2) status of cells after 24 h from seeding the cells. (e1,2) The results of culturing cells on the glass surface with PNIPAM coating and ITO electrodes: (e1) status of cells 10 min after seeding, (e2) status of cells after 24 h from seeding the cells.

4.3.4.2 ECM on the quartz crystal microbalance

4.3.4.2.1 Quartz crystal microbalance with only a culture medium

Figure 4-3 shows the changes in resonance frequency and resonance resistance with respect to the elapsed time of the measurement using only culture medium. After adding the medium in the chamber, the resonance frequency decreased and the resonance resistance increased due to overall loading on the quartz crystal microbalance, after which they were in a steady and stable state. Therefore, it was judged that evaluation by cell measurement was possible.

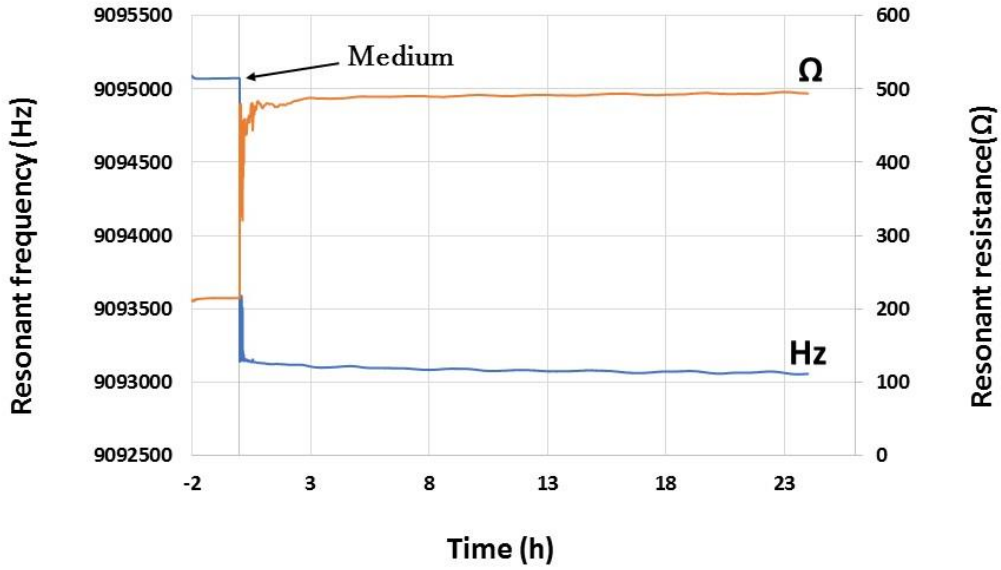

Figure 4-3. Changes in resonance frequency and resonance resistance with respect to the elapsed time of the measurement using only culture medium.

4.3.4.2.2 Adhesion of cultured cells to the surface of the quartz crystal microbalance with the blank mode

Figure 4-4 shows the changes in resonance frequency and resonance resistance with respect to the elapsed time of the experiment of adhesion of cultured cells to the surface of the quartz crystal microbalance with the blank mode. In Figure 4-4, the result when seeding cells directly and the result of seeding cells after 24 h of measurement are shown. After adding the medium in the chamber, the cells were seeded, and then the resonance frequency decreased slightly and the resonance resistance increased due to the loading of cells on the quartz crystal microbalance, after which they started to increase slightly over time due to the cell divisions taking place into the measurement chamber. In addition to the contact of some cells with the surface of the quartz crystal microbalance, as shown in Figure 4-5.

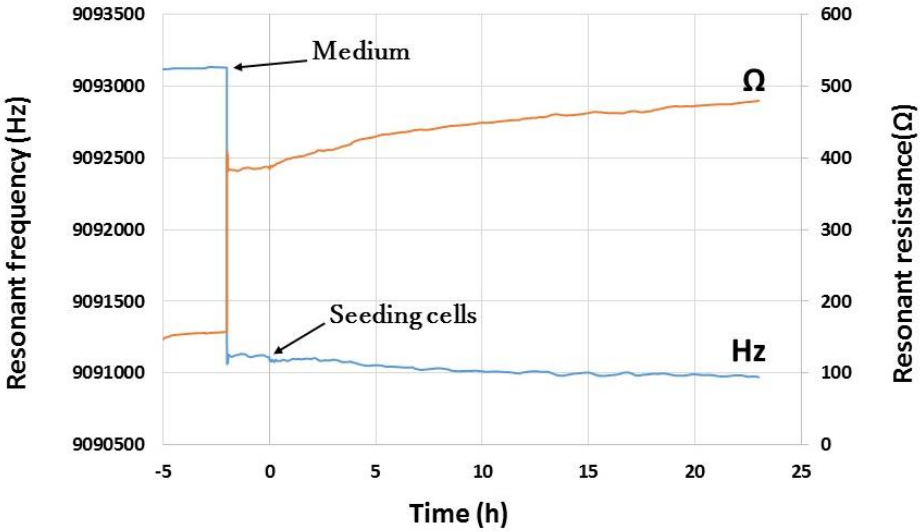

Figure 4-4. Changes in resonance frequency and resonance resistance with respect to the elapsed time of the experiment of adhesion of cultured cells to the surface of the quartz crystal microbalance with the blank mode, seeding cell densities of 0.63×10^3 cells/mm^2.

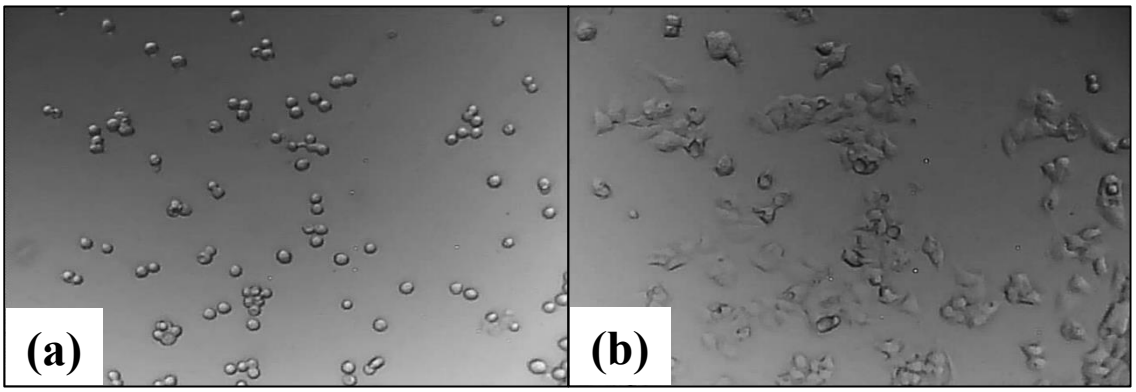

Figure 4-5. Changes in the cultured cells with respect to the elapsed time of the experiment of adhesion of cultured cells to the surface of the quartz crystal microbalance with the blank mode. (a) Result of cultured cells after 10 min of seeding the cells, (b) result of cultured cells after 24 h of seeding.

4.3.4.2.3 Adhesion of cultured cells to the surface of the quartz crystal microbalance with collagen

Figure 4-6 shows the changes in resonance frequency and resonance resistance with respect to the elapsed time of the experiment of adhesion of cultured cells to the surface of the quartz crystal microbalance with a collagen layer. Figure 4-6 shows the result when seeding cells directly on the collagen layer as well as the result of seeding cells after 24 h of measurement. After seeding the cells into the chamber, the resonance frequency decreased greatly and the resonance resistance also increased due to the loading of cells on the quartz crystal microbalance. Then, the resonance frequency began to decrease gradually over time due to the partial adhesion to the surface. Then it continued to decrease as a result of cells proliferation into the measurement chamber. In addition to its spread and adhesion to the surface of the quartz crystal microbalance, which means that the cells adhered to the collagen layer as shown in Figure 4-7.

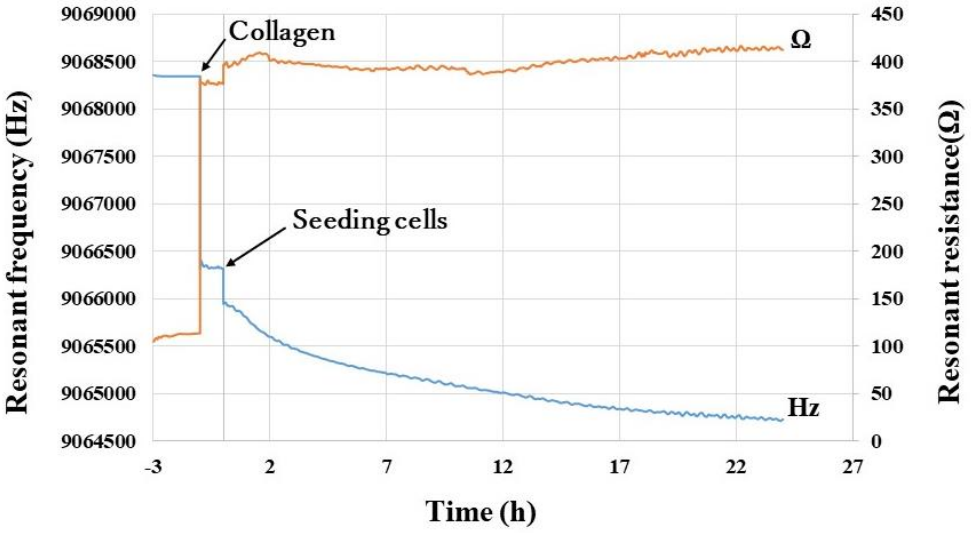

Figure 4-6. Changes in resonance frequency and resonance resistance with respect to the elapsed time of the experiment of adhesion of cultured cells to the surface of the quartz crystal microbalance with collagen, seeding cell densities of 0.63×10^3 cells/mm^2.

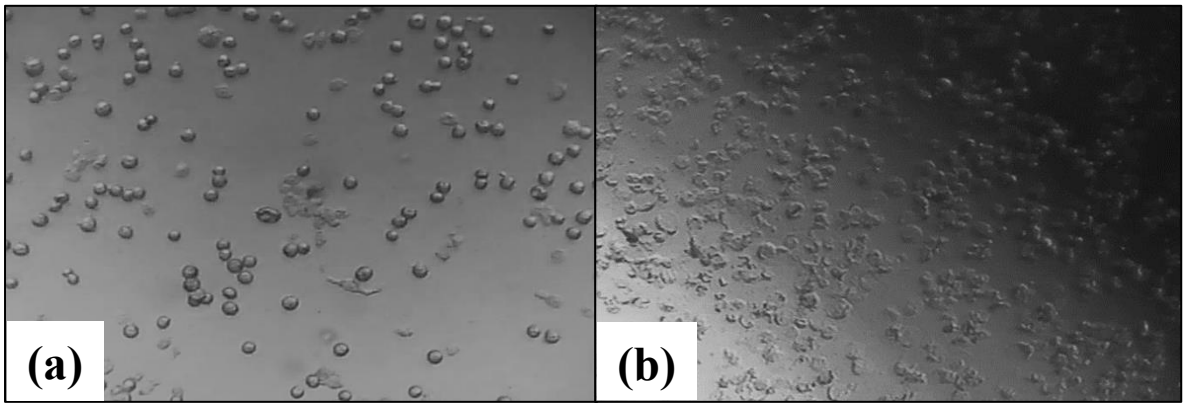

Figure 4-7. Changes in the cultured cells with respect to the elapsed time of the experiment of adhesion of cultured cells to the surface of the quartz crystal microbalance with collagen. (a) Result of cultured cells after 10 min of seeding the cells, (b) result of cultured cells after 24 h of seeding.

4.3.4.2.4 Adhesion of cultured cells to the surface of the quartz crystal microbalance with poly-L-lysine

Figure 4-8 shows the changes in resonance frequency and resonance resistance with respect to the elapsed time of the experiment of adhesion of cultured cells to the surface of the quartz crystal microbalance with a poly-L-lysine layer. Figure 4-8 shows the result when seeding cells directly on the PLL layer as well as the result of seeding cells after 24 h of measurement. After seeding the cells into the chamber, the resonance frequency decreased and the resonance resistance also increased due to the loading of cells on the quartz crystal microbalance. Then, the resonance frequency began to gradually decrease and the resonance resistance increased over time and they kept increasing. The result of cells' increase, spread, and adhesion to the surface, means that PLL is useful in the process of attaching cells to the surfaces as shown in Figure 4-9.

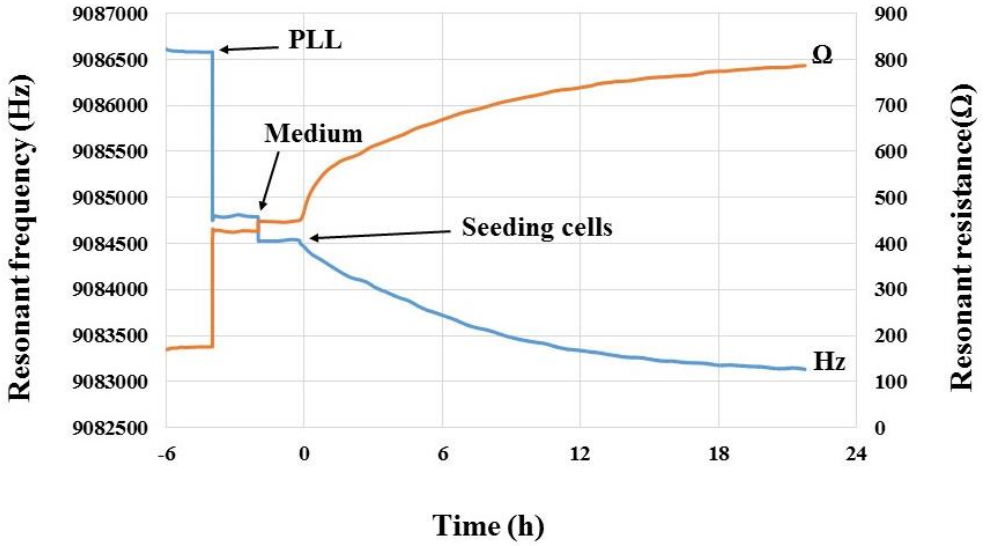

Figure 4-8. Changes in resonance frequency and resonance resistance with respect to the elapsed time of the experiment of adhesion of cultured cells to the surface of the quartz crystal microbalance with poly-L-lysine, seeding cell densities of 0.63×10^3 cells/mm^2.

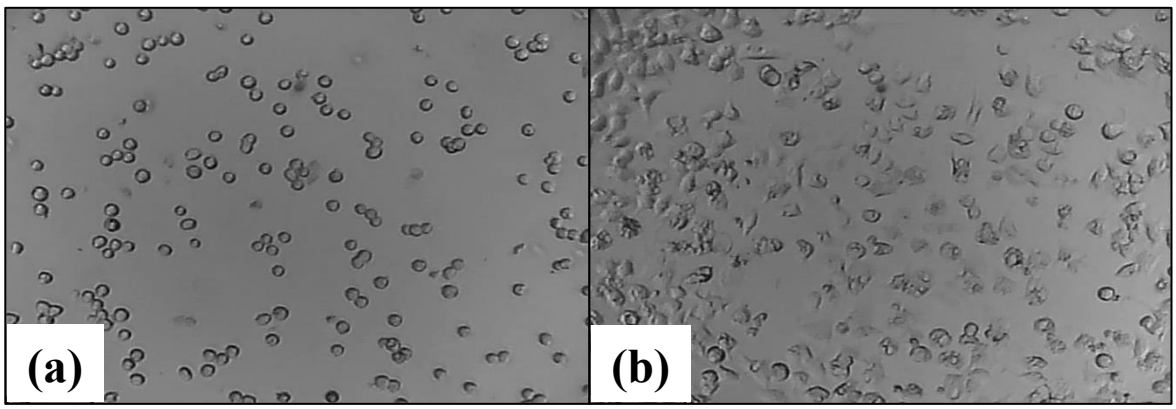

Figure 4-9. Changes in the cultured cells with respect to the elapsed time of the experiment of adhesion of cultured cells to the surface of the quartz crystal microbalance with poly-L-lysine. (a) Result of cultured cells after 10 min of seeding the cells, (b) result of cultured cells after 24 h of seeding.

4.3.4.2.5 Adhesion of cultured cells to the surface of the quartz crystal microbalance with PNIPAM polymer

Figure 4-10 shows the changes in resonance frequency and resonance resistance with respect to the elapsed time of the experiment of adhesion of cultured cells to the surface of the quartz crystal microbalance with a PNIPAM polymer. Figure 4-10 shows the result when seeding cells directly on the PNIPAM layer as well as the result of seeding cells over time to measurement. After seeding the cells into the chamber, the resonance frequency decreased slightly and the resonance resistance increased further due to the loading of cells on the quartz crystal microbalance. Then, the resonance frequency began to slightly decrease gradually due to the delay of cell adhesion to the surface while the resonance resistance increased over time as a result of cells viscosity factor. This means that the response of the cell-binding process to the PNIPAM polymer layer was delayed as shown in Figure 4-11, which I believe is due to the thermal factors of the PNIPAM polymer.

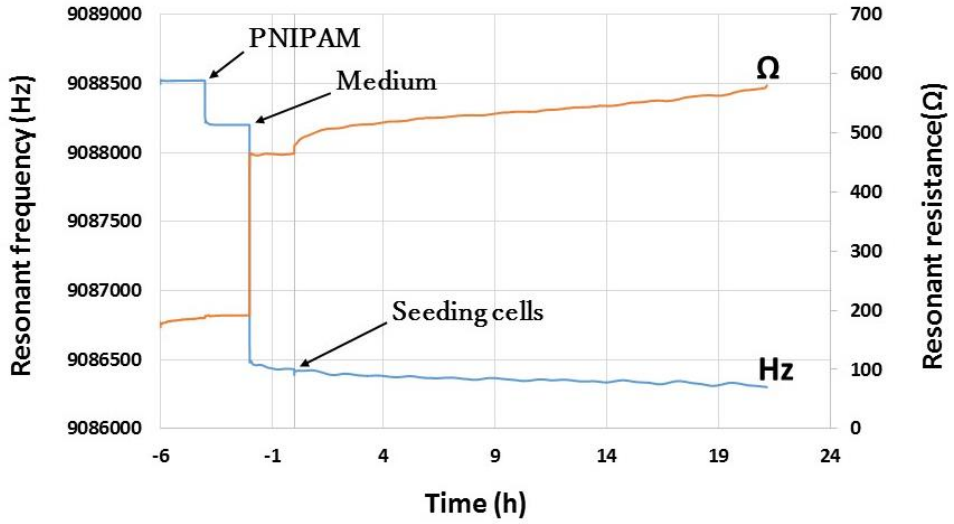

Figure 4-10. Changes in resonance frequency and resonance resistance with respect to the elapsed time of the experiment of adhesion of cultured cells to the surface of the quartz crystal microbalance with PNIPAM polymer, seeding cell densities of 0.63×10^3 cells/mm^2.

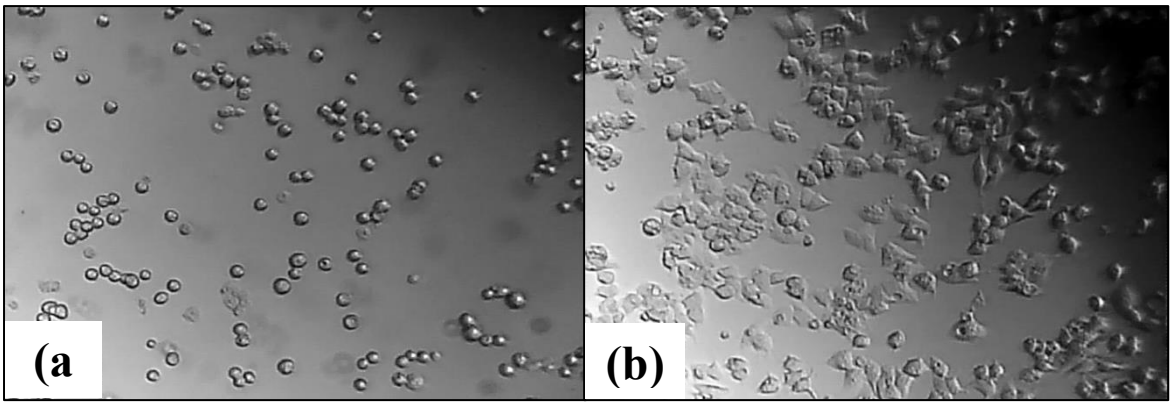

Figure 4-11. Changes in the cultured cells with respect to the elapsed time of the experiment of adhesion of cultured cells to the surface of the quartz crystal microbalance with PNIPAM polymer. (a) Result of cultured cells after 10 min of seeding the cells, (b) result of cultured cells after 24 h of seeding.

4.3.4.2.6 Adhesion of cultured cells to the surface of the quartz crystal microbalance with PLL on PNIPAM polymer

Figure 4-12 shows the changes in resonance frequency and resonance resistance with respect to the elapsed time of the experiment of adhesion of cultured cells to the surface of the quartz crystal microbalance with PLL on PNIPAM polymer. Figure 4-12 shows the result when seeding cells directly on the layers as well as the result of seeding cells after 24 hours of measurement. After seeding the cells into the chamber, the resonance frequency decreased and the resonance resistance was also increased due to the loading of cells on the quartz crystal microbalance. Then, the resonance frequency began to gradually decrease and the resonance resistance increased over time, and it continued to increase more quickly than measurements of the previous layers. The reason for this result is the increase of cells attachment and adhesion to the surface after cells divisions, which means that the coated PNIPAM polymer with PLL shows a high adherence layer that contributes to the attachment of cells to the surfaces as evidenced by this measurement and the images in Figure 4-13.

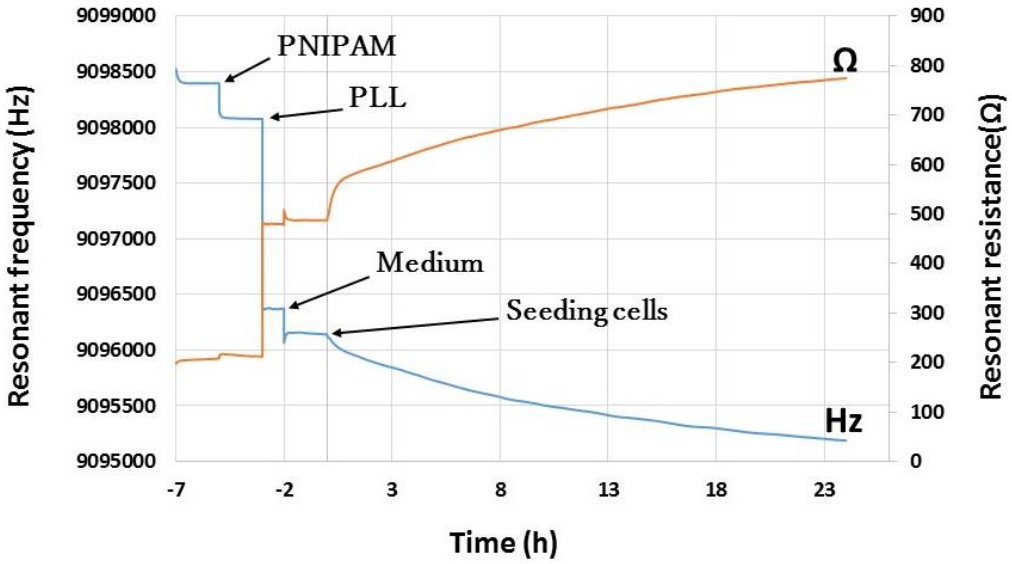

Figure 4-12. Changes in resonance frequency and resonance resistance with respect to the elapsed time of the experiment of adhesion of cultured cells to the surface of the quartz crystal microbalance with PLL on PNIPAM polymer, seeding cell densities of 0.63×10^3 cells/mm^2.

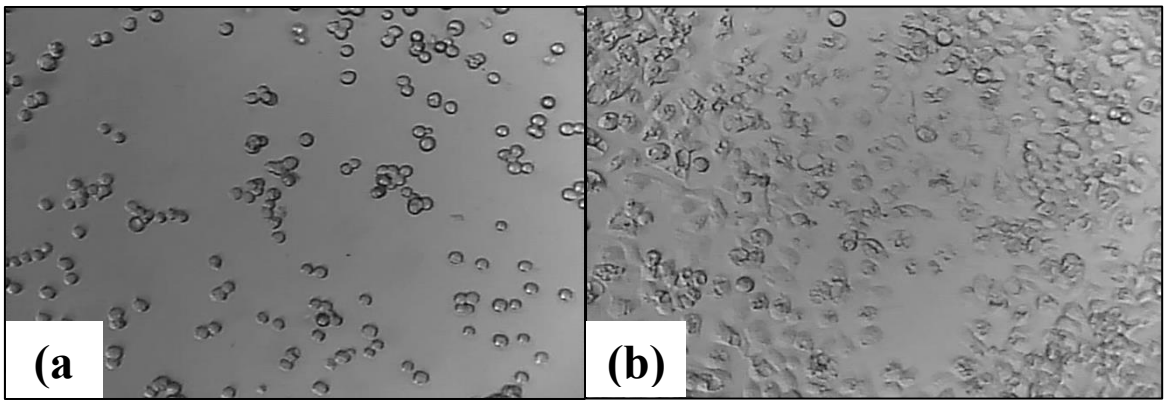

Figure 4-13. Changes in the cultured cells with respect to the elapsed time of the experiment of adhesion of cultured cells to the surface of the quartz crystal microbalance with PLL on PNIPAM polymer. (a) Result of cultured cells after 10 min of seeding the cells, (b) result of cultured cells after 24 h of seeding.

4.3.5 Discussion

All of the measurements show the changes in the resonance frequency and the resonance resistance in accordance to the elapsed time of the experiments of adhesion of cultured cells to the surface of the quartz crystal microbalance with the ECM treated surfaces, as well as the images of those measurements confirming proliferation and adhesion of cells to those surfaces. The changes in both the resonance frequency and resonance resistance were observed after cells seeding, and the response of the cells with the ECM over time was observed through proliferation and adhesion as well as the differences in the increase in cell mass and viscosity on the surface of the quartz crystal microbalance. This confirms the difference in the response of the resonance frequency and the resonance resistance according to the difference of the ECM treated surface on the quartz crystal microbalance.

PLL and collagen are widely used as ECM. PLL and ITO bind by ionic bonding between the amino groups of PLL and the hydroxy groups on ITO. Meanwhile, collagen molecules include amino acid residuals with amino groups that also ionically bond to the ITO surface. PNIPAM covalently bonds to the hydroxy groups on the ITO surface because it is triethoxysilane terminated. The CH3OH molecules were eliminated during the binding reaction. The PLL coating on the PNIPAM surface can form hydrophobic bonds because PNIPAM is hydrophobic at 37 °C [75].

To check the surface modification, the resonant frequency changes of PLL and PNIPAM were measured before and after the modification. The typical resonant frequency changes on the PLL and PNIPAM coatings were 53 Hz and 321 Hz in air, respectively. The resonant frequency change of collagen, measured during modification in solution, was typically 103 Hz. The resonant frequency change of the PLL coating on PNIPAM, also measured during modification in solution, was typically 13 Hz.

Figure 4-6 and Figure 4-8 show typical resonant frequency responses corresponding to cell attachment to a collagen-coated surface and a PLL-coated surface, respectively. In the two figures, the changes in frequency at 20 h are 1150 and 1380 Hz, respectively. The difference in the frequency change values is 15%. Figure 4-10 shows a typical resonant frequency response of the cell attachment to the PNIPAM-modified surface. The frequency change was 130 Hz at 20 h for the PNIPAM modified surface, which is 10 times smaller than the frequency changes for the PLL- and collagen-modified surfaces. This small resonant frequency change is attributed to the transverse vibration of the quartz crystal being damped in the PNIPAM layer. I further investigated this possibility in an experiment where PLL was additionally coated onto the PNIPAM, with the aim of checking whether the film was thick and unresponsive, the

response was obtained by performing the experiment with PLL, so collagen was not tried. The resonant frequency response of the cell attachment to the surface of PNIPAM with PLL is shown in Figure 4-12. The resonant frequency changed 880 Hz at 20 h, indicating that the small resonant frequency change for the PNIPAM-modified surface was caused by the interaction between the cells and the PNIPAM surface.

As shown in Figures 4-6, 4-8, 4-10, and 4-12, the resonant resistance changes were correlated with the resonant frequency responses of the PLL, PNIPAM, and PNIPAM with PLL surfaces. These changes reflected the increasing viscous effect of the cells as the attachment progressed. In contrast, the resonant resistance of the collagen surface changed scarcely, possibly because the binding protein was more active on the collagen surface than on the other surfaces. As the binding protein connects to the cytoskeleton inside the cell, its activity increases the cell rigidity and decreases the effect of the viscous property of the cell.

Figure 4-5 (a, b) shows simultaneously obtained microscope images of cells with the blank mode surface at 1 h and 24 h after the cells seeding in Figure 4-4. Figure 4-7 (a, b) shows simultaneously obtained microscope images of cells on the collagen-coated surface at 1 h and 24 h after the cell seeding in Figure 4-6. Figure 4-9 (a, b) shows simultaneously obtained microscope images of cells on the PLL-coated surface at 1 h and 24 h after the cell seeding in Figure 4-8. Figure 4-11 (a, b) shows simultaneously obtained microscope images of cells on the PNIPAM-coated surface at 1 h and 24 h after the cell seeding in Figure 4-10. Figure 4-13 (a, b) shows simultaneously obtained microscope images of cells on the PNIPAM-coated surface at 1 h and 24 h after the cell seeding in Figure 4-12.

The resonant frequency change curves resulting from the cells attachment process were analyzed by their fit to the model equation reported previously [47,48]. The model equation is expressed by three factors affecting the resonant frequency change. The density of adherent cells on the surface of a quartz crystal is one of these three factors, as cell numbers increase with cells divisions. The second factor is the effective mass, which depends on its distance from the quartz crystal, where the effect of mass appears with a delayed response of the first-order to the process of cells binding. The third factor is the extent of the effect of cellular communication resulting from cell-to-cell contact, as restricting their spread causes an effective increase in mass because it limits their spread and maintains the height of cells. In addition, the distribution of cells on the surface influences the initial difference of sedimentation.

I compared the differences among the curves by comparing the fitting parameters of the equations. Figures 4-14 to 4-17 show the fitting results of the modeling curves calculated using Microsoft Excel, where the calculation was carried out to obtain the maximum value of the

determination coefficient R2. The determination factor was calculated by regressing the experimental data against the data calculated using the modeling equation of the resonant frequency change. The resulting correlation plot should be a straight line with a slope of 1.0 passing through the origin. The modeling curves well fit the experimental curves; the calculated parameters are listed in Table 2.

In Figure 4-14, the curves for collagen show that the time constant for the first-order lag response for the cell attachment (T_1) is 16 h, but in Figure 4-15, the curves for PLL show that the time constant for the first-order lag response for the cell attachment (T_1) is 11 h. These results indicate that the cell attachment process for collagen takes slightly longer than that for PLL.

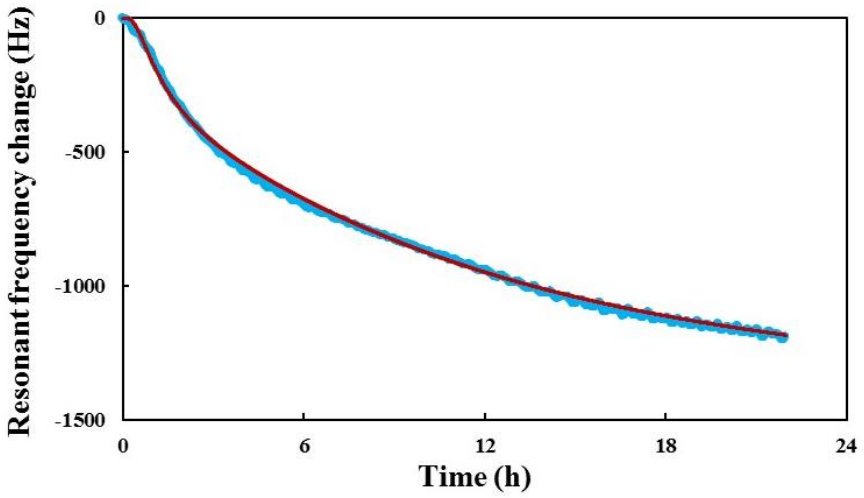

Figure 4-14. The fitting curve of the collagen obtained using the modeling equation of response curves of Figure 4-21.

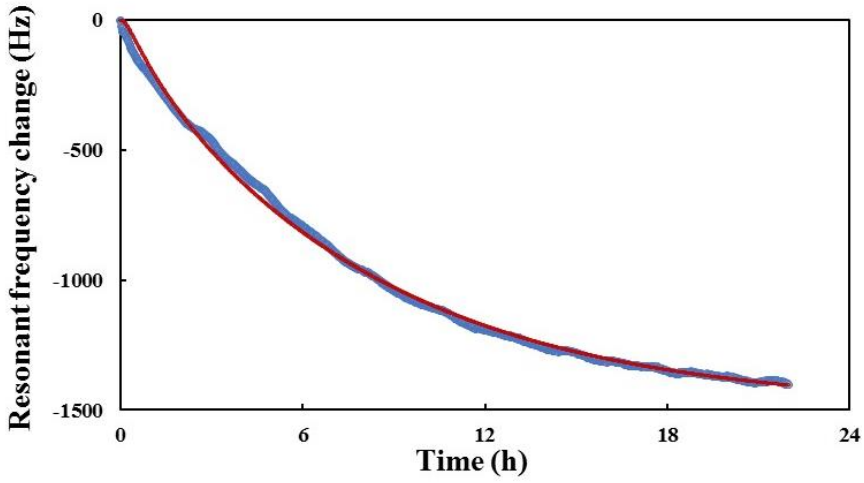

Figure 4-15. The fitting curve of the PLL obtained using the modeling equation of response curves of Figure 4-23.

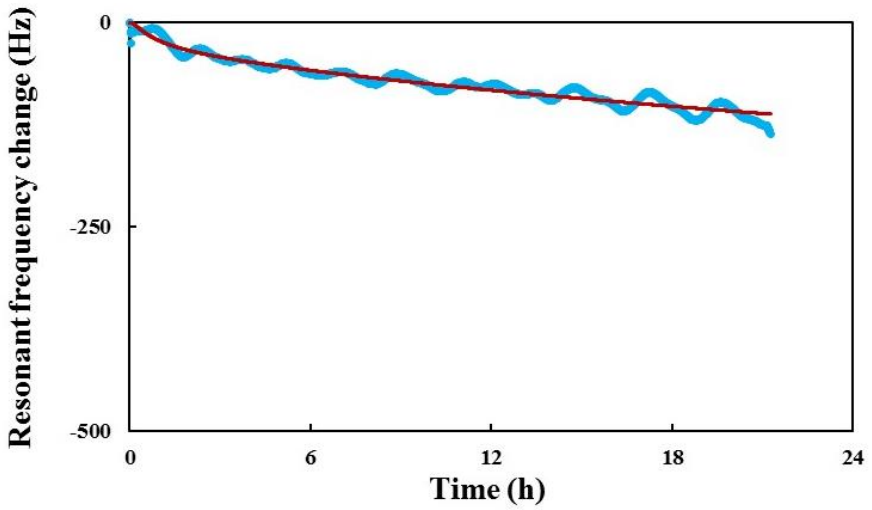

Figure 4-16. The fitting curve of the PNIPAM obtained using the modeling equation of response curves of Figure 4-25.

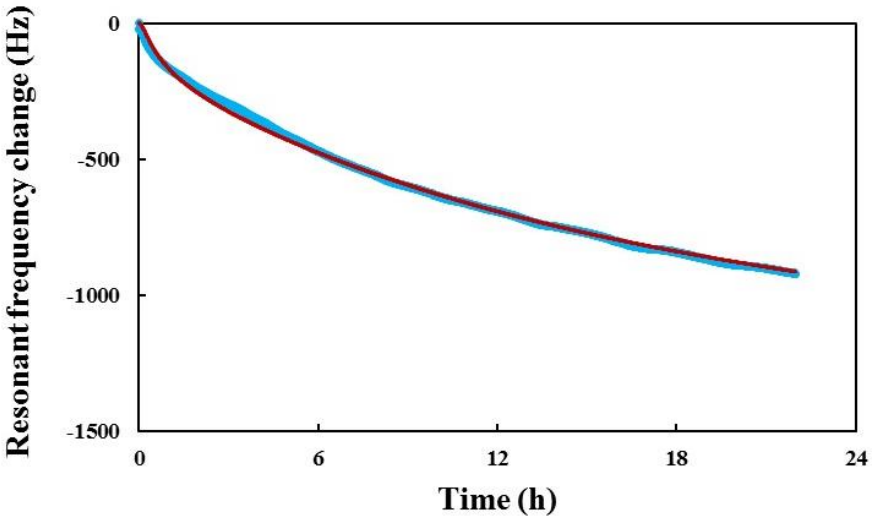

Figure 4-17. The fitting curve of the PNIPAM with PLL obtained using the modeling equation of response curves of Figure 4-27.

Table 2. Parameters used for the modeling curves in Figures 4-14 to 4-17.

Curves	*n(0)*	T_1 *(h)*	T_2 *(h)*	*K (Hz/cell)*	*β*	t_m *(h)*	t_s *(h)*	R^2
Collagen	900	16	70	0.68	0.2	ln(1)	ln(2)	0.9998
PLL	900	11	70	0.72	0.2	ln(1.1)	ln(3)	0.9997
PNIPAM	650	38	65	0.12	0.2	ln(0.8)	ln(3)	0.9934
PNIPAM + PLL	650	17	65	0.67	0.2	ln(0.6)	ln(3)	0.9997

In Figure 4-16, for the cell attachment process for PNIPAM, the conversion factor K is approximately six times smaller than that for PLL and collagen. This result means that the mass loading effect is smaller in PNIPAM than in PLL and collagen.

In Figure 4-17, the case of PLL-coated PNIPAM, the obtained time constant (T_1) was 17 h and the other parameters were similar to those for PLL and collagen. This result can be explained on the basis of the differences between the microscope images of cells on collagen and PNIPAM (Figure 4-7 (b) and Figure 4-11 (b), respectively). In the case of collagen (Figure 4-7 (b)), the widely spread cells on the surface provide a large mass effect because the mass effect of the viscoelastic material depends on its distance from the quartz crystal surface. In the case of PNIPAM (Figure 4-11 (b)), the cells are not as widely spread as those on PLL and collagen, resulting in a smaller total resonant frequency change. This weak cell spreading on PNIPAM results in a small total resonant frequency change. The value of time constant T_1 for PNIPAM was 38, which is triple as large as that for PLL. These results suggest that the attachment strength of cells to the PNIPAM surface was low and that the cells attached weakly onto the surface. The weak attachment strength of PNIPAM can be explained by the binding mechanism.

In PLL, the amino residues are targeted by binding the protein or forming ionic bonds with negatively charged molecules on the cell, whereas collagen includes amino groups in its amino acid residues (e.g., 5-hydroxylysine). In addition, the cell-binding proteins should have an affinity to the peptide sequence of collagen. Ionic and hydrogen bonds form between collagen and cells. On the contrary, the binding force of PNIPAM occurs by hydrophobic bonding. When not bound to a surface, a cell is spherical because a sphere is the most stable shape of a vesicle. When the binding strength is weak, the cell spreading cannot sufficiently overcome the force to retain its spherical form.

Figure 4-18 (a, b, c) shows a typical time course of the resonant frequency, resonant resistance, and temperature, respectively, of a PNIPAM-coated quartz crystal during a temperature cycle. Twenty-four hours after cell seeding, the temperature was lowered from 37 to 20°C; after the culture medium was replaced at the same temperature, the temperature was increased from 20 to 37 °C. Replacement of the culture medium was intended to provide an external force for detaching the PNIPAM film. The resonant frequency decreased during the cell attachment process (step A in Figure 4-18) and further decreased when the temperature was lowered to 20 °C (step B in Figure 4-18). The resonant frequency recovered when the temperature was increased to 37 °C and gradually decreased with an elapsed time (step C in Figure 4-18). The change in the resonant resistance of the quartz crystal was basically opposite the change in the resonant frequency. The microscope images of cells on the quartz crystal simultaneously obtained immediately before the temperature was lowered and immediately after the medium was replaced and the temperature was increased show no obvious change so they were not added. Replacing the medium apparently did not provide sufficient external force to remove the cells, even at 20 °C.

To analyze the change in the process, I plotted the resonant resistance as a function of the resonant frequency (Figure 4-18). In Figure 4-18 c, region A shows the initial cell attachment process. In this region, the slope of the decrease in resonant frequency and that of the increase in resonant resistance are almost constant. Region B corresponds to the temperature decrease. In region B, the slope of the resonant frequency and resonant resistance reflect the temperature change; that is, the viscosity of the medium increases with decreasing temperature.

In Figure 4-18 c, point X and point Y corresponded before and after the temperature cycle, respectively. After the temperature cycle, an increase in the resonance frequency and a decrease in the resonance resistance were observed. When the temperature was cycling, the interaction between cells and PNIPAM was temporarily weakened when the temperature was lowered, while the process was the opposite when the temperature was raised. However, when point X turns into point Y, this shows that the reverse process was not perfect. After increasing the temperature to 37 °C, there is a change in the resonance frequency and resonance resistance as shown in the region C in the (F – R) diagram. By comparing regions A and C, I find that the resonant frequency of region C has shifted to higher values than that of region A. This shift indicates an increase in the resonance frequency after the temperature cycle, due to the weakening of the mass loading effect by the temperature cycle. This is explained due to PNIPAM molecular brushes remain deformed after a temperature cycle.

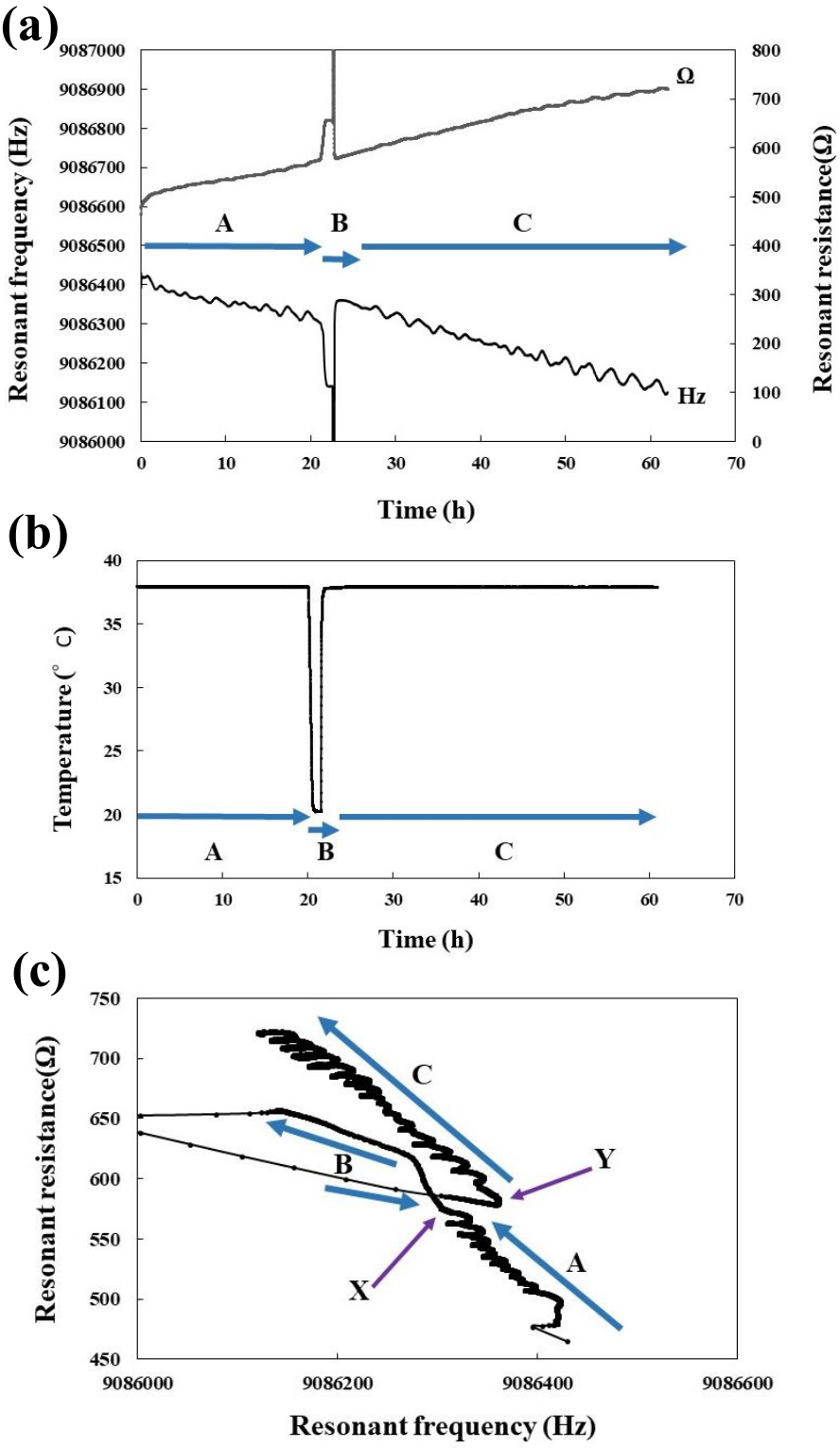

Figure 4-18. The typical time course of the cell reduction monitoring using the PNIPAM-coated quartz crystal. (a) Resonant frequency and resonant resistance, (b) temperature in the experiment, and (c) diagram of the resonant frequency and resonant resistance during the temperature cycle.

Finally, I have developed a measuring system that includes quartz crystals and a monitoring unit as well as a rapid temperature-control that can operate inside the CO_2 incubator. Cell adhesion and spreading on surfaces were monitored using three types of ECM, PLL, collagen and PNIPAM, then, the results of that monitoring were compared using modeling equations based on the response of the first-lag to curve fitting. These results also showed the time constants of the first-lag response, which was 11 h for PLL, 16 h for collagen and 38 h for PNIPAM. Through the results of the total resonance frequency change in the three coating materials, it was found that PNIPAM is the smallest among those changes, due to the low adhesion force between cells and the surface of PNIPAM. Microphotographs obtained at the same time supported this speculation. The F-R schematic diagram of the PNIPAM thermal cycle experiments showed the process of cells adhesion to the surface, as the strength of cells-attached were decreased due to the heat cycle and the effect of the PNIPAM molecular brush remained disturbed after the thermal cycle.

In fact, the number of cells is higher than the target cell concentration in some previous experiments. This is because the cells are not mixed evenly in the medium due to insufficient pipettes. Also, some of these experiences took place at varying lengths. This led to the repetition of culturing the original cells with the aim of conducting more of these experiments, consequently extending the life of these cells until they are used. This caused an increase in their number and then poor visibility of all cells in the counting chamber during their counting.

Chapter 5: Evaluation and analysis of cell response to antitumor using quartz crystal microbalance

5.1 Introduction

According to recent stastical data shown in Cancer Today, cancer is a leading cause of death worldwide, accounting for nearly 10 million deaths in 2020 [76]. Cancer is a disease in which some of the body's cells grow uncontrollably and spread to other parts of the body, and thus it can cause damage to some or all of the human body's systems, or even death. Therefore, it is important to cure this disease.

In general, the primary goal of cancer therapy is to prolong the life span of patient. Improving the patient's quality of life is also an important goal. Many cancers can be removed if diagnosed early and treated appropriately [76]. Treatment usually includes radiotherapy, chemotherapy, and/or surgery. Chemotherapy is one of cancer treatment that uses drugs to kill cancer cells. Traditional chemotherapeutic agents kill cells that divide rapidly, a critical property of most cancer cells and some of normal cells. Therefore, these treatments help you fight a life-threatening disease.

Cisplatin, cisplatinum, or cis-diamminedichloroplatinum (II) is an antitumor that is widely used in the treatment of cancerous tumors. It has been used to treat many human cancers including head and neck, lung, bladder, ovarian, and testicular cancers. It is effective against different types of cancers. It is generally considered a cytotoxic drug, as it has the ability to cross-link with purine bases on DNA and Interfering with the mechanisms of DNA repair, causing DNA damage and inhibiting its synthesis, thereby inducing apoptosis in cancer cells [77].

In this thesis, I have developed a measurement system that allows live cell monitoring cultured cells a CO_2 incubator. Using this system, I monitored and analyzed cell response to antitumor using quartz crystal microbalance. This is to understand the effects of chemical stimuli and stress and to analyze the physical properties of cells according to the reversals of the state of the cytoskeleton and the state of activity as a result of exposure to such antitumor. This is also studied by fitting curves of the model equations onto the experimental curves of the resonant frequency change. It will also appear in the content of this chapter.

5.2 Purpose

In this chapter, I monitor the life and death process of cultured cells as a result of their antitumor response using quartz crystal microbalance, in addition to the analysis of apoptosis

based on the measurement results. The process of cells attachment to surfaces as well as the response to the antitumor reagent cisplatin were studied using the fitting of model equations curves on the experimental curves of the resonance frequency change. Also their response were explained by building response model equations and defining the parameters of the equations. The purpose is to comprehensively understand the response of cells with antitumor drugs by measuring using quartz crystal microbalance, therefore to be able to analyze their response to the drugs.

5.3 Experimental instruments/reagents

The experimental equipment and reagents used in this experiment are shown below:

Experimental instruments

- Developed experiment device (Figure 3-1)
- CO_2 incubator (temperature 37 ℃, CO_2 concentration 5%)
- Crystal oscillator chemical measurement system QCA922
- Peltier device controller
- Camera/light switch
- Focus controller
- Computer
- Measurement software

(WinQCM (Seiko EG & G), USB Video Selector & Capture (laboratory original)) and thermal control & adjustment program using Visual Basic

- Centrifuge
- Gas burner
- Hemocytometer (counting chamber)
- Culture petri dish (100 mm/Collagen-Coated Dish)
- 15 mL tube centrifuge tube

- Electric pipettor
- Pipette (2 mL, 5 mL)
- Micropipette (20 μL, 200 μL, 1000 μL)
- Chip (20 μL, 200 μL, 1000 μL)
- Driver
- Quartz crystal microbalance (ITO electrodes)
- Measurement cell (attached: O-ring, screw)

Reagents

- DMEM medium (with FBS, Antibiotic-Antimycotic, Amphotericin B solution)
- Trypsin
- PBS
- HepG2 cells
- Poly-L-lysine (PLL)
- Cisplatin
- Ethanol 76.9–81.4%
- Acetone 99.8%
- Sterilized water

5.4 Experiments

Before the measurement, the measurement cell for the crystal unit was assembled. Figure 3-12 shows a photograph of the measurement cell parts and quartz crystal microbalance, and Figure 3-13 shows the procedure after they are collected in the measurement cell. The target cells' concentration in these experiments was 0.63×10^3 cells/chamber. Experiments to evaluate and analyze the cell response to antitumor were performed using quartz crystal microbalance with poly-L-lysine (PLL), and then the results of the cells' response to the

antitumor were described.

5.4.1 Cisplatin

A drug effect evaluation trial was conducted using cisplatin. The cell concentration was 0.63×10^3 cells/mm^2, and the final cisplatin concentration was 83.3 μM and 16.7 μM. The procedure of the experiment is shown below.

5.4.2 Evaluation and analysis of cells cultured under cisplatin

1. The quartz crystal microbalance was integrated into the measuring cell and washed with sterile water.
2. The measuring cell was connected to the experiment device by QCA multiplier in the incubator, the measuring program "WinQCM" was started, and the measuring cell was allowed to stand about 1 to 2 h until the resonant frequency and resonant resistance became stable.
3. 60 μL of PLL (100 μL/mL) was added dropwise to the measurement cell for surface treatment on the crystal unit substrate.
4. After 1 h of adding PLL, the PLL was removed with 100 μL of added PBS and gently removed to wash the surface of the quartz crystal microbalance, and then 200 μL of medium was added dropwise, and the mixture was allowed to stand for 2 h.
5. After culturing the HepG2 cells, the cells were seeded into the measurement cell at the target concentration.
6. After 10 min of seeding the cells into the measuring cell, the "USB Video Selector & Capture" turned on, and then CMOS camera focus was set, after which cells were imaged at 30 min intervals.
7. Once imaging was completed after 24 h, the target concentration of cisplatin was added dropwise.
8. The measurement was completed approximately 72 h after seeding the cell.

5.4.3 Response analysis setting items for cisplatin

Table 3 shows the setting items for drugs response analysis. In the response analysis of cells with antitumor drugs, Excel VBA is used based on the measurement data to obtain the values of these items so that the coefficient of determination of the measurement curve and the model curve is maximized by fitting curves of model equations to the experimental curves of the resonant frequency change as mentioned in Section 2.3.

Table 3. Setting items for drugs response analysis.

Setting items	Details
Time constant 1 T_1 (h)	Time to reach 63% of cell adhesion process
Doubling time T_2 (h)	Time for cells to double
Number of cells n_0	Number of harvest cells
Basic mass coefficient K (Hz/cell)	Basic mass per cell
Initial adhesion mass coefficient β	Cell mass sensed by the crystal oscillator sensor in the early stages of cell adhesion
Initial adhesion average time t_m (h)	Average cell sedimentation time in the early stages of cell adhesion
Initial adhesion standard deviation t_s (h)	Degree of variation in average data of cell sedimentation time in the initial stage of cell adhesion
Average response time 1 t_{m1} (h)	Average time for cells to peel and curl
Standard deviation 1 t_{s1} (h)	Degree of variation in average data for cell rounding time
Cell viability γ	Percentage of living cells after addition of anticancer drug
Addition time t_{inj} (h)	Time when anti-cancer drug was added
Mass coefficient 1 k_1	Changes in cell mass during the process of cell rounding
Average response time 2 t_{m2} (h)	Average time involved in cell contraction
Standard deviation 2 t_{s2} (h)	Degree of variation in average data of time involved in cell contraction
Mass coefficient 2 k_2	Changes in cell mass during cell contraction

5.5 Results and discussion

5.5.1 Results and discussion of evaluation and analysis of cells cultured under cisplatin

Figure 5-1 shows the changes in resonance frequency and resonance resistance with respect to the elapsed time of a cisplatin measurement experiment at a concentration of 16.7 μM. Figure 5-2 shows the diagram of the resonant frequency and resonant resistance for the same experiment. Also, changes in the cultured cells with respect to the elapsed time of the cisplatin measurement experiment at a concentration of 16.7 μM are shown. The figure shows (a) the result of cultured cells after 10 min of seeding the cells, (b) the result of cultured cells after 24 h of seeding, (c) the result of cultured cells after 24 h after adding of cisplatin, (d) the result of cultured cells after 72 h after adding of cisplatin.

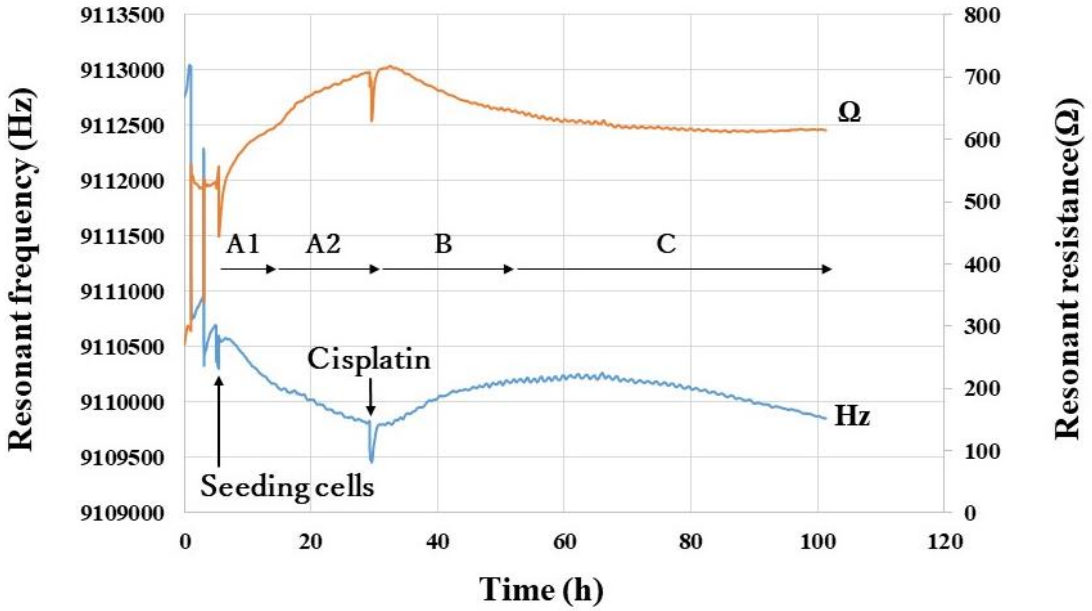

Figure 5-1. Changes in resonance frequency and resonance resistance with respect to the elapsed time of a cisplatin measurement experiment at a concentration of 16.7 μM, seeding cell densities of 0.63 × 10^3 cells/mm^2.

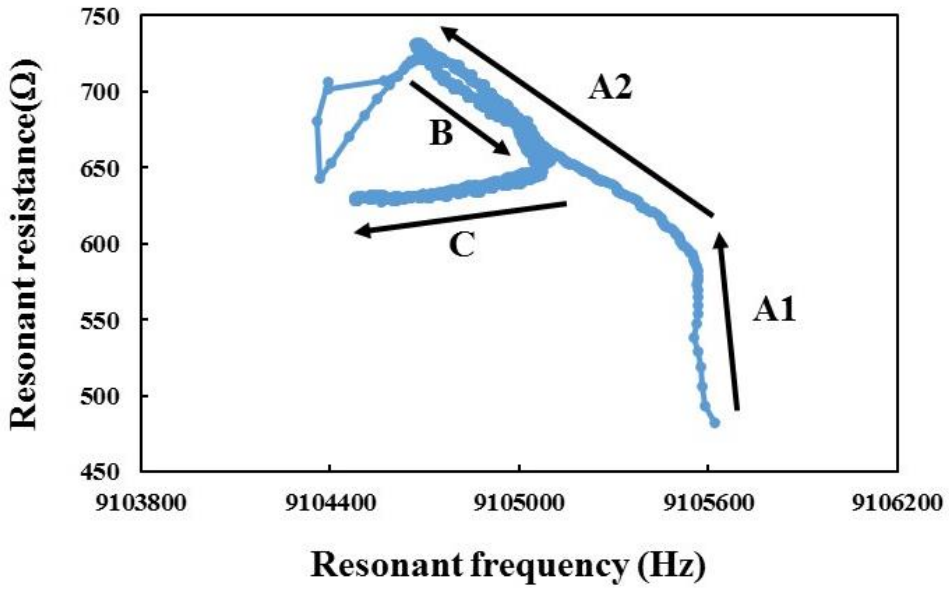

Figure 5-2. The diagram of the resonant frequency and resonant resistance of a cisplatin measurement experiment at a concentration of 16.7 μM.

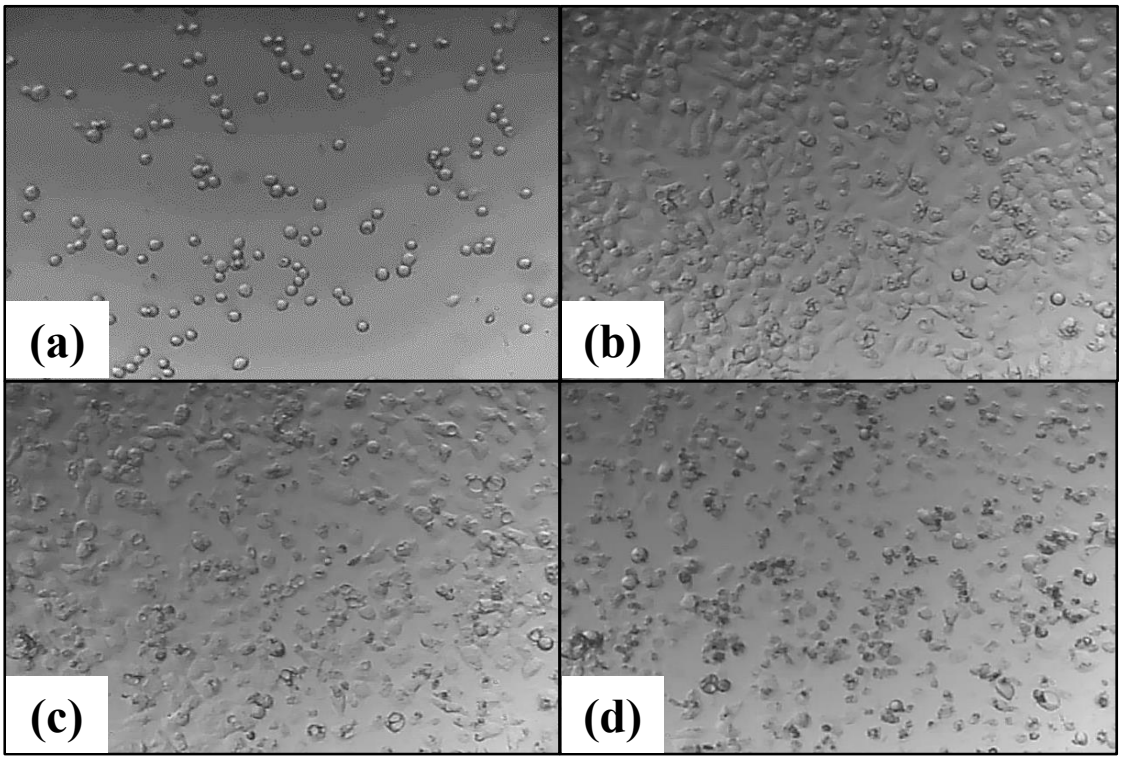

Figure 5-3. Changes in the cultured cells with respect to the elapsed time of the cisplatin measurement experiment at a concentration of 16.7 μM. (a) Result of cultured cells after 10 min of seeding the cells, (b) result of cultured cells after 24 h of seeding, (c) result of cultured cells after 24 h after adding of cisplatin, (d) result of cultured cells after 72 h after adding of cisplatin.

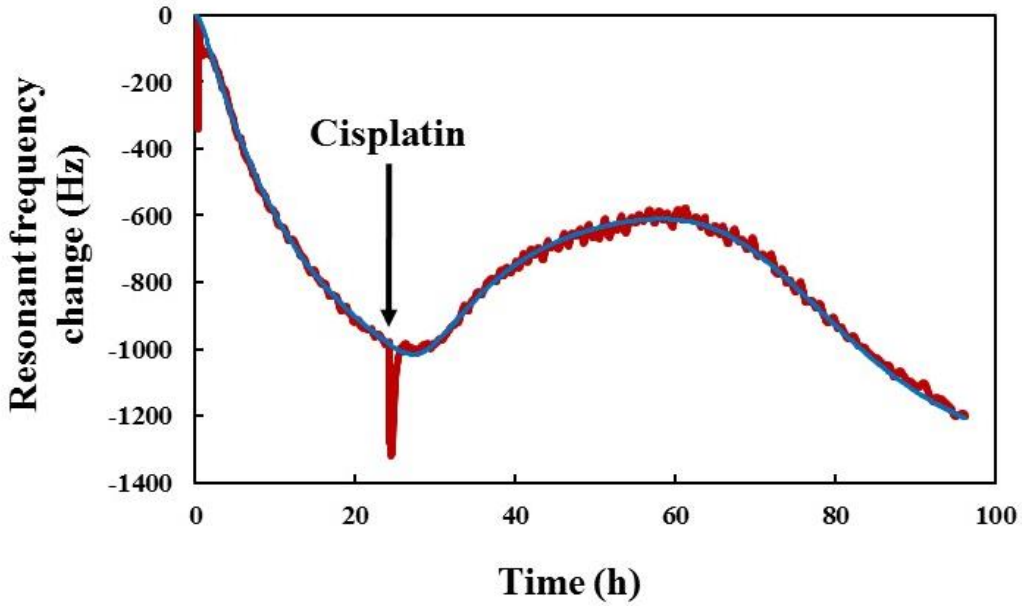

Figure 5-4. The fitting curve of the cisplatin obtained using the modeling equation of

response curves of Figure 5-1 at cisplatin concentration of 16.7 µM.

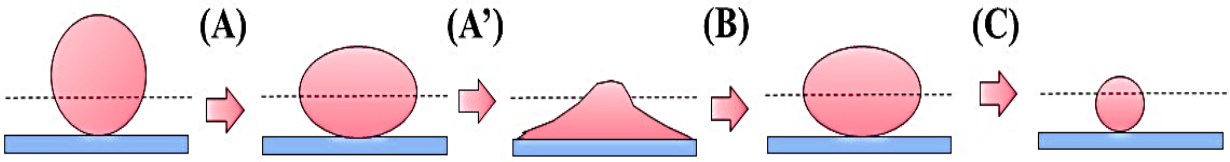

Figure 5-5. Illustration of the cell morphology change in the cell attachment process.

Table 4. Parameters used for the modeling curves in Figure 5-4 at cisplatin concentration of 16.7 µM.

Curves	$n(0)$	T_1 (h)	T_2 (h)	K (Hz/cell)	β	t_m (h)	t_s (h)
16.7 µM	460	12	65	0.82	0.2	ln(2.8)	ln(3)
83.3 µM	510	8.5	65	0.75	0.2	ln(2.8)	ln(3)

Curves	γ	k_1	t_{m1} (h)	t_{s1} (h)	k_2	t_{m2} (h)	t_{s2} (h)	R^2
16.7 µM	0.2	0.66	ln(12)	ln(2.2)	0.7	ln(54)	ln(1.25)	0.9989
83.3 µM	0.1	0.66	ln(12.5)	ln(4.2)	0.7	ln(64)	ln(1.4)	0.9989

When the measurement was made, several changes in the structure of cells over time, which were observed through the microscopic images obtained in conjunction with the measurement, as the cells began to shrink until they reached the stage of atrophy with the stop proliferation and spread, and they appear in black. This reason is attributed to programmed death or necrosis as cells are known to die as a result of their response to the antitumor drug [78, 79, 80, 81, 85, 86]. These changes correspond to the amount of changes in the resonant frequency, from which the amount of change is analyzed and the rate of cell death γ is determined.

Figure 5-2 shows the result of the resonant frequency-resonant resistance plot of cells after exposure to cisplatin. In the (part A), refers to the process of cells adhesion, in which the resonance frequency was decreased and the resonance resistance increased, this change

corresponds to the change in cells morphology as in Fig. 5-3(a, b). In particular, the resonance resistance showed a sharp increase in the initial part of the A1 part, due to the shift of cells from the spherical phase in the initial state (part A1) to the viscous, rubbery phase as seen in (part A2). This change is consistent with the change in cells adhesion reported in the literature [20,43,44]. In contrast, in the first half of the cell response to cisplatin as seen in (Part B), the change was partially reversed than in (Part A2). This change also corresponds to the change in the morphology of the cells as in Figure 5-3(b, c), this change indicates that there are many cells transformed into a spherical state while retaining their viscosity and flexibility. This change is consistent with the cell removing process reported in the literature [44], but the amount of change is lower than in the case of the literature [44], in which cells are still adherent to the ECM. In the last step (part C) the curve shows a decrease in the resonance frequency and almost no change in the resonance resistance, this change corresponds to the morphological changes of the cells in Figure 5-3(c, d). This change is due to an increase in the mass factor on the QCM surface due to the cellular decrease due to apoptosis and solidification of its molecules.

This can be explained by damage to the cells membranes, which led to the leakage of fluids inside the cells, and thus their particles became nearly semi-solid. In general, the cells remain attached to the QCM surface by the ECM. Basically, the response of cells to cisplatin can be understood as a cell necrosis or apoptosis reaction, since cisplatin binds to DNA in cells and thus disrupts cells generation leading to cells death [78−80]. The process of apoptosis is related to the cell cycle. Although the response of cells to cisplatin stresses is expected to be a first-order delay response, thus the frequency-change curve cannot be fitted through a first-order lag curve only. Cisplatin diffuses into the cell very rapidly [81]; therefore, the response does not appear to occur via the rate-controlling step. Namely, the response curve can be explained by the sum of different cells responses resulting from cell cycle shifts. Figure 5-4 shows the obtained modeling curve. The modeling curve corresponds well to the experimental data.

Table 4 shows the determined parameters of the modeling curves which were obtained from Figure 5-4. Through the parameters of Table 4 T_1, T_2, K_0, β, tm, and t_s, it is clear that attaching cells is not much different from the parameters of Table 2 in Chapter 4. In parameters of cell response to cisplatin, the survival rate is estimated as 0.2 when the cisplatin concentration is 16.7 μmol/L while it is estimated as 0.1 when the cisplatin concentration is 83.3 μmol/L. The survival rate in the reference literature [82, 83] was 0.1 to 0.9 from 10 to 150 μmol/L cisplatin. The survival rate I obtained in our analysis does not appear to be very

different from the values found in the literature, due to the variability of the rate by determination methods [86]. The reaction time course has not been extensively studied with traditional experimental methods and techniques, so QCM technique is an effective way to study the mechanism of drugs action. In Table 4, the first response parameters, tm_1, and standard deviation, ts_1, are shown to be similar for both concentrations, as for the second response parameters, the tm_2 value for a concentration of 16.7 μmol/L of cisplatin is smaller than the concentration value of 83.3 μmol/L. It is possible that these values are within the variable if the value of tm_2 does not depend on the concentration of cisplatin.

The obtained k_1 value is shown in Table 4 as 0.66 for the amplitude of the first response to cisplatin. This indicates a 66% decreasing mass effect in cells during the reverse process of cells attachment from the attached state. For the second response to cisplatin, the k_2 value obtained was 0.7. This indicates a 70% mass increase by contraction effect in the cells.

5.5.2 Simulation of responsive curve

When apoptosis begins, the frequency begins to change and this change increases with increasing cell death. By this change, the amount of cell death can be calculated which is obtained by survival rates γ. The response time for the antitumor reagent is calculated by simulation curves of the resonant frequency change for the cell response to cisplatin when cisplatin is injected 24 hours after seeding the cells, the survival rates are $\gamma = 0, 0.25, 0.5, 0.75, 1$, with which I can evaluate the antitumor reagent as Figure 5-6.

In future applications, it is possible that our obtaining the cell death ratio from the response curve will be useful in evaluating the effects of drugs. Using the other parameters, it is possible to simulate the response curve as a function of cell density and survival rate, in addition to using typical values of the parameters I was able to simulate response curves for several survival rates as in Figure 5-6.

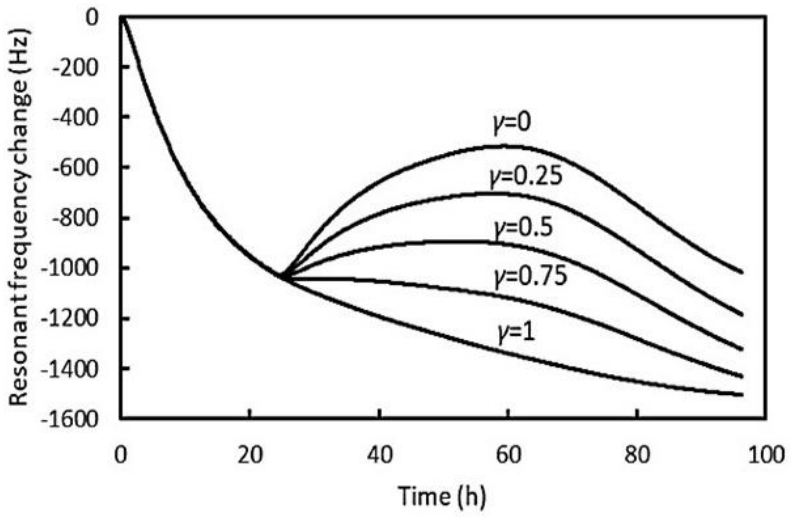

Figure 5-6. The curves simulate the change in resonant frequency of the cell response to cisplatin when cisplatin was injected 24 h after cell transplantation, survival rates are γ = 0, 0.25, 0.5, 0.75, 1.

Chapter 6: Conclusions

In this thesis, a new quartz crystal microbalance system has been developed which is considered the first method in the world. This system supports the previous methods, but uses QCM measurement technology and a micro-CMOS camera simultaneously with a model for analysis. In addition, it works with easy and low cost applications and gives quick results without exposure to experiments on humans or animals. This system can help in studying and evaluating some drugs or toxins on cultured cells and conducting preliminary tests on them in simple and quick ways, and knowing their effectiveness before applying them directly to humans or animals.

Through this system, to analyze the results and determine the relationship between the change of resonant frequency and the cell number on a QCM, the cell-cell interaction model has been proposed using the binomial equation to determine the relationship between the resonance frequency change and the number of cells on the QCM. In the proposed equation the variable mass ratio was 1.75, and the close contact probability 1/2400, which was determined to correct the resonance frequency modeling curves of the experimental results obtained. For the cell attachment process, a first-order lag response model for cell attachment was also proposed, and cell generation was also considered. The generation time T_2 = 65 to 70 h, and the constant response time T_1 = 8.5 to 16.5 h were calculated. In addition, two steps of cell response to cisplatin were observed, and log-normal distributions were applied to match both steps. The measured curves and the modeling curves are in good agreement with the two cisplatin concentration results. By fitting results, I obtained survival rates of 0.1 and 0.2 when the cisplatin concentrations were 83.3 and 16.7 μmol/L, respectively.

The results showed that QCM could be used to monitor and analyze the physical and morphological changes of cells. Through this system, chemical stresses applied directly to cells can be monitored and their effect analyzed, which helps in understanding their mechanism of action. It was found through previous experiments that:

1) Cell attachment onto the QCM surface.
2) Cells adhere to the surface.
3) Shrinkage and decrease in cell size when cisplatin is added.

For the cell attachment onto the QCM surface, when cells were seeded on the surface treated with ECM, it was confirmed that the cells were attached to the QCM surface over time of measurement. This was observed by the resonance frequency results and micrographs.

For cell adhered to the surface, all of the measurements show the changes in both the resonance frequency and the resonance resistance were observed after cells seeding and

attached to the QCM surface, the response of the cells with the ECM over time was observed through proliferation and adhesion as well as the differences in the increase in cell mass and viscosity on the surface of the QCM. This system was able to confirm the difference in the resonant frequency response and the resonant resistance according to the difference of the ECM-treated surface on the QCM. It can therefore help to study and evaluate different types of ECM and understand their mechanism of action, thus contributing to new diagnoses and potential therapeutic targets.

When cisplatin was added to cells, the micrographs showed shrinkage and decrease in cell size over time. Shrinkage and decrease in cell size on the surface is the typical cell-death process. These results found through the microscope image and QCM resonance frequency data. The images showed a typical cell-death process, in which surface adhering cells shrink and decrease, these results are consistent with changes in resonance frequency. This system was also able to monitor the life and death of programmed cells. It can help in studying and evaluating some drugs or toxins on cultured cells, and knowing their effectiveness without applying them directly to humans or animals.

I expect that more future additional experiments will provide information regarding the dependence of response model parameters on cisplatin concentration. It is necessary to work on improving the response model to be able to obtain a better fit through future studies and applying it in evaluating the effects of drugs or toxins on cultured cells.

Acknowledgment

I would like to express my sincere gratitude and appreciation to my supervisor Prof. Dr. MURAMATSU Hiroshi for providing him with ideas and guidance for recognizing my mistakes and giving me valuable suggestions and constant encouragement, had it not been for his great patience and constant encouragement, this work would not have been possible.

I would like to thank Prof. Dr. NAEMURA Kiyoshi, Prof. Dr. SUGIYAMA Tomoyasu, Prof. Dr. SASAKI Satoshi and Prof. Dr. MATSUI Takeshi for providing many advice and guidance to advance my research.

I extend my special thanks to my wife, Amnah, who has always accompanied me throughout my scholarship, helped and encouraged me during difficult times and happy times, and was patient with me despite the harsh conditions of immigration. Thanks to my children Abdulrahman, Jinan, Abdulmalik and Sahab, who spent the days of immigration with us, and made me happy with their presence with us.

I dedicate my success to the spirit of my late father, who struggled with illness throughout my scholarship until he passed away while I was far from him. I also dedicate my success to my mother, who was patient with my separation throughout my scholarship until she sees this success.

I would like to commend the scholarship from King Salman bin Abdulaziz, which provided the necessary financial support for living expenses for my living expenses, my family and my studies in Japan.

Finally, I thank the staff of the Cultural Office of the Saudi Embassy in Japan for their constant assistance and support, and everyone who contributed to this success.

Published papers

- Alsaleem, A. H. A., Ito, S., Naemura, K., & Muramatsu, H. (2021). Comparison of cultured cell attachment on a temperature-responsive polymer, poly-l-lysine, and collagen using modeling curves and a thermal-controlled quartz crystal microbalance. *Journal of Biological Physics*, 47(2), 117-129.

- Muramatsu, Hiroshi, Sae Ito, and Abdullah Hussain A. Alsaleem. "Monitoring and modeling of living cell responses in the attachment process and reaction to the antitumor reagent cisplatin studied by a quartz crystal microbalance combined with a microscope." *Analytical chemistry* 92.11 (2020): 7907-7914.

References

1. Alberts, B., Johnson, A., Lewis, J., Raff, M., Roberts, K., & Walter, P. (2002). The extracellular matrix of animals. *Molecular Biology of the Cell. 4th edition*. Garland Science: 2767-2768.
2. Folkman, Judah, and Anne Moscona. "Role of cell shape in growth control." *Nature* 273.5661 (1978): 345-349.
3. Huang, Sui, and Donald E. Ingber. "The structural and mechanical complexity of cell-growth control." *Nature cell biology* 1.5 (1999): E131-E138.
4. Hinshaw, D. B., Sklar, L. A., Bohl, B., Schraufstatter, I. U., Hyslop, P. A., Rossi, M. W., ... & Cochrane, C. G. "Cytoskeletal and morphologic impact of cellular oxidant injury." *The American journal of pathology* 123.3 (1986): 454.
5. Massia, Stephen P., and Jeffrey A. Hubbell. "Convalent surface immobilization of Arg-Gly-Asp-and Tyr-Ile-Gly-Ser-Arg-containing peptides to obtain well-defined cell-adhesive substrates." *Analytical biochemistry* 187.2 (1990): 292-301.
6. Fotakis, George, and John A. Timbrell. "In vitro cytotoxicity assays: comparison of LDH, neutral red, MTT and protein assay in hepatoma cell lines following exposure to cadmium chloride." *Toxicology letters* 160.2 (2006): 171-177.
7. Śliwka, L., Wiktorska, K., Suchocki, P., Milczarek, M., Mielczarek, S., Lubelska, K., ... & Chilmonczyk, Z. "The comparison of MTT and CVS assays for the assessment of anticancer agent interactions." *PloS one* 11.5 (2016): e0155772.
8. Zhi, Q. M., Chen, X. H., Ji, J., Zhang, J. N., Li, J. F., Cai, Q., ... & Yu, Y. Y. "Salinomycin can effectively kill ALDHhigh stem-like cells on gastric cancer." *Biomedicine & Pharmacotherapy* 65.7 (2011): 509-515.
9. Xu, F. Y., Shang, W. Q., Yu, J. J., Sun, Q., Li, M. Q., & Sun, J. S. "The antitumor activity study of ginsenosides and metabolites in lung cancer cell." *American journal of translational research* 8.4 (2016): 1708.
10. Kaneshiro, E. S., Wyder, M. A., Wu, Y. P., & Cushion, M. T. Reliability of calcein acetoxy methyl ester and ethidium homodimer or propidium iodide for viability assessment of microbes. *Journal of microbiological methods*, 17(1), (1993):1-16.
11. Papadopoulos, N. G., Dedoussis, G. V., Spanakos, G., Gritzapis, A. D., Baxevanis, C. N., & Papamichail, M. "An improved fluorescence assay for the determination of lymphocyte-mediated cytotoxicity using flow cytometry". *Journal of immunological methods*, 177(1-2), (1994):101-111.
12. Li, X., Tian, M., Zhang, G. E., Zhang, R., Feng, R., Guo, L., ... & He, X. "Spatially dependent fluorescent probe for detecting different situations of mitochondrial membrane potential conveniently and efficiently." *Analytical chemistry* 89.6 (2017): 3335-3344.
13. Sauerbrey, G. J. Z. P. "The use of quarts oscillators for weighing thin layers and for microweighing." *Z. Phys.* 155 (1959): 206-222.
14. Redepenning, J., Schlesinger, T. K., Mechalke, E. J., Puleo, D. A., & Bizios, R. "Osteoblast attachment monitored with a quartz crystal microbalance." *Analytical chemistry* 65.23 (1993): 3378-3381.
15. Gryte, David M., Michael D. Ward, and Wei Shou Hu. "Real-time measurement of anchorage-dependent cell adhesion using a quartz crystal microbalance." *Biotechnology progress* 9.1 (1993): 105-108.
16. Li, J., Thielemann, C., Reuning, U., & Johannsmann, D. "Monitoring of integrin-mediated adhesion of human ovarian cancer cells to model protein surfaces by quartz

crystal resonators: evaluation in the impedance analysis mode." *Biosensors and Bioelectronics* 20.7 (2005): 1333-1340.

17. Chronaki, D., Stratiotis, D. I., Tsortos, A., Anastasiadou, E., & Gizeli, E. "Screening between normal and cancer human thyroid cells through comparative adhesion studies using the Quartz Crystal Microbalance." *Sensing and Bio-Sensing Research* 11 (2016): 99-106.
18. Kao, W. L., Chang, H. Y., Lin, K. Y., Lee, Y. W., & Shyue, J. J. "Effect of surface potential on the adhesion behavior of NIH3T3 cells revealed by quartz crystal microbalance with dissipation monitoring (QCM-D)." *The Journal of Physical Chemistry C* 121.1 (2017): 533-541.
19. Kang, H. W., Otani, N., Hiroshi, M., Chang, S. M., & Kim, J. M. "Investigation of the extracellular matrix effect for the QCM/CCD cell activity monitoring system." *Journal of nanoscience and nanotechnology* 18.8 (2018): 5777-5784.
20. Zhou, T., Marx, K. A., Dewilde, A. H., McIntosh, D., & Braunhut, S. J. "Dynamic cell adhesion and viscoelastic signatures distinguish normal from malignant human mammary cells using quartz crystal microbalance." *Analytical biochemistry* 421.1 (2012): 164-171.
21. Nomura, T., and M. Okuhara. "Frequency shifts of piezoelectric quartz crystals immersed in organic liquids." *Analytica Chimica Acta* 142 (1982): 281-284.
22. Bruckenstein, Stanley, and Michael Shay. "Experimental aspects of use of the quartz crystal microbalance in solution." *Electrochimica Acta* 30.10 (1985): 1295-1300.
23. Hager, Harold E. "Fluid property evaluation by piezoelectric crystals operating in the thickness shear mode." *Chemical Engineering Communications* 43.1-3 (1986): 25-38.
24. Muramatsu, Hiroshi, Eiichi Tamiya, and Isao Karube. "Computation of equivalent circuit parameters of quartz crystals in contact with liquids and study of liquid properties." *Analytical Chemistry* 60.19 (1988): 2142-2146.
25. Muramatsu, H., Ye, X., Suda, M., Sakuhara, T., & Ataka, T. "In-situ monitoring of microrheology on electrochemical deposition using an advanced quartz crystal analyzer and its application to polypyrrole deposition." *Journal of Electroanalytical Chemistry* 322.1-2 (1992): 311-323.
26. Muramatsu, Hiroshi, and Kazuhiko Kimura. "Quartz crystal detector for microrheological study and its application to phase transition phenomena of Langmuir-Blodgett films." *Analytical Chemistry* 64.21 (1992): 2502-2507.
27. Muramatsu, Hiroshi, Xuanjing Ye, and Tatsuaki Ataka. "Micro-rheology changes of Nafion® films with electrochemical mass-transport in hydroquinone solutions and in situ measurement using a quartz crystal analyzer." *Journal of Electroanalytical Chemistry* 347.1-2 (1993): 247-255.
28. Rodahl, Michael, Fredrik Höök, and Bengt Kasemo. "QCM operation in liquids: An explanation of measured variations in frequency and Q factor with liquid conductivity." *Analytical Chemistry* 68.13 (1996): 2219-2227.

29. Redepenning, J., Schlesinger, T. K., Mechalke, E. J., Puleo, D. A., & Bizios, R. "Osteoblast attachment monitored with a quartz crystal microbalance." *Analytical chemistry* 65.23 (1993): 3378-3381.

30. Gryte, David M., Michael D. Ward, and Wei Shou Hu. "Real-time measurement of anchorage-dependent cell adhesion using a quartz crystal microbalance." *Biotechnology progress* 9.1 (1993): 105-108.

31. Wegener, Joachim, Andreas Janshoff, and H-J. Galla. "Cell adhesion monitoring using a quartz crystal microbalance: comparative analysis of different mammalian cell lines." *European biophysics journal* 28.1 (1998): 26-37.

32. Wegener, J., Seebach, J., Janshoff, A., & Galla, H. J. "Analysis of the composite response of shear wave resonators to the attachment of mammalian cells." *Biophysical journal* 78.6 (2000): 2821-2833.

33. Kang, H. W., Ida, K., Yamamoto, Y., & Muramatsu, H. "Monitoring of morphology and physical properties of cultured cells using a micro camera and a quartz crystal with transparent indium tin oxide electrodes after injections of glutaraldehyde and trypsin." *Analytica chimica acta* 624.1 (2008): 154-161.

34. Watarai, E., Matsuno, R., Konno, T., Ishihara, K., & Takai, M. "QCM-D analysis of material–cell interactions targeting a single cell during initial cell attachment." *Sensors and Actuators B: Chemical* 171 (2012): 1297-1302.

35. Chen, Jennifer Y., Lynn S. Penn, and Jun Xi. "Quartz crystal microbalance: Sensing cell-substrate adhesion and beyond." *Biosensors and Bioelectronics* 99 (2018): 593-602.

36. Rodahl, M., Höök, F., Fredriksson, C., Keller, C. A., Krozer, A., Brzezinski, P., ... & Kasemo, B. "Simultaneous frequency and dissipation factor QCM measurements of biomolecular adsorption and cell adhesion." *Faraday discussions* 107 (1997): 229-246.

37. Fredriksson, C., Khilman, S., Kasemo, B., & Steel, D. M. "In vitro real-time characterization of cell attachment and spreading." *Journal of Materials Science: Materials in Medicine* 9.12 (1998): 785-788.

38. Fohlerová, Zdenka, Petr Skládal, and Jaroslav Turánek. "Adhesion of eukaryotic cell lines on the gold surface modified with extracellular matrix proteins monitored by the piezoelectric sensor." *Biosensors and Bioelectronics* 22.9-10 (2007): 1896-1901.

39. Lord, M. S., Modin, C., Foss, M., Duch, M., Simmons, A., Pedersen, F. S., ... & Milthorpe, B. K. "Extracellular matrix remodelling during cell adhesion monitored by the quartz crystal microbalance." *Biomaterials* 29.17 (2008): 2581-2587.

40. Molino, P. J., Yue, Z., Zhang, B., Tibbens, A., Liu, X., Kapsa, R. M., ... & Wallace, G. G. "Influence of Biodopants on PEDOT Biomaterial Polymers: Using QCM□D to Characterize Polymer Interactions with Proteins and Living Cells." *Advanced Materials Interfaces* 1.3 (2014): 1300122.

41. Noiri, M., Kushiro, K., Togo, S., Sato, K., Yoshikawa, H. Y., Takai, M., & Teramura, Y. "Influence of cell adhesive molecules attached onto PEG-lipid-modified fluid surfaces on cell adhesion." *Colloids and Surfaces B: Biointerfaces* 175 (2019): 375-383.

42. Zhou, T., Marx, K. A., Warren, M., Schulze, H., & Braunhut, S. J. "The quartz crystal microbalance as a continuous monitoring tool for the study of endothelial cell surface attachment and growth." *Biotechnology Progress* 16.2 (2000): 268-277.

43. Marx, K. A., Zhou, T., Montrone, A., Schulze, H., & Braunhut, S. J. "A quartz crystal microbalance cell biosensor: detection of microtubule alterations in living cells at nM nocodazole concentrations." *Biosensors and Bioelectronics* 16.9-12 (2001): 773-782.

44. Marx, K. A., Zhou, T., Montrone, A., McIntosh, D., & Braunhut, S. J. "Quartz crystal microbalance biosensor study of endothelial cells and their extracellular matrix following cell removal: Evidence for transient cellular stress and viscoelastic changes during detachment and the elastic behavior of the pure matrix." *Analytical Biochemistry* 343.1 (2005): 23-34.

45. Marx, K. A., Zhou, T., Montrone, A., McIntosh, D., & Braunhut, S. J. "A comparative study of the cytoskeleton binding drugs nocodazole and taxol with a mammalian cell quartz crystal microbalance biosensor: Different dynamic responses and energy dissipation effects." *Analytical biochemistry* 361.1 (2007): 77-92.

46. Wei, X. L., Mo, Z. H., Li, B., & Wei, J. M. "Disruption of HepG2 cell adhesion by gold nanoparticle and Paclitaxel disclosed by in situ QCM measurement." *Colloids and Surfaces B: Biointerfaces* 59.1 (2007): 100-104.

47. Kang, H. W., & Muramatsu, H. "Monitoring of cultured cell activity by the quartz crystal and the micro CCD camera under chemical stressors." *Biosensors and Bioelectronics* 24.5 (2009): 1318-1323.

48. Tan, L., Jiang, X., Zhang, Y., Tang, H., Yao, S., & Xie, Q. "In vitro study on the individual and synergistic cytotoxicity of adriamycin and selenium nanoparticles against Bel7402 cells with a quartz crystal microbalance." *Biosensors and Bioelectronics* 24.7 (2009): 2268-2272.

49. Kang, H. W., Muramatsu, H., Lee, B. J., & Kwon, Y. S. "Monitoring of anticancer effect of cisplatin and 5-fluorouracil on HepG2 cells by quartz crystal microbalance and micro CCD camera." *Biosensors and Bioelectronics* 26.4 (2010): 1576-1581.

50. Wang, G.; Dewilde, A. H.; Zhang, J.; Pal, A.; Vashist, M.; Bello, D.; Marx, K. A.; Braunhut, S. J.; Therrien, J. M. A living cell quartz crystal microbalance biosensor for continuous monitoring of cytotoxic responses of macrophages to single-walled carbon nanotubes. *Particle and fibre toxicology* 8.1 (2011): 1-17

51. Fatisson, Julien, Fereshteh Azari, and Nathalie Tufenkji. "Real-time QCM-D monitoring of cellular responses to different cytomorphic agents." *Biosensors and Bioelectronics* 26.7 (2011): 3207-3212.

52. Tymchenko, N., Nilebäck, E., Voinova, M. V., Gold, J., Kasemo, B., & Svedhem, S. "Reversible changes in cell morphology due to cytoskeletal rearrangements measured in real-time by QCM-D." *Biointerphases* 7.1 (2012): 43.

53. Alessandrini, A., Croce, M. A., Tiozzo, R., & Facci, P. "Monitoring cell-cycle-related viscoelasticity by a quartz crystal microbalance." *Applied physics letters* 88.8 (2006): 083905.

54. Lee, D. Y., Kang, H. W., Kaneko, S., Kwon, Y. S., & Muramatsu, H. "Direct monitoring of paraquat induced cell death using quartz crystal sensor." *Thin Solid Films* 518.2 (2009): 707-710.

55. Marx, K. A., Zhou, T., Warren, M., & Braunhut, S. J. "Quartz crystal microbalance study of endothelial cell number dependent differences in initial adhesion and steady□state behavior: Evidence for cell□cell cooperativity in initial adhesion and spreading." *Biotechnology progress* 19.3 (2003): 987-999.

56. Zhou, T., Marx, K. A., Dewilde, A. H., McIntosh, D., & Braunhut, S. J. "Dynamic cell adhesion and viscoelastic signatures distinguish normal from malignant human mammary cells using quartz crystal microbalance." *Analytical biochemistry* 421.1 (2012): 164-171.

57. Ozawa, S., Sugiyama, Y., Mitsuhashi, J., & Inaba, M. "Kinetic analysis of cell killing effect induced by cytosine arabinoside and cisplatin in relation to cell cycle phase specificity in human colon cancer and Chinese hamster cells." *Cancer research* 49.14 (1989): 3823-3828.

58. Montalenti, F., Sena, G., Cappella, P., & Ubezio, P. "Simulating cancer-cell kinetics after drug treatment: application to cisplatin on ovarian carcinoma." *Physical Review E* 57.5 (1998): 5877.

59. Arias, L. Renea, Carla A. Perry, and Liju Yang. "Real-time electrical impedance detection of cellular activities of oral cancer cells." *Biosensors and Bioelectronics* 25.10 (2010): 2225-2231.

60. Mason, Warren P., and Hans Baerwald. "Piezoelectric crystals and their applications to ultrasonics." *Physics Today* 4.5 (1951): 23.

61. Bottom, V. E. "Introduction to quartz crystal unit design" Van Nostrand Reinhold Co." (1982) : 13-16

62. Elmlund, L., Käck, C., Aastrup, T., & Nicholls, I. A. "Study of the interaction of trastuzumab and SKOV3 epithelial cancer cells using a quartz crystal microbalance sensor." *Sensors* 15.3 (2015): 5884-5894.

63. Latif, U., Can, S., Hayden, O., Grillberger, P., & Dickert, F. L. "Sauerbrey and anti-Sauerbrey behavioral studies in QCM sensors—Detection of bioanalytes." *Sensors and Actuators B: Chemical* 176 (2013): 825-830.

64. Xiao, X., Guo, M., Li, Q., Cai, Q., Yao, S., & Grimes, C. A. "In-situ monitoring of breast cancer cell (MCF-7) growth and quantification of the cytotoxicity of anticancer drugs fluorouracil and cisplatin." *Biosensors and Bioelectronics* 24.2 (2008): 247-252.

65. Galli Marxer, C., Collaud Coen, M., Greber, T., Greber, U. F., & Schlapbach, L. "Cell spreading on quartz crystal microbalance elicits positive frequency shifts indicative of viscosity changes." *Analytical and bioanalytical chemistry* 377.3 (2003): 578-586.

66. Zhou, T., Marx, K. A., Dewilde, A. H., McIntosh, D., & Braunhut, S. J. "Dynamic cell adhesion and viscoelastic signatures distinguish normal from malignant human

mammary cells using quartz crystal microbalance." *Analytical biochemistry* 421.1 (2012): 164-171.

67. Tan, L., Jiang, X., Zhang, Y., Tang, H., Yao, S., & Xie, Q. "In vitro study on the individual and synergistic cytotoxicity of adriamycin and selenium nanoparticles against Bel7402 cells with a quartz crystal microbalance." *Biosensors and Bioelectronics* 24.7 (2009): 2268-2272.
68. Nowacki, L., Follet, J., Vayssade, M., Vigneron, P., Rotellini, L., Cambay, F., ... & Rossi, C. "Real-time QCM-D monitoring of cancer cell death early events in a dynamic context." *Biosensors and Bioelectronics* 64 (2015): 469-476.
69. Williams, C., Quinn, K. P., Georgakoudi, I., & Black III, L. D. "Young developmental age cardiac extracellular matrix promotes the expansion of neonatal cardiomyocytes in vitro." *Acta biomaterialia* 10.1 (2014): 194-204.
70. Lam, A. T. L., Li, J., Chen, A. K. L., Reuveny, S., Oh, S. K. W., & Birch, W. R. "Cationic surface charge combined with either vitronectin or laminin dictates the evolution of human embryonic stem cells/microcarrier aggregates and cell growth in agitated cultures." *Stem cells and development* 23.14 (2014): 1688-1703.
71. Dorenvanck, K. M. "*Micropatterns on Polyacrylamide Hydrogel for Controlled Cardiomyocyte Attachment using PLL-PEG and ECM Proteins*". MS thesis. University of Twente, 2019.
72. Akiyama, Y., Kikuchi, A., Yamato, M., & Okano, T. "Ultrathin poly (N-isopropylacrylamide) grafted layer on polystyrene surfaces for cell adhesion/detachment control." *Langmuir* 20.13 (2004): 5506-5511.
73. Nishimura, A., Nakajima, R., Takagi, R., Zhou, G., Suzuki, D., Kiyama, M., ... & Takeda, S. "Fabrication of tissue-engineered cell sheets by automated cell culture equipment." *Journal of tissue engineering and regenerative medicine* 13.12 (2019): 2246-2255.
74. Muramatsu, Hiroshi, Sae Ito, and Abdullah Hussain A. Alsaleem. "Monitoring and Modeling of Living Cell Responses in the Attachment Process and Reaction to the Antitumor Reagent Cisplatin Studied by a Quartz Crystal Microbalance Combined with a Microscope." *Analytical chemistry* 92.11 (2020): 7907-7914.
75. Alsaleem, A. H. A., Ito, S., Naemura, K., & Muramatsu, H. "Comparison of cultured cell attachment on a temperature-responsive polymer, poly-l-lysine, and collagen using modeling curves and a thermal-controlled quartz crystal microbalance." *Journal of Biological Physics* 47.2 (2021): 117-129
76. Ferlay J ،Ervik M ،Lam F ،Colombet M ،Mery L ،Piñeros M ،Znaor A ،

Soerjomataram I ،Bray F. Global Cancer Observatory: Cancer Today. Lyon: International Agency for Research on Cancer; 2020 (https://gco.iarc.fr/today, accessed February 2021).

77. Dasari, Shaloam, and Paul Bernard Tchounwou. "Cisplatin in cancer therapy: molecular mechanisms of action." *European journal of pharmacology* 740 (2014): 364-378.
78. Rosenberg, B., Vancamp, L., Trosko, J. E., & Mansour, V. H. "Platinum compounds: a new class of potent antitumour agents." *Nature* 222.5191 (1969): 385-386.
79. Harder, Harold C., and Barnett Rosenberg. "Inhibitory effects of anti□tumor platinum compounds on DNA, RNA and protein syntheses in mammalian cells in vitro." *International Journal of Cancer* 6.2 (1970): 207-216.
80. Van Cruchten, Steven, and Wim Van Den Broeck. "Morphological and biochemical aspects of apoptosis, oncosis and necrosis." *Anatomia, histologia, embryologia* 31.4 (2002): 214-223.
81. Eljack, N. D.; Ma, H.-Y. M.; Drucker, J.; Shen, C.; Hambley, T. W.; New, E. J.; Friedrich, T.; Clarke, R. J. Metallomics. "Mechanisms of cell uptake and toxicity of the anticancer drug cisplatin." *Metallomics* 6.11 (2014): 2126-2133.
82. Furusawa, C., Suzuki, T., Kashiwagi, A., Yomo, T., & Kaneko, K. "Ubiquity of log-normal distributions in intra-cellular reaction dynamics." *Biophysics* 1 (2005): 25-31.
83. Serpeloni, J. M., Barcelos, G. R. M., Angeli, J. P. F., Mercadante, A. Z., Bianchi, M. L. P., & Antunes, L. M. G. "Dietary carotenoid lutein protects against DNA damage and alterations of the redox status induced by cisplatin in human derived HepG2 cells." *Toxicology in Vitro* 26.2 (2012): 288-294.
84. Zhang, K., Chew, M., Yang, E. B., Wong, K. P., & Mack, P. "Modulation of cisplatin cytotoxicity and cisplatin-induced DNA cross-links in HepG2 cells by regulation of glutathione-related mechanisms." *Molecular pharmacology* 59.4 (2001): 837-843.
85. Eastman, Alan. "The mechanism of action of cisplatin: from adducts to apoptosis. Chemistry and biochemistry of a leading anticancer drug." *Verlag Helvetica Chimica Acta*, (1999): 111-134.
86. Gonzalez, V. M., Fuertes, M. A., Alonso, C., & Perez, J. M. "Is cisplatin-induced cell death always produced by apoptosis?." *Molecular pharmacology* 59.4 (2001): 657-663.

Appendices

Appendix 1:

Operation manual for sputtering equipment (CFS-4ES)

1 Outline of the device

1-1 Front view of sputtering equipment

Figure 1-1 Front view of CFS-4ES.

1-2 Front view of RF power supply

Figure 1-2 Front view of RF power supply.

2 Operation method

2-1 Start of exhaust system

① Open the water supply valve (0.2 to 0.3 MPa) and supply cooling water to the device.

(2) Turn on the power breakers on the wall surface (two places) to supply power to the device.

③ Pull-out valve (Fig. 1-1 ⑥), auxiliary valve (Fig. 1-1 ⑧), roughing valve (Fig. 1-1 ⑦), chamber leak valve (Fig. 1-1 ⑩), gas introduction valve (Fig. 1-1 ⑪), after confirming that the rotary pump leak valve (Fig. 1-1 ⑰) and turbo pump leak valve (Fig. 1-1 ⑱) are all closed, turn on the power breaker (Fig. 1-1 ①) of the device. .. (The power POWER lamp (Fig. 1-1 (2)) lights up).

④ When the rotary pump switch (Fig. 1-1 ③) is turned on, the lamp lights up.

⑤ When the operating noise stabilizes, open the auxiliary valve and exhaust the turbo pump.

Note) Before turning on the turbo pump, turn on the turbo pump OK (Fig. 1-1 ⑤) Lamp lights up to confirm. If the turbo pump ON OK lamp does not light, check the following items.

① Is cooling water flowing in the turbo pump?

(2) Is setting 1 of PG2 (Pirani vacuum gauge (Fig. 1-1 ⑫)) turned on?

Note) When turning on the turbo pump, make sure that the internal pressure of the pump is 100 Pa or less.

⑥ After confirming the above precautions, turn on the turbo pump switch (Fig. 1-1 ④). Make sure the turbo controller display is LOCAL and press START.

★ When the number of revolutions exceeds 800 rpm, the exhaust system is ready.

2-2 Sample installation
(1) Make sure the Pull-out valve and roughing valve are closed.
(2) Open the main plug of the N2 gas cylinder and adjust the gas pressure to 0.1 MPa with a regulator.
③ Open the chamber leak valve and let N2 gas flow.
When you hear the gas leaking, close the chamber leak valve.
★ Atmospheric pressure inside the chamber allows samples to be taken in and out.
④ Attach the sample to the holder and close the lid.

2-3 Vacuum tank exhaust
① Close the auxiliary valve and open the roughing valve.
When the inside of the vacuum chamber is exhausted and becomes 2 KPa or less, the pointer of the Pirani vacuum gauge starts to move.
PG1 exhaust (inside the chamber) lights up when SET1 is (about 100Pa).
Note) If the degree of vacuum does not rise, press the lid of the vacuum chamber for a few seconds.
② Wait for a few minutes after SET1 of PG1 lights up.
Then close the roughing valve and open the auxiliary valve.
* The reason why the roughing valve is not closed immediately is that gas is released from the vacuum chamber and the sample.
③ After confirming that the turbo pump ON OK lamp is lit and that the rotation speed of the turbo controller has reached 48000 rpm, open the main valve.
④ Turn on the POWER of the ionization vacuum gauge IG1 (Fig. 1-1 ⑬), and turn on Filament (green button) after the change in the numerical value has subsided.
* If an error occurs, press OFF (red button) once, and then press ON again.
⑤ Wait until the pressure drops below 3×10^{-3} Pa. (15-20 minutes)
⑥ Turn off Filament when it becomes 3×10-3 Pa or less.

2-4 RF sputtering

Target	Membrane formation rate [nm/min]	Gas used (introduction amount)
Ti	3.5□	Ar (21.0)
Cr	7	
Au	20.5	
SiO_2	3	Ar (21.0) O_2 (0.20)
TiO_2	1.3	
ITO	10	

① Open the main plug of the gas cylinder according to the target to be used, and adjust the gas pressure with the regulator. (Both pressures are 0.25 to 0.30 MPa)
② Open the gas introduction valve and turn the knob of the mass control box to adjust the amount of gas introduced.
③ After adjusting the gas introduction amount, turn on the Filament of IG1 and wait for a few minutes until it stabilizes at a vacuum degree of about 0.5 to 0.6 Pa.
Note) When flowing O2, immediately after checking the degree of vacuum to protect the Filament.
Turn off Filament and perform subsequent operations with Filament OFF.
④ Turn the P-GUN cooling water valve (Fig. 1-1 ⑤⓪) at the bottom left of the front of the device upward on both the left and right sides. This prepares the target for cooling water. (Water does not flow unless the SPUTTER INTERLOCK OK switch is pressed)
⑤ The chamber cooling water valve (Fig. 1-1 ○ 51) and the etching table cooling water valve (Fig. 1-1 ○ 52) also flow cooling water upward on both the left and right sides.
Note) Be sure to check if the pressure of the cooling water has dropped. (0.2-0.3 MPa)

⑥ Press and hold the SPUTTER INTERLOCK OK switch (Fig. 1-1 ㉓) to turn on the lamp.
Note) If the lamp does not light up, check the following items.
① Is the cooling water flowing sufficiently?
② Is the safety cover firmly attached?
(7) Target selection Select the target number for RF sputtering with the shutter and P-GUN switch.
Note) When changing the target number with the P-GUN switch, be sure to pull the handle toward you before rotating it. If you rotate it forcibly, the shaft will be damaged.
⑧ Turn on JIG ROTATION and set the rotation speed to 20 rpm.
⑨ Adjust MATCHING and TUNING. (Refer to the magnet sheet for the value)
⑩ Turn on the POWER switch of the RF power supply (Fig. 1-1 ○ 60).
⑪ When the RF ON switch (Fig. 1-1 ○ 61) is pressed, the ON lamp lights up and the RF power supply oscillates.
⑫ Turn the POWER CONT (Fig. 1-1 ○ 62) dial to set FORWARD POWER to about 30W, and press the SPUTTER INTERLOCK OK switch. The glow starter lights up and discharge starts. Confirm that REFLECTED POWER becomes 0.
★ If REFLECTED POWER does not reach 0 (discharge does not start), refer to "3 Supplement".
⑬ Turn the POWER CONT dial to set it to the specified value. (100 W)
⑭ Rematch so that REFLECTED POWER is minimized.

(FORWARD POWER: REFLECTED POWER = 10: 1 or less)

⑮ Set the SPUTTER TIMER (Fig. 1-1 ㉔) according to the target film thickness.

⑯ Turn the shutter open / close knob (Fig. 1-1 ㉚) to open the shutter.

Start sputtering.

⑰ Immediately turn on the switch of SPUTTER TIMER.

⑱ When the sputtering is completed and the buzzer sounds for a few seconds, close the shutter.

⑲ Turn off the IG1 Filament and turn off the IG1 power.

⑳ Turn off JIG ROTATION, stop the rotation of the jig, and return the rotation speed dial to 0.

㉑ Return the POWER CONT dial to 0.

㉒ Close the gas introduction valve. Twice

★ When performing continuous sputtering work, repeat the operations of "2 Operation method" 2-3 to 2-5 as necessary.
When performing continuous sputtering by switching only the target: 2-4 → 2-4 → 2-5
When performing sputtering again after exchanging the sample: 2-4 → 2-5 → 2-3 → 2-4 → 2-5

★ If you do not want to perform continuous sputtering, return the dial to 0 with ㉑ and then turn off the main power of the RF device.

2-5 Leakage in vacuum tank, sample removal

① Close the main valve.

② Open the chamber leak valve and let N2 gas flow.

③ Take out the sample when the vacuum chamber reaches atmospheric pressure.

* When performing sputtering again, attach the sample to the holder and close the lid.

2-6 Stopping the device

① Perform the operation of "2-3 Exhaust of vacuum chamber (page 97)" to exhaust the inside of the vacuum chamber.

② Turn off the POWER of IG1.

③ Close the main valve.

④ Press STOP on the turbo controller and wait until the turbo pump stops. (About 5 minutes)

⑤ After stopping the turbo pump, close the auxiliary valve.

⑥ Turn off the turbo pump switch.

⑦ Open the turbo pump leak valve (Fig. 1-1 ⑱) and introduce N2 gas into the turbo pump. After about 20 seconds, close the turbopump leak valve.

⑧ Turn off the rotary pump switch.

⑨ Open the rotary pump leak valve and introduce N2 gas into the rotary pump. After about 10 seconds, close the turbopump leak valve.

⑩ Make sure that all valves are completely closed and all pumps are turned off, and then turn off the power breaker of the device.

⑪ Close the main plug of the used gas (N2, Ar, O2).

⑫ Close the P-GUN cooling water valve, chamber cooling water valve, and table cooling water valve, and close the main cooling water valve.

⑬ Turn off the power breaker on the wall.

3 Supplement

3-1 When discharge does not start in ⑫ of "2-4 RF sputtering"

① Press the SPUTTER INTERLOCK OK switch at the same time as opening the shutter, and close the shutter immediately. If the discharge still does not start, perform ②.

② Close the gas introduction valve once, wait for a few seconds, and then open the gas introduction valve again.

3-2 Processing at the time of power failure

① Close the main valve.

② Close the gas introduction valve.

③ Close the auxiliary valve and roughing valve.

④ Turn off the switches of the rotary pump and turbo pump.

⑤ Wait until the turbo pump stops. (About 10 minutes)

⑥ Open the turbo pump leak valve.

⑦ Open the rotary pump leak valve.

3-3 Target replacement procedure * Be sure to turn off the power.

① Turn the P-GUN cooling water valve downward. (Cooling water in the target is discharged)

(2) Open the main plug of the N2 gas cylinder and adjust the gas pressure to 0.1 MPa with a regulator.

③ Open the chamber leak valve and let N2 gas flow.

When you hear the gas leaking, close the chamber leak valve and open the sample chamber.

④ Remove the cover on the main valve and cover it with aluminum foil to prevent water from entering.

⑤ Remove the shutter, shutter plate, anode, and target in this order with a hexagon.

⑥ If there is dirt, wipe it off with alcohol and reapply grease to the O-ring.

⑦ Reassemble in order.

Install the shutter at a position slightly away from the shutter plate.

Please note that the shutter cannot be opened and closed smoothly if they are in close contact with each other.

Don't forget to change the target display magnet.

Appendix 2:

The ITO electrode film formation, optimization, and setting conditions

Sample	A1	A2	A3	B1	B2	B3	C1	C2	C3	D1	D2	D3	A0
Ar	21MPa												-
O_2	0.2MPa												-
Watt	400W												-
Spattering Time	40m			20m			15m			10m			-
Ω	5 ～ 8Ω	5 ～ 7Ω	4.5 ～ 5Ω	11～13Ω	11～13Ω	11～13Ω	16～19Ω	16～20Ω	16～19Ω	23～26Ω	25～28Ω	25～28Ω	-
Transmittance%	63.04%	65.01%	60.48%	69.63%	67.89%	70.55%	73.42%	71.97%	73.1%	75.32%	74.37%	75.73%	91.32%
Heat Treatment time	3h												-
Heat Treatment temperature	200℃	160℃	120℃	200℃	160℃	120℃	200℃	160℃	120℃	200℃	160℃	120℃	-
Ω after Heat Treatment	4.5 ～14Ω	3.5 ～ 6Ω	3.5 ～4.5Ω	160～460Ω	12～14Ω	11～13Ω	1450～2700Ω	22～26Ω	17～18Ω	900～2300Ω	33～45Ω	26～30Ω	-
Transmittance% after Heat Treatment	70.75%	67.84%	63.127%	73.34%	69.76%	71.63%	75.89%	73.40%	73.44%	73%	75.45%	75.88%	-

ITO Film transmittance results

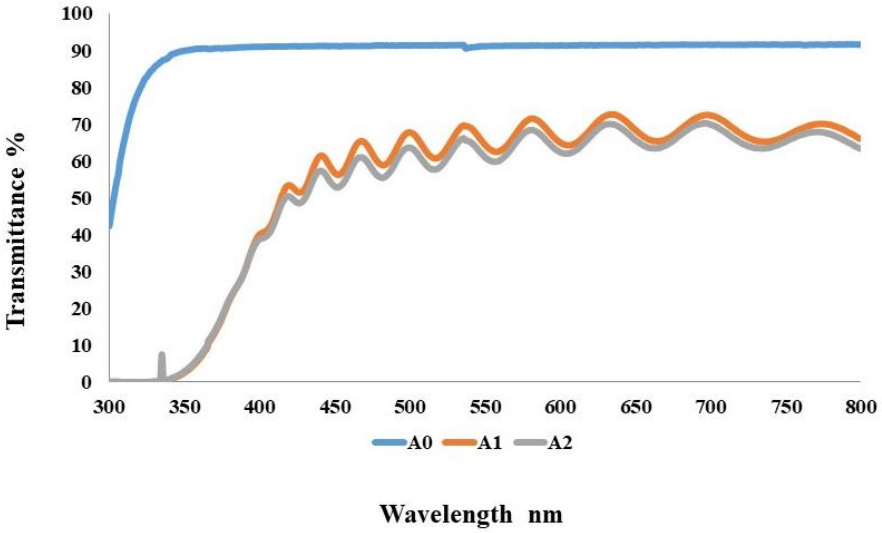

(a) ITO Film transmittance results, the condition of spattering when 400 W, A0 when no film.

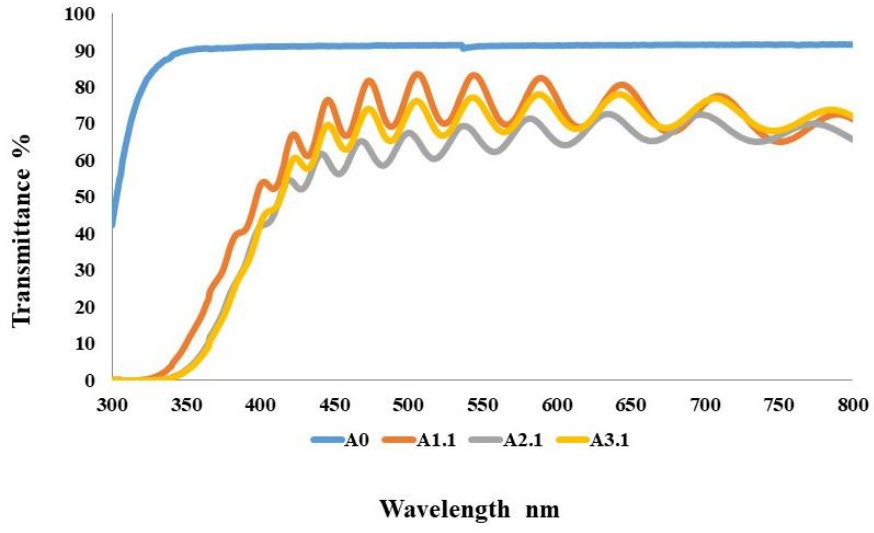

(b) ITO Film transmittance results after heat treatment , the condition of spattering when 400 W and the heat treatment temperature when A1: 200℃, A2: 120℃, A3: 160℃, A0 when no film.

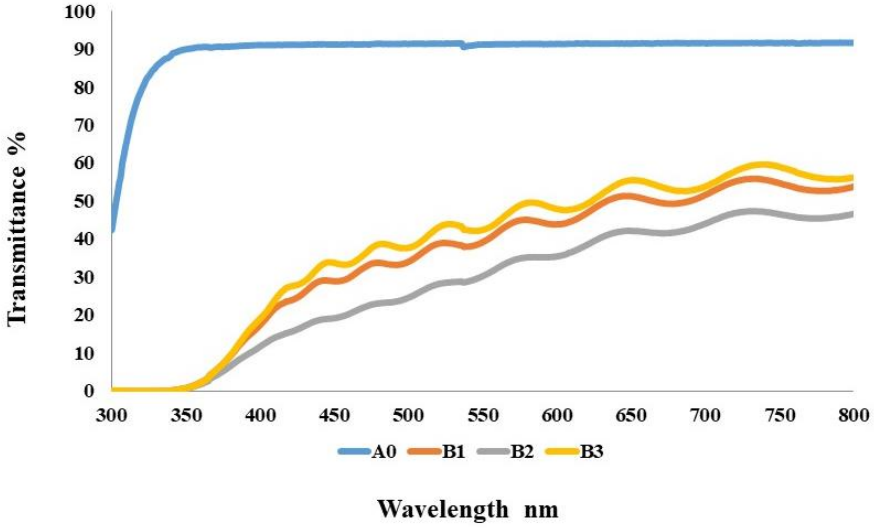

(c) ITO Film transmittance results, the condition of spattering when 300 W, A0 when no film.

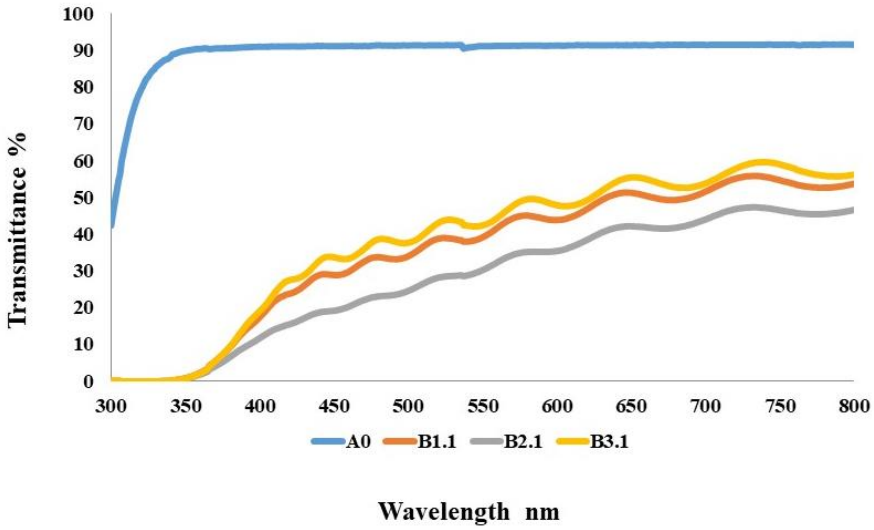

(d) ITO Film transmittance results after heat treatment , the condition of spattering when 300 W and the heat treatment temperature when A1: 200℃, A2: 120℃, A3: 160℃, A0 when no film.

Appendix 3:

Experimental procedures for consideration to using quartz crystal microbalance with ECM:

1. **Experimental procedure for consideration to using quartz crystal microbalance with only a culture medium**
    1. The quartz crystal microbalance was integrated into the measuring cell and washed with sterile water.
    2. The measuring cell was connected to the experiment device by QCA multiplier in the incubator, the measuring program "WinQCM" was started, and the measuring cell was allowed to stand about 1 to 2 h until the resonant frequency and resonant resistance became stable.
    3. After resonant frequency and resonant resistance became stabled, 200 μL of the medium was added dropwise and the measurement was allowed to complete about 24 h.

2. **Experimental procedure for the adhesion of cultured cells to the surface of the quartz crystal microbalance with the blank mode**
    1. The quartz crystal microbalance was integrated into the measuring cell and washed with sterile water.
    2. The measuring cell was connected to the experiment device by QCA multiplier in the incubator, the measuring program "WinQCM" was started, and the measuring cell was allowed to stand about 1 to 2 h until the resonant frequency and resonant resistance became stable.
    3. After two hours, 200 μL of the medium was added dropwise, and the mixture was allowed to stand for two hours.
    4. After culturing the HepG2 cells, the cells were seeded into the measurement cell at the target concentration.
    5. After 10 minutes of seeding the cells into the measuring cell, the "USB Video Selector & Capture" turned on, and then CMOS camera focus was set, after which cells were imaged at 30 min intervals.
    6. The measurement was completed approximately 72 h after seeding the cell.

3. Experimental procedure for the adhesion of cultured cells to the surface of the quartz crystal microbalance with collagen

1. The quartz crystal microbalance was integrated into the measuring cell and washed with sterile water.
2. The measuring cell was connected to the experiment device by QCA multiplier in the incubator, the measuring program "WinQCM" was started, and the measuring cell was allowed to stand about 1 to 2 h until the resonant frequency and resonant resistance became stable.
3. 100 μL of collagen solution was added dropwise to the measurement cell for surface treatment on the crystal unit substrate.
4. After 1 h of adding collagen solution, the collagen solution was removed with 100 μL of added PBS and gently removed to wash the surface of the quartz crystal microbalance, and then 200 μL of medium and cells at target concentration were added dropwise into the measuring cell.
5. After 10 min of seeding the cells into the measuring cell, the "USB Video Selector & Capture" turned on, and then CMOS camera focus was set, after which cells were imaged at 30 min intervals.
6. The measurement was completed approximately 72 h after seeding the cell.

4. Experimental procedure for adhesion of cultured cells to the surface of quartz crystal microbalance with poly-L-lysine

1. The quartz crystal microbalance was integrated into the measuring cell and washed with sterile water.
2. The measuring cell was connected to the experiment device by QCA multiplier in the incubator, the measuring program "WinQCM" was started, and the measuring cell was allowed to stand about 1 to 2 h until the resonant frequency and resonant resistance became stable.
3. 60 μL of PLL (100 μL/mL) was added dropwise to the measurement cell for surface treatment on the crystal unit substrate.
4. After 1 hour of adding PLL, the PLL was removed with 100 μL of added PBS and gently removed to wash the surface of the quartz crystal microbalance, and then 200 μL of medium was added dropwise, and the mixture was allowed to stand for 2 h.
5. After culturing HepG2 cells, cells were seeded into the measurement cell at the target concentration.

6. After 10 minutes of seeding the cells into the measuring cell, the “USB Video Selector & Capture” turned on, and then CMOS camera focus was set, after which cells were imaged at 30 min intervals.
7. The measurement was completed approximately 72 h after seeding the cell.

5. Experimental procedure for the adhesion of cultured cells to the surface of the quartz crystal microbalance with PNIPAM polymer

1. The quartz crystal microbalance was integrated into the measuring cell and washed with sterile water.
2. The measuring cell was connected to the experiment device by QCA multiplier in the incubator, the measuring program “WinQCM” was started, and the measuring cell was allowed to stand about 1 to 2 h until the resonant frequency and resonant resistance became stable.
3. To form a PNIPAM film, the measurement was paused and the quartz crystal was removed from the measurement cell, after which the quartz crystal was washed with methanol for 10 minutes and heated at 150 °C for 30 min, after which its surface was treated with PNIPAM – triethoxysilane 5% – in methanol for 10 min. After heating the crystal at 150 °C for 60 min, its surface was rinsed with distilled water. The crystal was then heated again at 150 °C for 30 min.
4. After the PNIPAM film was formed, the quartz crystal was returned to the measuring cell, the measurement was continued after being paused, the measuring cell was allowed to stand for 2 h, after which 200 μL of the medium was added dropwise, and the mixture was left for 2 h as well.
5. After culturing HepG2 cells, cells were seeded into the measurement cell at the target concentration.
6. After 10 minutes of seeding the cells into the measuring cell, the “USB Video Selector & Capture” turned on, and then CMOS camera focus was set, after which cells were imaged at 30 min intervals.
7. In a cell reduction monitoring experiment, the temperature was lowered from 37 °C to 20 °C for half an hour, after which the temperature was raised to 37 °C.
8. The measurement was completed approximately 72 h after seeding the cell.

6. Experimental procedure for the adhesion of cultured cells to the surface of the quartz crystal microbalance with PLL on PNIPAM polymer

1. The quartz crystal microbalance was integrated into the measuring cell and washed with sterile water.
2. The measuring cell was connected to the experiment device by QCA multiplier in the incubator, the measuring program "WinQCM" was started, and the measuring cell was allowed to stand about 1 to 2 h until the resonant frequency and resonant resistance became stable.
3. To form a PNIPAM film, the measurement was paused and the quartz crystal was removed from the measurement cell, after which the quartz crystal was washed with methanol for 10 min and heated at 150 °C for 30 min, after which its surface was treated with PNIPAM – triethoxysilane 5% – in methanol for 10 min. After heating the crystal at 150 °C for 60 min, its surface was rinsed with distilled water. The crystal was then heated again at 150 °C for 30 min.
4. After the PNIPAM film was formed, the quartz crystal was returned to the measuring cell and connected to the experiment device by QCA multiplier in the incubator, the measurement was continued after being paused, the measuring cell was allowed to stand for 2 h, after which 200 μL of the medium was added dropwise, and the mixture was left for 2 h as well.
5. To form a PLL film, 50 μL of PLL (100 μL/mL) was added dropwise to the measurement cell for surface treatment on the PNIPAM film.
6. After 1 hour of adding PLL, the PLL was removed with 100 μL of added PBS and gently removed to wash the surface of the quartz crystal microbalance, and then 200 μL of medium was added dropwise, and the mixture was allowed to stand for 2 hours.
7. After culturing HepG2 cells, cells were seeded into the measurement cell at the target concentration.
8. After 10 min of seeding the cells into the measuring cell, the "USB Video Selector & Capture" turned on, and then CMOS camera focus was set, after which cells were imaged at 30 min intervals.
9. The measurement was completed approximately 72 h after seeding the cell.